

AN ABSTRACT OF THE DISSERTATION OF

Kent C. Abel for the degree of Doctor of Philosophy in Nuclear Engineering presented on August 25, 2005.

Title: Stability Improvement of the One-Dimensional Two-Fluid Model for Horizontal Two-Phase Flow with Model Unification.

Redacted for privacy

Abstract approved:

José N. Reyes, Jr.

Qiao Wu

The next generation of nuclear safety analysis computer codes will require detailed modeling of two-phase fluid flow. The most complete and fundamental model used for these calculations is known as the two-fluid model. It is the most accurate of the two-phase models since it considers each phase independently and links the two phases together with six conservation equations.

A major drawback is that the current two-fluid model, when area-averaged to create a one-dimensional model, becomes ill-posed as an initial value problem when the gas and liquid velocities are not equal. The importance of this research lies in obtaining a model that overcomes this difficulty. It is desired to develop a modified one-dimensional two-fluid model for horizontal flow that accounts for the pressure difference between the two phases, due to hydrostatic head, with the implementation of a void fraction distribution parameter. With proper improvement of the one-dimensional two-fluid model, the next generation of nuclear safety analysis computer codes will be able to predict, with greater precision, the key safety parameters of an accident scenario.

As part of this research, an improved version of the one-dimensional two-fluid model for horizontal flows was developed. The model was developed from a theoretical point of view with the three original distribution parameters simplified down to a single parameter. The model was found to greatly enhance the numerical

stability (hyperbolicity) of the solution method. With proper modeling of the phase distribution parameter, a wide range of flow regimes can be modeled. This parameter could also be used in the future to eliminate the more subjective flow regime maps that are currently implemented in today's multiphase computer codes. By incorporating the distribution parameter and eliminating the flow regime maps, a hyperbolic model is formed with smooth transitions between various flow regimes, eliminating the unphysical oscillations that may occur near transition boundaries in today's multiphase computer codes.

©Copyright by Kent C. Abel
August 25, 2005
All Rights Reserved

Stability Improvement of the One-Dimensional Two-Fluid Model for Horizontal Two-Phase Flow with Model Unification

by
Kent C. Abel

A DISSERTATION

submitted to

Oregon State University

in partial fulfillment of
the requirements for the
degree of

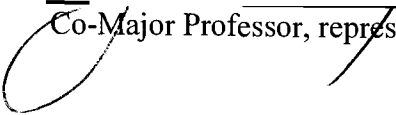
Doctor of Philosophy

Presented August 25, 2005
Commencement June 2006

Doctor of Philosophy dissertation of Kent C. Abel presented on August 25, 2005.

APPROVED:

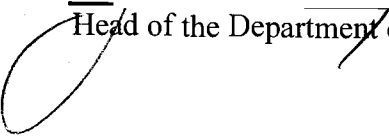
Redacted for privacy

_____
Co-Major Professor, representing Nuclear Engineering

Redacted for privacy

Co-Major Professor, representing Nuclear Engineering

Redacted for privacy

_____
Head of the Department of Nuclear Engineering and Radiation Health Physics

Redacted for privacy

Dean of the Graduate School

I understand that my dissertation will become part of the permanent collection of Oregon State University libraries. My signature below authorizes release of my dissertation to any reader upon request.

Redacted for privacy

Kent C. Abel, Author

ACKNOWLEDGMENTS

I would like to take this opportunity to thank Dr. José N. Reyes, Jr. for all of his support, ideas, and positive input throughout the research and writing phases of this dissertation. He has been instrumental in my education.

I also owe Dr. Qiao Wu a debt of gratitude for all of his help and guidance through the model development portion of this work. He has provided exceptional guidance with both theoretical and applied information based upon his vast experience within this field. He has had a large influence on my education and I am thankful for that.

I would also like to thank the other members of my committee, Dr. Deborah V. Pence, Dr. Brian Woods and Dr. Vinod Narayanan, for their valuable comments and their time.

I finally would like to thank my wife, Micki, for putting up with the late hours of work and providing support throughout this dissertation. Lastly, I want to thank my family back home, especially my mother, for their support throughout my college education.

TABLE OF CONTENTS

	<u>Page</u>
1 INTRODUCTION	1
2 LITERATURE REVIEW	3
2.1 TYPES OF FLOW REGIMES.....	3
2.2 TWO-PHASE FLOW MODELS	8
2.2.1 Homogenous model	9
2.2.2 Drift-flux model	10
2.2.3 Two-fluid model	13
2.3 TWO-FLUID MODEL FOR ONE-DIMENSIONAL HORIZONTAL FLOW .	16
2.3.1 Bubbly/Intermittent flow model	18
2.3.2 Separated (stratified/annular) flow two-fluid model.....	19
2.4 TWO-FLUID MODEL STABILITY FOR HORIZONTAL FLOW	23
2.4.1 Stratified wavy-to-slug flow regime transition	23
2.4.2 Numerical stability	26
2.5 VOID DISTRIBUTION MEASUREMENT (HORIZONTAL FLOW).....	34
2.6 INTERFACIAL PRESSURE MODELING	37
2.7 INTERFACIAL AREA TRANSPORT EQUATION.....	38
2.8 INTERFACIAL AREA MEASUREMENT	43
2.9 LITERATURE REVIEW SUMMARY	47
3 TWO-PRESSURE TWO-FLUID MODEL DEVELOPMENT	49
3.1 FULLY-MIXED FLOW VS. SEPARATED FLOW EQUATIONS.....	51
3.2 INTERFACIAL PRESSURE TERM.....	55
3.2.1 Stratified flow - pressure terms	55
3.2.2 Bubbly flow - pressure terms	57
3.2.3 Interfacial pressure term unification	62
3.3 PHASE DISTRIBUTION PARAMETER.....	64
3.3.1 Development of the phase distribution parameters.....	64
3.3.2 Comparison of the phase distribution parameters.....	67
3.3.3 Simplification of the phase distribution parameters	72
4 MODEL RESULTS AND COMPARISON	77
4.1 AVERAGE PHASE PRESSURE BASED ON EXPERIMENTAL DATA.....	77

TABLE OF CONTENTS (Continued)

	<u>Page</u>
4.2 DISTRIBUTION PARAMETER BASED ON EXPERIMENTAL DATA	81
4.3 DISTRIBUTION PARAMETER SIMPLIFICATION VERIFICATION	86
4.4 EFFECTS OF DISTRIBUTION PARAMETER ON STABILITY	90
4.4.1 Phase transition	90
4.4.2 Characteristic analysis	90
4.5 MODELING OF THE DISTRIBUTION PARAMETER	103
4.5.1 Using void fraction distribution to calculate parameter	104
4.5.1.1 Determine void distribution using a force balance approach	104
4.5.1.2 Determine void distribution using fits of experimental data	106
4.5.1.3 Determine void distribution using a physical modeling approach	106
4.5.2 Determine distribution parameter in terms of non-dimensional numbers ..	107
4.5.2.1 Discussion of parameters to describe flow regime transition	107
4.5.2.2 Functional relation between θ and non-dimensional numbers	113
4.6 COMPARISON OF MODEL TO PREVIOUS MODELS	124
5 DISCUSSION AND FUTURE WORK	125
6 CONCLUSIONS	128
BIBLIOGRAPHY	129
NOMENCLATURE	136
APPENDICES	138
APPENDIX A: STRATIFIED TWO-FLUID MODEL DERIVATION	139
APPENDIX B: PHASE DISTRIBUTION PARAMETERS DERIVATION	147

LIST OF FIGURES

<u>Figure</u>	<u>Page</u>
2.1: Flow patterns in vertical flow.....	4
2.2: Flow patterns in horizontal flow	5
2.3: Flow map for horizontal flow (<i>Mandhane et al., 1974</i>)	7
2.4: Flow map for vertical flow (<i>Hewitt and Roberts, 1969</i>)	7
2.5: Kelvin-Helmholtz problem.....	32
3.1: Stratified flow channel definitions	50
3.2: Control volume for continuity equation	51
3.3: Control volume for momentum equation	52
3.4: Stratified flow pressure development.....	56
3.5: Interface definitions.....	58
3.6: Pressure force on bubbly flow.....	59
3.7: Fully-mixed flow pressure development.....	60
3.8: Phase distribution for different flow regimes.....	67
3.9: Comparison of the theoretical limits of the θ_0 distribution parameter	70
3.10: Comparison of the theoretical limits of the θ_1 distribution parameter	71
3.11: Comparison of the theoretical limits of the θ_2 distribution parameter	71
4.1: Comparison of theoretical vs. experimental pressure due to gravity force	79
4.2: Relative pressure difference between two phases	81
4.3: Experimental void fraction profiles, $\langle j_f \rangle = 1.65 \text{ m/s}$	82

LIST OF FIGURES (Continued)

<u>Figure</u>	<u>Page</u>
4.4: Experimental void fraction profiles, $\langle j_f \rangle = 3.8$ m/s	82
4.5: Experimental void fraction profiles, $\langle j_f \rangle = 4.67$ m/s	83
4.6: Experimental void fraction profiles, $\langle j_f \rangle = 5.0$ m/s	83
4.7: Comparison of the θ_0 distribution parameter with experimental data.....	87
4.8: Comparison of the θ_1 distribution parameter with experimental data.....	87
4.9: Comparison of the θ_2 distribution parameter with experimental data.....	88
4.10: Calculation of error in v_r for using the $\langle\langle P_i \rangle\rangle = \langle\langle P_g \rangle\rangle$ approximation.....	100
4.11: Influence of the distribution parameter on stability limit (2" duct, $\rho_f/\rho_g = 100$)	101
4.12: Influence of the distribution parameter on stability limit (2" duct, $\rho_f/\rho_g = 500$)	102
4.13: Influence of the distribution parameter on stability limit (2" duct, $\rho_f/\rho_g = 1000$)	102
4.14: Flow regime area of focus for distribution parameter modeling.....	108
4.15: Possible function describing the distribution parameter in terms of Fr	115
4.16: The resulting collapsed curve for describing the distribution parameter	116
4.17: Using average liquid velocity for Fr, $v_f = j_f/(1-\alpha)$	117
4.18: Using superficial liquid velocity for Fr	118

LIST OF TABLES

<u>Table</u>	<u>Page</u>
2.1: Summary of previous work in improving two-fluid model stability.....	47
3.1: Comparison of theoretical values of the phase distribution parameters.....	70
4.1: Experimental data test conditions.....	78
4.2: Pressure of gas and liquid phases based on experimental data	85
4.3: Comparison of experimentally obtained distribution parameters and their theoretical values	89
4.4: Comparison of experimental Froude numbers	112
4.5: Average relative error of Fr_f based on average liquid velocity	121
4.6: Maximum relative error of Fr_f based on average liquid velocity	121
4.7: Average relative error of Fr_f based on superficial liquid velocity.....	122
4.8: Maximum relative error of Fr_f based on superficial liquid velocity.....	122

Stability Improvement of the One-Dimensional Two-Fluid Model for Horizontal Two-Phase Flow with Model Unification

1 INTRODUCTION

Within the area of two-phase fluid flow, there is still little understanding of the complex nature in which phases interact with each other. The proper modeling of flow structure is important in determining heat transfer coefficients, pressure drop, and other important parameters in many research and industrial applications such as chemical reactors and nuclear power plants. The most complete of the two-phase flow models is known as the two-fluid model. The two-fluid model is incorporated in important multiphase computer codes used for modeling transients in nuclear power plants such as RELAP5 and TRACE. Although the two-fluid model is complete from a theoretical point of view, there is a lack of complete understanding of the interaction mechanisms and rates between the different phases.

The current two-fluid model, when area-averaged to produce a one-dimensional model, has a few problems with respect to computationally modeling two-phase flow. The current one-dimensional two-fluid model possess unphysical instabilities in the case where the gas velocity is not equal to the liquid velocity. During these instabilities, the governing equations become ill-posed as an initial value problem and are not able to be solved as the solution method is no longer consistent with the equations. The second downfall of current use of the two-fluid model is that the two-fluid model equations are typically developed for either the stratified flow case or the fully mixed bubbly flow case. Due to these restrictions, the flow is not properly modeled when the flow structure falls outside of these categories. In addition, due to the assumptions used within the fully mixed case, the two-phase flow no longer has the ability to become separated in order to transition back into stratified flow.

With this research, however, the intent is to incorporate phase (void fraction) distribution parameters into the two-fluid model in order to unify the one-dimensional two-fluid model. In this case, everything from stratified to fully mixed flow will have the ability to be properly modeled once the phase distribution parameters are known. The phase distribution parameter will create a difference in pressure between the two phases (due to the hydrostatic head). This pressure difference should add to the stability of the flow, allowing the problem to remain hyperbolic in nature, so that the problem may properly be solved with one-dimensional multiphase computer codes. In addition, with this added ability, the two-phase modeling codes will not have to switch from one flow model to the next, which tends to cause numerical oscillations in current multiphase computer programs. With proper modeling of the phase distribution parameters, the multiphase computer codes will no longer need to be based on the more subjective flow regime maps, as the distribution parameters are all that would be needed in order to describe the flow. As a result, a smooth transition from one flow regime type to the next can occur, eliminating the unphysical oscillations that may occur near transition boundaries using current two-phase flow codes.

2 LITERATURE REVIEW

2.1 TYPES OF FLOW REGIMES

The use of flow regimes is a way to visually categorize the void distribution patterns of gas-liquid flows. These patterns depend upon gas and liquid flow rates, channel geometry, pressure and orientation to gravity. In the nuclear engineering industry, the two most important flow orientations are vertical and horizontal. In other fields such as petroleum engineering, inclined flows are also important. In the nuclear engineering field, upward, vertical, co-current flow is used in simulating a Boiling Water Reactor (BWR) fuel assembly. The horizontal co-current flow is important for simulation of a Light Water Reactor (LWR) piping during transients.

The distinct flow regimes in the vertical flow orientation are bubbly, slug, churn, and annular. A representation of these flows is given in Figure 2.1. The bubbly flow regime is characterized by the existence of dispersed bubbles in a continuous liquid phase. Smaller bubbles are typically spherical, but larger bubbles tend to be between spherical and ellipsoid in shape. Slug flow is constructed of large gas bubbles separated by liquid slugs. Within the liquid slug, small bubbles like those in bubbly flow exist. In addition, in the case of slug flow, a thin liquid film surrounding the slug bubble falls downward as the slug rises. Churn flow is similar to slug flow but is more chaotic. The annular flow regime exists at high gas flow rates and is characterized by a gas core surrounded by a liquid film. The annular flow regime may also contain liquid droplets within the gas core depending on the flow rates used.

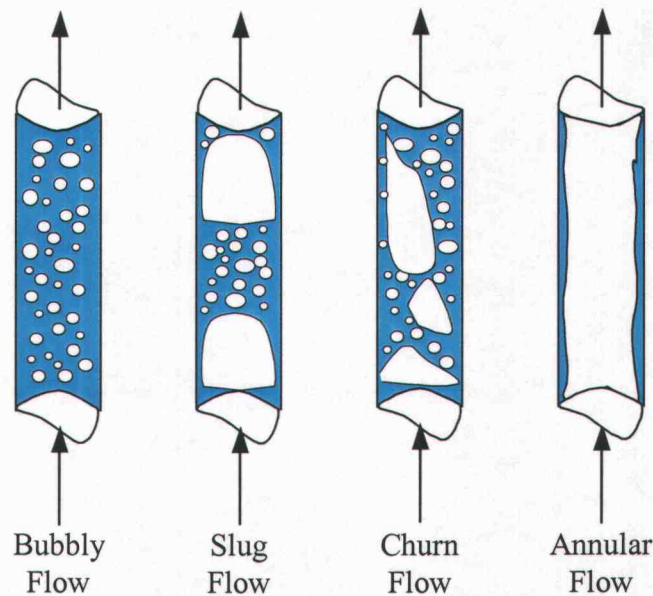


Figure 2.1: Flow patterns in vertical flow

Flow in a horizontal section has the ability to become stratified and thus contains more flow regimes than in the vertical case. The flow regimes for the horizontal case are given in Figure 2.2. An additional difference between the vertical and horizontal flow is the radial location of the maximum void fraction. The void fraction distribution is normally peaked in the center of the pipe for the vertical case, whereas, due to the bubble buoyancy, the void fraction distribution peak for horizontal flow is near the top of the pipe. Another important distinction between horizontal flow and vertical two-phase flow is how the flow develops along the length of pipe. In the case of vertical flow, the flow quickly develops as the frictional and buoyancy forces become in balance with the gravitational force. However, in the case of horizontal flow, one does not obtain fully developed flow as in vertical or inclined flows. This is due to the constant acceleration from the pressure losses caused by wall friction and the lack of an opposing force along the flow direction, such as gravity.

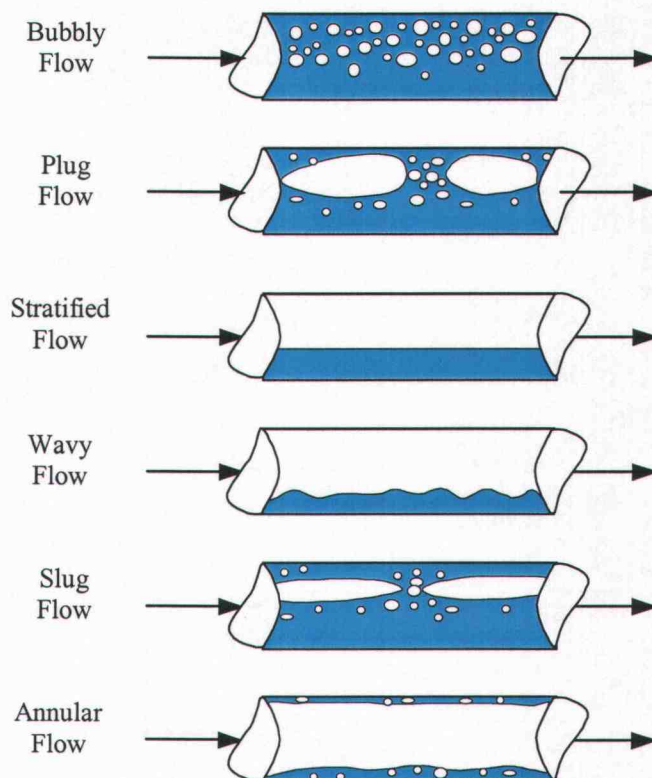


Figure 2.2: Flow patterns in horizontal flow

Knowing the type of flow regime that the channel is currently experiencing is important in trying to model two-phase flow. This is due to the fact that many important parameters such as pressure drop and heat transfer coefficients are flow regime dependent. The flow regimes are typically determined with the use of flow regime maps. Examples of some typical flow regime maps used for horizontal and vertical flow cases are given in Figure 2.3 and Figure 2.4, respectively. Flow regime maps are typically plotted using superficial gas and liquid velocities, j_g and j_f , which are defined as follows:

$$j_g = \frac{Q_g}{A} \quad (2.1)$$

$$j_f = \frac{Q_f}{A} \quad (2.2)$$

where A is the cross-sectional flow area of the channel and Q_g and Q_f are the volumetric flow rates of the gas and liquid phases, respectively. These flow regime maps vary with pipe orientation, pipe diameter, fluid type, etc., so separate maps are needed for each particular flow case. Also, these maps are created for fully developed flow, so they are not applicable to entrance regions or regions near bends, piping expansions, nozzles, etc. The other difficulty with standard flow regime maps is that some of the transition lines are based only on experimental observation instead of through a mechanistic approach which adds a subjective nature to these maps. In addition, numerical oscillations may be created because each region has its own correlations for pressure drop and other flow parameters, which combined with the logical switching between regimes, can create unphysical oscillations near flow transition boundaries. This is because there is no blending of the boundary so, as an example, one side of the transition boundary could be stratified wavy flow with its own correlations used and on the other side of the boundary may be slug flow with a completely different set of correlations. Near this transition boundary, the numerical calculation may switch back and forth between these two regimes with only small variations in the calculated flow. This is how these unphysical oscillations can be created.

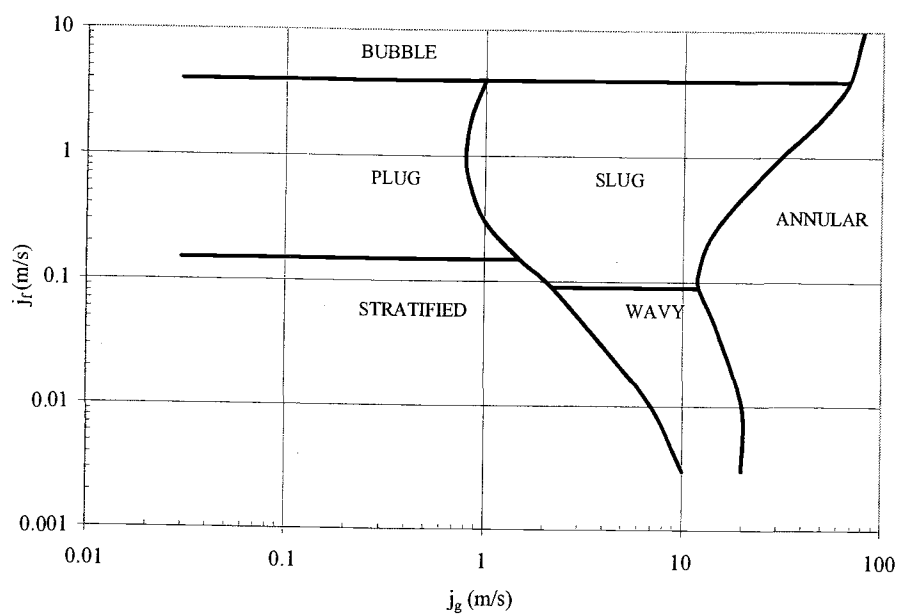


Figure 2.3: Flow map for horizontal flow (*Mandhane et al., 1974*)

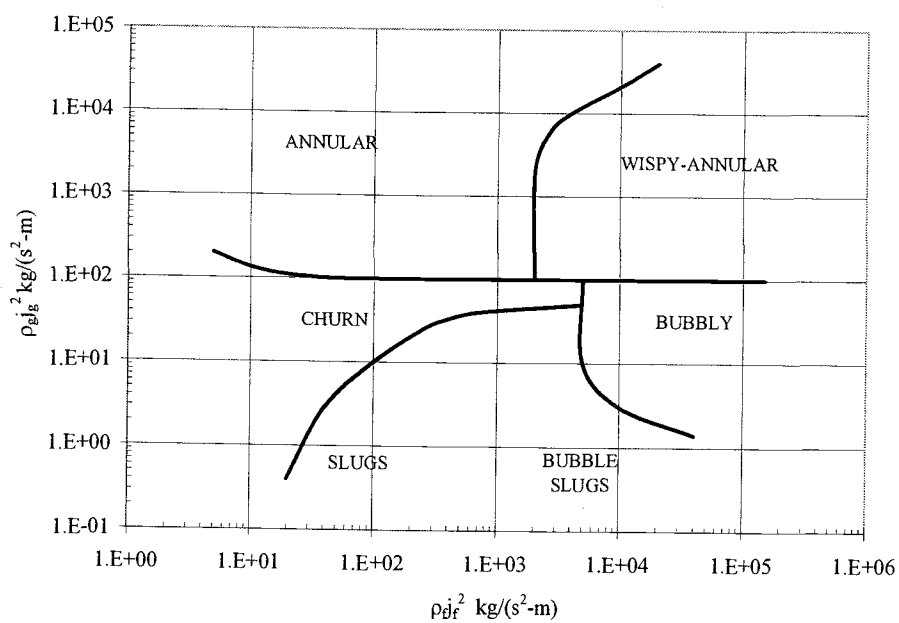


Figure 2.4: Flow map for vertical flow (*Hewitt and Roberts, 1969*)

2.2 TWO-PHASE FLOW MODELS

In the field of two-phase flow, three major models have been proposed. These models include the homogeneous flow model, the drift flux model and the two-fluid model. A brief description of each of these models is given:

1. **Homogeneous model** – In this model, the two phases are assumed to move with the same velocity and have the same temperature. This allows the two-phase mixture to be treated as a single fluid. This model is useful at high pressure and high flow rate conditions. The temperature is the saturation temperature for that pressure. Since at high flow rates, the gas and liquid move with the approximately same velocity, the equal velocity of the two phases is a good assumption.
2. **Drift flux model** – This model is similar to the homogeneous model except it allows the two phases to move with different velocities or a slip ratio. This model requires that the relative velocity between the two phases be given by a predetermined relationship. This model is useful for low pressure or low flow rate flows in which the system is at steady-state condition.
3. **Two-fluid model** – This is the most advanced of these three models. The two-fluid model allows the two phases to have unequal temperatures as well as unequal velocities. The model uses conservation of mass, momentum, and energy transfer equations. This model is most useful where transient and non-equilibrium conditions exist. However, since this is the most descriptive of the three models, the two-fluid model may also be applied to the simpler flow conditions.

A more in depth coverage of each two-phase flow model will be covered in the upcoming subsections.

2.2.1 Homogenous model

The homogeneous model is the most simplistic of these three models since it assumes that both phases are at the same temperature and move with the same velocity. Although the homogenous model is the least complex of the traditional two-phase flow models, it still has important applications for which it is applicable. These include applications in which the fluids are at saturation temperature, moving at high flow rates, and at a steady-state condition. An example in which the homogenous model may work well is in modeling a BWR fuel channel during normal steady-state operation. The area averaged void fraction given by the homogenous model is given in equation (2.3).

$$\langle \alpha \rangle = \frac{1}{1 + \frac{1-x}{x} \frac{\rho_g}{\rho_f}} \quad (2.3)$$

Where x is the vapor quality, ρ_g is the density of the gas, and ρ_f is the liquid density. The vapor quality is defined as the mass flow rate of the vapor divided by the mass flow rate of the two-phase mixture. The homogenous model, also referred to as the three-equation model, treats the flow similar to single-phase flow by incorporating the use of mixture properties along with the three conservation equations: mass, momentum and energy. The three governing equations for the one-dimensional homogenous flow model are as follows:

continuity equation:

$$\frac{\partial \rho_m}{\partial t} + \frac{\partial \rho_m u_m}{\partial x} = 0 \quad (2.4)$$

momentum equation:

$$\frac{\partial \rho_m u_m A}{\partial t} + \frac{\partial}{\partial x} (\rho_m u_m u_m A) = -\frac{\partial P_m}{\partial x} A + A \rho_m g \cos \varphi - \tau_w \xi_w \quad (2.5)$$

enthalpy energy equation:

$$\frac{\partial \rho_m H_m A}{\partial t} + \frac{\partial}{\partial x} (\rho_m H_m u_m A) = q_w'' \xi_w \quad (2.6)$$

Both the mixture density, ρ_m , and the mixture enthalpy, H_m , are functions of the mixture quality, x . The subscript w identifies the values at the wall and P , u , ξ , ρ , q'' and τ are pressure, axial velocity component, perimeter, density, heat flux, and shear stress, respectively.

2.2.2 Drift-flux model

The drift flux model is currently the most widely used model in two-phase flow. This is due to the fact that the drift flux model offers more flexibility than the homogeneous model but is much less complex than the two-fluid model. The drift flux model assumes that everything is at a uniform temperature, similar to the homogenous model, but allows for each phase to move at its own velocity. A common application for the drift flux model is the analysis of the pool boiling phase during a Loss of Coolant Accident (LOCA). In this application, both phases are at saturation temperature with the vapor bubbles rising in a pool of stagnant liquid. The drift flux model is most commonly used for co-current upward, vertical flows. However, Franca and Lahey (Franca and Lahey, 1992) successfully applied the drift flux model to horizontal flows. The drift flux model stems from the work of Zuber and Findley (Zuber and Findley, 1965). This basic drift flux model has been revised by other researchers over the years. The one dimensional drift flux model for a relative velocity v_r is given by:

$$(1-\alpha)v_r = (C_o - 1)j + \langle\langle V_{gj} \rangle\rangle \quad (2.7)$$

where C_o , j , and $\langle\langle V_{gj} \rangle\rangle$ are the volumetric distribution parameter, total volumetric flux, and the void fraction weighted area average of the local drift velocity, respectively. The total volumetric flux is defined as:

$$j = j_g + j_f \quad (2.8)$$

where j_g and j_f are the superficial gas and liquid velocities respectively. The relative velocities between the phases is given by:

$$v_r = u_g - u_f \quad (2.9)$$

where $u_g = j_g/\alpha$ and $u_f = j_f/(1-\alpha)$. By combining these relations, one can find the void fraction as follows:

$$\alpha = \frac{j_g}{C_o j + \langle\langle V_{gj} \rangle\rangle} \quad (2.10)$$

The volumetric distribution parameter, C_o , is defined by equation (2.11). Often the volumetric distribution parameter is found by using one of the many correlations that exist. For fully developed bubbly and slug flows, the value of C_o is approximately 1.2. Kataoka and Ishii (Kataoka and Ishii, 1987) used the drift flux model to apply towards a large diameter pipe to develop a correlation for pool void fraction. Kataoka and Ishii found that the drift velocity of a pool system depends upon vessel diameter, pressure, gas flux, and the physical properties of the fluid being studied. The paper found that the drift velocity and the void fraction measured experimentally could be quite different from those predicted by the conventional correlations at the time. The correlation that Kataoka and Ishii developed based on the drift flux model fit the existing experimental data much better than the conventional correlations.

$$C_o = \frac{\langle \alpha j \rangle}{\langle \alpha \rangle \langle j \rangle} \quad (2.11)$$

Kataoka et al. (Kataoka et al., 1987) applied the drift flux model to a vertical column in which the liquid phase was stagnant. Kataoka et al. found that the distribution parameters for the stagnant flow case were higher than those found at higher liquid flow rates. Kataoka et al. also observed that the drift velocity remained nearly the same for the various liquid flow rates used. Kaminaga (Kaminaga, 1992) compared experiments that were in vertical columns with small diameters and having a low liquid velocity to three different correlations. The correlations that are compared include Ishii's correlation, Kataoka's (Kataoka and Ishii, 1987) correlation based on stagnant liquid, and a correlation for stagnant or low liquid velocities in an air-water system determined by Ellis. Kaminaga determined that the void fraction correlations of Ishii and Ellis were valid with experimental data within a 30% error for gas velocities over 0.2 m/s in a round tube with a diameter less than 50 mm. However, if the gas velocity is less than 0.2 m/s, Kaminaga found that none of the correlations selected for this study could be applied and suggested that a correlation that is applicable in this velocity range for small diameter tubes needed to be determined.

Chen and Fan (Chen and Fan, 1989) applied the drift flux model to a vertical column consisting of air, water, and 3.04 mm diameter glass beads. It was found that the drift flux model can be applied to a three phase system such as this one and return a value for the bubble velocity with an error of less than 10% and 2% error in liquid holdup for the liquid-solid sedimentation region. This paper demonstrates that the drift flux model can be applied to more than a gas-liquid system.

Franca and Lahey (Franca and Lahey, 1992) applied the drift flux model to the horizontal flow orientation and found that horizontal two-phase flows could be well correlated using the drift flux model. Franca and Lahey also discovered that the standard variables $\langle j_g \rangle / \langle \alpha \rangle$ and $\langle j \rangle$ work well for plug and slug flows while

$\langle \alpha \rangle / (1 - \langle \alpha \rangle)$ and $\langle j_g \rangle / \langle j_f \rangle$ are more appropriate for stratified and annular flows. For plug, wavy-stratified, and annular flow, the distribution parameter, C_o , is equal to about 1.0 while for slug flow the distribution parameter is equal to 1.2. For a value of C_o that is approximately equal to 1.0, indicates a nearly flat profile while values of C_o greater than 1.0, indicates a more center peaked profile such as a parabolic shape. The drift velocity, $\langle \langle v_{gj} \rangle \rangle$, found in horizontal flow ranged from -0.20 m/s, for slug flow, up to 2.7 m/s for annular flow. A negative value for the drift velocity indicates that the liquid phase is moving faster than the vapor phase.

2.2.3 Two-fluid model

The two-fluid model is considered the most comprehensive of these models because this model considers each phase separately in terms of two sets of conservation equations (Hibiki et al., 1998; Hibiki and Ishii, 1999; Revankar and Ishii, 1992; Wu et al., 1998; Ghiaasiaan et al., 1995) along with interfacial transfer terms in order to link the two sets of conservation equation together. These conservation equations include a balance of mass, energy and momentum of each phase. Since mass, energy, and momentum can transfer between the two phases; one needs to accurately predict these transfer terms. The weakest link of this model is the difficulty in accurately predicting or measuring the interfacial transfer terms. Since the interfacial transfer terms are related to the area between the two phases, one needs to be able to find the interfacial area or interfacial area concentration. Thus, interfacial area and interfacial area concentration are two important parameters in the field of two-phase flow. The interfacial area concentration has units of area per volume and is defined as:

$$\frac{1}{L_s} = a_i = \frac{\text{Interfacial area}}{\text{Mixture volume}} \quad (2.12)$$

where L_s is the length scale at the interface and a_i is the interfacial area concentration. The three conservation equations for each phase are given as follows (Revankar and Ishii, 1992):

continuity equation:

$$\frac{\partial \alpha_k \rho_k}{\partial t} + \nabla \cdot (\alpha_k \rho_k \mathbf{v}_k) = \Gamma_k \quad (2.13)$$

momentum equation:

$$\begin{aligned} \frac{\partial \alpha_k \rho_k \mathbf{v}_k}{\partial t} + \nabla \cdot (\alpha_k \rho_k \mathbf{v}_k \mathbf{v}_k) = & -\alpha_k \nabla P_k + \nabla \cdot \alpha_k (\bar{\boldsymbol{\tau}}_k + \boldsymbol{\tau}_k^t) \\ & + \alpha_k \rho_k \mathbf{g} + \mathbf{v}_{ki} \Gamma_k + M_{ik} - \nabla \alpha_k \cdot \boldsymbol{\tau}_i \end{aligned} \quad (2.14)$$

enthalpy energy equation:

$$\begin{aligned} \frac{\partial \alpha_k \rho_k H_k}{\partial t} + \nabla \cdot (\alpha_k \rho_k H_k \mathbf{v}_k) = & \nabla \cdot \alpha_k (\bar{q}_k + \mathbf{q}_k^t) \\ & + \alpha_k \frac{D_k}{Dt} P_k + H_{ki} \Gamma_k + \frac{q_{ki}''}{L_s} + \Phi_k \end{aligned} \quad (2.15)$$

The symbols Γ_k , M_{ik} , $\boldsymbol{\tau}_i$, q_{ki}'' , and Φ_k are the mass generation per unit volume, interfacial drag, the interfacial shear stress, the interfacial heat flux and the dissipation term, respectively. The subscript ki indicates the value of the term for phase k at the interface i . The terms α_k , ρ_k , \mathbf{v}_k , P_k , and H_k represent the void fraction, density, velocity, pressure and enthalpy of phase k , respectively. The terms $\bar{\boldsymbol{\tau}}_k$, $\boldsymbol{\tau}_k^t$, \bar{q}_k , \mathbf{q}_k^t , and \mathbf{g} are the average viscous stress, turbulent stress, mean conduction heat flux, the turbulent heat flux, and the acceleration due to gravity, respectively. H_{ki} symbolizes the enthalpy of phase k at the interface. The right hand sides of equations (2.13) - (2.15) are the interfacial transfer terms and are related to each other by using averaged local jump conditions. If one rewrites equations (2.13) - (2.15) in terms of the average mass transfer per unit area, \dot{m}_k , which is defined as $\Gamma_k = \dot{m}_k / L_s$, one can write the

right hand side of these equations as an interfacial area multiplied by a driving force. The results are as follows:

continuity equation:

$$\frac{\partial \alpha_k \rho_k}{\partial t} + \nabla \cdot (\alpha_k \rho_k \mathbf{v}_k) = \frac{\dot{m}_k}{L_s} \quad (2.16)$$

momentum equation:

$$\begin{aligned} \frac{\partial \alpha_k \rho_k \mathbf{v}_k}{\partial t} + \nabla \cdot (\alpha_k \rho_k \mathbf{v}_k \mathbf{v}_k) = & -\alpha_k \nabla P_k + \nabla \cdot \alpha_k \left(\overline{\boldsymbol{\tau}}_k + \boldsymbol{\tau}_k^t \right) \\ & + \alpha_k \rho_k \mathbf{g} + \frac{1}{L_s} (\mathbf{v}_{ki} \dot{m}_k + \zeta_{ik}) - \nabla \alpha_k \cdot \boldsymbol{\tau}_i \end{aligned} \quad (2.17)$$

enthalpy energy equation:

$$\begin{aligned} \frac{\partial \alpha_k \rho_k H_k}{\partial t} + \nabla \cdot (\alpha_k \rho_k H_k \mathbf{v}_k) = & \nabla \cdot \alpha_k \left(\overline{\mathbf{q}}_k + \mathbf{q}_k^t \right) \\ & + \alpha_k \frac{D_k}{D_t} P_k + \frac{1}{L_s} (\dot{m}_k H_{ki} + q_{ki}'') + \Phi_k \end{aligned} \quad (2.18)$$

With ζ_{ik} in equation (2.17) being the interfacial drag force per cross-sectional bubble area. Equations (2.16) – (2.18) shows that the interfacial transfer terms are proportional to the interfacial area concentration multiplied by a driving force. The importance of interfacial area concentration is shown by the appearance of interfacial area concentration in each one of the conservation equations. Although, the interfacial area concentration is an important value, measurement of interfacial area concentration in the real world is very difficult, so there are very few data sets with good local interfacial area concentration data. Most of the interfacial area data sets are limited to averaged values over a section of pipe due to many of the interfacial area concentration data sets being determined by a first order chemical reaction.

The driving force for the energy equation is the heat flux between the two phases based on:

$$q_{ki}'' = h_{ki}(T_i - T_k) \quad (2.19)$$

where T_i and T_k are the interfacial and bulk temperatures based on the mean enthalpy and h_{ki} is the interfacial heat transfer coefficient. The driving force for the continuity equation is the mass generation per volume and for the momentum equation; the driving force is based on the interfacial drag and velocity. By separating out the length scale, L_s , from each of the conservation equations, one is able to determine each of the driving forces independently of the interfacial area concentration. This allows one to perform separate experiments for interfacial area concentration and the driving forces independently and then recombine the information to construct the set of conservation equations.

2.3 TWO-FLUID MODEL FOR ONE-DIMENSIONAL HORIZONTAL FLOW

The motivation behind this dissertation is the development of the two-fluid model equations for horizontal two-phase flow geometry. Typically, two-phase flow in a horizontal channel is modeled using a one-dimensional two-fluid model. The one-dimensional two-fluid model for horizontal flow is then typically subdivided into two categories: stratified/annular flow and bubbly/slug flow. Each model has its own assumptions about the flow conditions, most importantly, the difference in phase pressure caused by the transverse pressure term. The stratified/annular flow model accounts for the pressure difference between the two phases caused by gravity head, the key mechanism for phase separation. The bubbly/slug model in its current form, however, does not include the gravity head effects on the two phases and gas phase pressure is assumed to be in equilibrium with the liquid phase pressure (when surface tension effects are neglected). The difficulty lies in the fact that since the bubbly/slug model does not include this transverse pressure term, there is no mechanism governing

the vertical phase distribution and thus, the flow is not able to separate back into a stratified or annular type of flow. It is desired to create a unified one-dimensional two-fluid model that allows for a proper transition from bubbly/slug flows to stratified/annular flow and anything in between. The one-dimensional flow model is created by taking the general three-dimensional two-fluid model equations, equations (2.13) – (2.15), then integrating over a cross-section and introducing proper mean values. The one-dimensional two-fluid model is derived using the following definitions:

Area averaged quantities are defined by:

$$\langle F \rangle = \frac{1}{A} \int_A F dA \quad (2.20)$$

While, the void fraction weighted mean value is given by:

$$\langle \langle F \rangle \rangle = \frac{\langle \alpha_k F_k \rangle}{\langle \alpha_k \rangle} \quad (2.21)$$

The density of each phase is assumed to be uniform such that $\rho_k = \langle \rho_k \rangle$. The weighted mean velocity along the axial flow direction is given by:

$$\langle \langle u_k \rangle \rangle = \frac{\langle \alpha_k u_k \rangle}{\langle \alpha_k \rangle} \quad (2.22)$$

With the use of these definitions, the one-dimensional two-fluid model will be developed and discussed in the upcoming subsections for bubbly/intermittent flow as well as stratified/annular flow.

2.3.1 Bubbly/Intermittent flow model

Several authors have incorporated the bubbly/intermittent one-dimensional two-fluid model for predicting two-phase flows with common application to the nuclear industry (Ulke, 1984; Gidaspow et al., 1983; Murata, 1991; Ishii and Mishima, 1984). However, due to the assumptions that are typically placed upon this flow model, several problems appear. There can be numerical stability issues if the phase velocities do not match, there is problem with predicting flow regime transition as this model is not able to achieve flow separation, and real horizontal flows tend to have a void fraction peak near the top wall whereas this model assumes that the void is uniformly distributed. Assuming thermal processes are unimportant, in order to eliminate the need of the energy equation, the general one-dimensional two-fluid model for bubbly/slug regime horizontal flow is as follows (Song and Ishii, 2001):

continuity equation:

$$\frac{\partial \langle \alpha_k \rangle \rho_k}{\partial t} + \frac{\partial \langle \alpha_k \rangle \rho_k \langle u_k \rangle}{\partial x} = \langle \Gamma_k \rangle \quad (2.23)$$

momentum equation:

$$\begin{aligned} \frac{\partial \langle \alpha_k \rangle \rho_k \langle u_k \rangle}{\partial t} + \frac{\partial \langle \alpha_k \rangle \rho_k C_{vk} \langle u_k \rangle^2}{\partial x} = & -\langle \alpha_k \rangle \frac{\partial \langle P_k \rangle}{\partial x} + \frac{\partial}{\partial x} \left(\langle \alpha_k \rangle \langle \tau_k + \tau_k' \rangle \right) - \frac{4\alpha_{kw} \tau_w}{D} \\ & + \langle \alpha_k \rangle \rho_k g \cos \phi + \langle v_{ki} \rangle \langle \Gamma_k \rangle + \langle M_{ik} \rangle + \left(\langle P_{ki} \rangle - \langle P_k \rangle \right) \frac{\partial \langle \alpha_k \rangle}{\partial x} \end{aligned} \quad (2.24)$$

With these assumptions, the set of equations, (2.13)-(2.15), is reduced to a set of two area-averaged equations for each phase. If it is assumed that no phase change is taking place, such as in the case of air-water flow, the two-fluid model can be simplified to even a greater extent. The area-averaged form of the shear stress is rewritten as $4\alpha_{kw} \tau_w / D$, where D is the hydraulic diameter of the channel. This general form is

applicable for both square channels and round tubes. The quantity C_{vk} in the above momentum equation is known as the momentum flux parameter and is defined as:

$$C_{vk} = \frac{\langle \alpha_k u_k u_k \rangle}{\langle \alpha_k \rangle \langle u_k \rangle^2} \quad (2.25)$$

In addition, the set of governing differential equations are typically simplified even further to be directly applied to the bubbly/slug flow regime. It is typically assumed that the interface pressure, $\langle \langle P_{ki} \rangle \rangle$, is equal to the phase pressure, $\langle \langle P_k \rangle \rangle$, so that the term $(\langle \langle P_{ki} \rangle \rangle - \langle \langle P_k \rangle \rangle) \frac{\partial \langle \alpha_k \rangle}{\partial x}$ can be eliminated. In addition, it is assumed that locally the gas phase pressure, P_g , is in equilibrium with the liquid phase pressure, P_f , if the effect of surface tension is ignored. As a result of this assumption, the void fraction weighted area-averaged pressure of the gas phase equals that of the liquid phase or $\langle \langle P_g \rangle \rangle = \langle \langle P_f \rangle \rangle$.

2.3.2 Separated (stratified/annular) flow two-fluid model

A description of the general one-dimensional two-fluid separated flow model is given in Kocamustafaogullari (Kocamustafaogullari, 1985). First the continuity and momentum equations are written for each phase assuming that the flow is one-dimensional and both phases are incompressible. It is also assumed that the gas phase is moving faster than the liquid phase: this determines the sign on the interfacial shear terms. The equations are developed assuming that the cross-sectional flow area does not change with liquid height. This assumption is suitable for rectangular flow channels as well as flow over a flat plate.

Kinematic field equations:

$$\frac{\partial \langle 1 - \alpha \rangle}{\partial t} + \frac{\partial}{\partial x} [\langle 1 - \alpha \rangle \langle u_f \rangle] = - \frac{m_{fi}}{\rho_f} \left(\frac{\xi_i}{A} \right) \quad (2.26)$$

$$\frac{\partial \langle \alpha \rangle}{\partial t} + \frac{\partial}{\partial x} [\langle \alpha \rangle \langle u_g \rangle] = - \frac{m_{gi}}{\rho_g} \left(\frac{\xi_i}{A} \right) \quad (2.27)$$

Dynamic field equations:

$$\begin{aligned} \rho_l \left(\frac{\partial \langle u_f \rangle}{\partial t} + \langle u_f \rangle \frac{\partial \langle u_f \rangle}{\partial x} \right) = & - \frac{\partial \langle P_f \rangle}{\partial x} + \rho_f g \cos \varphi + \left(\frac{1}{\langle 1 - \alpha \rangle} \right) \left\{ (P_{fi} - \langle P_f \rangle) \frac{\partial \langle \alpha \rangle}{\partial x} \right. \\ & \left. - m_{fi} (u_{fi} - \langle u_f \rangle) \left(\frac{\xi_i}{A} \right) + \tau_{fi} \left(\frac{\xi_i}{A} \right) - \tau_{fe} \left(\frac{\xi_{fe}}{A} \right) - \frac{\partial}{\partial x} [\langle 1 - \alpha \rangle \rho_f \text{Cov}(u_f^2)] \right\} \end{aligned} \quad (2.28)$$

$$\begin{aligned} \rho_g \left(\frac{\partial \langle u_g \rangle}{\partial t} + \langle u_g \rangle \frac{\partial \langle u_g \rangle}{\partial x} \right) = & - \frac{\partial \langle P_g \rangle}{\partial x} + \rho_g g \cos \varphi + \left(\frac{1}{\langle \alpha \rangle} \right) \left\{ (P_{gi} - \langle P_g \rangle) \frac{\partial \langle \alpha \rangle}{\partial x} \right. \\ & \left. - m_{gi} (u_{gi} - \langle u_g \rangle) \left(\frac{\xi_i}{A} \right) - \tau_{gi} \left(\frac{\xi_i}{A} \right) - \tau_{ge} \left(\frac{\xi_{ge}}{A} \right) - \frac{\partial}{\partial x} [\langle \alpha \rangle \rho_g \text{Cov}(u_g^2)] \right\} \end{aligned} \quad (2.29)$$

Where subscripts f and g correspond to the liquid phase and gas phase, respectively. The subscripts i and e identify the internal and external boundaries. The quantities m and α corresponds to the interfacial mass flux transfer rate and the area averaged void fraction, respectively. The $\text{Cov}(F)$ in the above equation is the covariance of a quantity. The covariance term is defined as follows for this situation:

$$\text{Cov}(F^2) = \langle F^2 \rangle - \langle F \rangle^2 \quad (2.30)$$

The average phasic pressures are determined by:

$$\langle P_f \rangle = P_{fi} + \frac{(1 - \alpha) \rho_f g_y}{2} \left(\frac{A}{\xi_i} \right) \quad (2.31)$$

$$\langle\langle P_g \rangle\rangle = P_{gi} + \frac{\alpha \rho_g g_y}{2} \left(\frac{A}{\xi_i} \right) \quad (2.32)$$

Due to the fact that the macroscopic fields of one phase are not independent of the other phase, the interaction terms which couple the transport of mass and momentum across the interface appear in the field equations. By performing a mass and momentum balance on the interface, the three following relations can be found:

$$\dot{m}_{fi} + \dot{m}_{gi} = 0 \quad (2.33)$$

$$P_{fi} - P_{gi} = \dot{m}_{fi}^2 \left(\frac{\Delta \rho}{\rho_f \rho_g} \right) + \left(\frac{\sigma A}{\xi_i} \right) \frac{\partial^2 \alpha}{\partial x^2} \quad (2.34)$$

$$\tau_{fi} - \tau_{gi} = 0 \quad (2.35)$$

These balance equations need to be supplemented with an additional relation since there are more unknowns than there are equations. A physical additional relation that can be implemented is the kinematic no relative velocity at the interface (no slip condition).

$$u_{fi} = u_{gi} \equiv u_i \quad (2.36)$$

The momentum equations can now be combined and simplified with the use of the above relations. Subtracting the liquid phase momentum equation from the gas phase momentum equation and applying the relations, equations (2.33) - (2.36), the pressure terms can be completely eliminated from the equation. Thus,

$$\begin{aligned}
& \rho_g \left(\frac{\partial \langle \langle u_g \rangle \rangle}{\partial t} + \langle \langle u_g \rangle \rangle \frac{\partial \langle \langle u_g \rangle \rangle}{\partial x} \right) - \rho_f \left(\frac{\partial \langle \langle u_f \rangle \rangle}{\partial t} + \langle \langle u_f \rangle \rangle \frac{\partial \langle \langle u_f \rangle \rangle}{\partial x} \right) = \sigma \left(\frac{A}{\xi_i} \right) \frac{\partial^3 \langle \alpha \rangle}{\partial x^3} \\
& + 2 \left(\frac{\Delta \rho}{\rho_f \rho_g} \right) \dot{m}_{fi} \frac{\partial \dot{m}_{fi}}{\partial x} - \Delta \rho g_x + \left[\frac{u_i - \langle \langle u_g \rangle \rangle}{\langle \alpha \rangle} + \frac{u_i - \langle \langle u_f \rangle \rangle}{1 - \langle \alpha \rangle} \right] \dot{m}_{fi} \left(\frac{\xi_i}{A} \right) \\
& - \tau_{fi} \left(\frac{1}{\langle \alpha \rangle} + \frac{1}{1 - \langle \alpha \rangle} \right) \left(\frac{\xi_i}{A} \right) - \frac{\tau_{ge}}{\langle \alpha \rangle} \left(\frac{\xi_{gc}}{A} \right) + \frac{\tau_{fe}}{1 - \langle \alpha \rangle} \left(\frac{\xi_{fe}}{A} \right) \\
& + \left\{ \Delta \rho g_y \left(\frac{A}{\xi_i} \right) - \left[\frac{\rho_g \text{Cov}(u_g^2)}{\alpha} + \frac{\rho_f \text{Cov}(u_f^2)}{1 - \alpha} \right] \right\} \frac{\partial \langle \alpha \rangle}{\partial x} + \rho_f \frac{\partial \text{Cov}(u_f^2)}{\partial x} - \rho_g \frac{\partial \text{Cov}(u_g^2)}{\partial x}
\end{aligned} \tag{2.37}$$

This combined momentum equation replaces the dynamic field equations while eliminating $\langle \langle P_f \rangle \rangle$, $\langle \langle P_g \rangle \rangle$, P_{fi} , and P_{gi} from the formulation in the process. There are now three equations (one combined momentum equation and two continuity equations) and three basic dependent variables: $\langle \alpha \rangle$, $\langle \langle u_f \rangle \rangle$, $\langle \langle u_g \rangle \rangle$. The remaining seven variables, \dot{m}_{fi} (or \dot{m}_{gi}), u_i , τ_{fi} , τ_{fe} , τ_{ge} , $\text{Cov}(u_f^2)$, and $\text{Cov}(u_g^2)$ are known as supplementary variables. These variable are flow regime dependent, but should be functionally related to the three basic dependant variables. In general, this functional relationship may be expressed as:

$$f = f(\langle \alpha \rangle, \langle \langle u_f \rangle \rangle, \langle \langle u_g \rangle \rangle) \tag{2.38}$$

Sadatom et al. (Sadatom et al., 1993) incorporated the one-dimensional two-fluid model momentum equation to predict the axial distribution of liquid level or void fraction in gas-liquid stratified concurrent flows in horizontal circular and rectangular flow channels during steady conditions. The driving force behind Sadatom et al. was to incorporate the effect of having an appreciable interface level gradient since many previous works had not studied the case of stratified flow with an interfacial level gradient present. Two different critical liquid levels at the channel exits were found, under certain flow conditions, from the momentum equation and were incorporated as

boundary conditions in order to calculate the void fraction upstream of the channel exit. Based upon these two critical exit conditions, the model that was created would be applicable to both a free-discharge condition as well as for discharge into a pool. The predicted void fraction profiles were then compared to existing experimental data as well as data gathered by the authors and were found to agree well with the model presented for all cases with a smooth interface.

2.4 TWO-FLUID MODEL STABILITY FOR HORIZONTAL FLOW

There are two primary types of instabilities that need to be addressed regarding the two-fluid model for horizontal flow. The first is a numerical instability that occurs when the governing flow equations are not properly modeled. This can create unphysical numerical oscillations and can cause the problem to be unable to be solved because the equations become inconsistent with the numerical scheme (Lyczkowski et al., 1978; Song and Ishii, 2001; Song, 2003). The second type of instability is an interfacial instability of the flow (Trapp, 1986; Kocamustafaogullari, 1985). The interest of this type of instability lies in the prediction of the flow regime transition from stratified wavy flow to slug flow. The physical mechanism behind this type of flow regime transition is due to interfacial wave instability. When the gas flow exceeds a critical value, the inertia force from the gas phase acting upon the interface overcomes the gravity force, causing intermittent flow to occur.

2.4.1 Stratified wavy-to-slug flow regime transition

One of the primary ways for determining the flow regime transition point from stratified wavy flow to slug flow is with the use of a linear perturbation analysis. By incorporating a linear perturbation analysis, the flow instability of the system can be determined. The two-fluid model equations are perturbed using the independent variables of the model. The perturbation is assumed to be very small in order to neglect the nonlinear effects. The steady-state portion of the equations is then

subtracted from the perturbed set of equations and the result is a set of equations that may be analyzed to determine under what conditions flow instability will occur. Under conditions where the instability point lies, any small perturbation in velocity or void fraction will cause the inertia force of the gas to overcome the force due to gravity on the liquid phase. Under these conditions, the crest of the liquid wave is pulled to the top of the pipe and slug flow is then created.

The process of determining this interfacial instability is given in Kocamustafaogullari (Kocamustafaogullari, 1985). First, the continuity and momentum equations are written and constitutive relations are applied for each phase assuming that the flow is one-dimensional and both phases are incompressible. To determine under what conditions waves appearing on the interface lead to instability, the behavior of very small perturbations can be examined using the perturbed flow equations. Because it is assumed that the perturbations are very small compared to the mean variable values, the higher order (nonlinear) terms of the perturbed equations may be dropped. This procedure is known as a linear perturbation analysis. In order to obtain the perturbed flow equations, first the three basic flow variables, $\langle \alpha \rangle$, $\langle \langle u_f \rangle \rangle$ and $\langle \langle u_g \rangle \rangle$ are written as:

$$F = \bar{F} + F' \quad (2.39)$$

where \bar{F} is the time-averaged mean value of any flow variable, F , while F' is the perturbation from the mean value. Next, the supplementary variables are expressed by performing a Taylor Series expansion:

$$\begin{aligned} f\left(\langle \bar{\alpha} \rangle + \langle \alpha' \rangle, \langle \langle \bar{u}_f \rangle \rangle + \langle \langle u_f \rangle \rangle', \langle \langle \bar{u}_g \rangle \rangle + \langle \langle u_g \rangle \rangle'\right) \\ = \bar{f} + \frac{\partial \bar{f}}{\partial \langle \bar{\alpha} \rangle} \langle \alpha' \rangle + \frac{\partial \bar{f}}{\partial \langle \langle \bar{u}_f \rangle \rangle} \langle \langle u_f \rangle \rangle' + \frac{\partial \bar{f}}{\partial \langle \langle \bar{u}_g \rangle \rangle} \langle \langle u_g \rangle \rangle' + \text{NT's} \end{aligned} \quad (2.40)$$

where NT's stands for the nonlinear terms. The perturbations are now substituted into equations (2.29), (2.30), and (2.40). By considering the mean flow equations and discarding the nonlinear perturbation terms, the flow equations are now linearized. The linearization applies to long waves (small amplitude in comparison to wavelength) so that the perturbations considered will be only applicable to long wavelengths. This restriction is due to forces, such as surface tension, that become important in short wavelength analyses which adds nonlinearity to the wave problem. It is assumed that the mean flow variables are fully developed and do not change appreciably along the flow direction. Due to this assumption, any perturbed value multiplied by quantities of x-derivatives of the mean flow variables are considered to be second order and may be dropped during the linearization process.

Following the above procedure, and assuming that no phase change is taking place in order to simplify the problem, the perturbed flow equations obtained from equations (2.26), (2.27), and (2.37), respectively, are as follows:

$$-\frac{\partial \langle \alpha \rangle'}{\partial t} - \langle \langle u_f \rangle \rangle \frac{\partial \langle \alpha \rangle'}{\partial x} + (1 - \langle \bar{\alpha} \rangle) \frac{\partial \langle \langle u_f \rangle \rangle'}{\partial x} = 0 \quad (2.41)$$

$$\frac{\partial \langle \alpha \rangle'}{\partial t} + \langle \langle u_g \rangle \rangle \frac{\partial \langle \alpha \rangle'}{\partial x} + \langle \bar{\alpha} \rangle \frac{\partial \langle \langle u_g \rangle \rangle'}{\partial x} = 0 \quad (2.42)$$

$$\begin{aligned} \rho_g \left(\frac{\partial \langle \langle u_g \rangle \rangle'}{\partial t} + \langle \langle \bar{u}_g \rangle \rangle \frac{\partial \langle \langle u_g \rangle \rangle'}{\partial x} \right) - \rho_f \left(\frac{\partial \langle \langle u_f \rangle \rangle'}{\partial t} + \langle \langle \bar{u}_f \rangle \rangle \frac{\partial \langle \langle u_f \rangle \rangle'}{\partial x} \right) = a_1 \frac{\partial^3 \langle \alpha \rangle'}{\partial x^3} \\ + a_2 \frac{\partial \langle \alpha \rangle'}{\partial x} - a_3 \frac{\partial \langle \langle u_g \rangle \rangle'}{\partial x} + a_4 \frac{\partial \langle \langle u_f \rangle \rangle'}{\partial x} + a_5 \langle \alpha \rangle' - a_6 \langle \langle u_g \rangle \rangle' + a_7 \langle \langle u_f \rangle \rangle' \end{aligned} \quad (2.43)$$

The coefficients a_1 through a_7 are defined in terms of the main flow variables and are used in order to simplify the form of the shown equation. The above set of

perturbed equations can be combined into a equation. The process used to combine the perturbed equations is to first differentiate equation (2.43) with respect to the flow direction, x , while equations (2.41) and (2.42) are used to express the derivatives of $\langle\langle u_g \rangle\rangle'$ and $\langle\langle u_f \rangle\rangle'$ in terms of those of $\langle\alpha\rangle'$. The combined perturbed equation becomes:

$$\begin{aligned}
 & a_1 \frac{\partial^4 \langle\alpha\rangle'}{\partial x^4} + \left[a_2 - \left(\frac{a_3 \langle\langle \bar{u}_g \rangle\rangle}{\langle\bar{\alpha}\rangle} + \frac{a_4 \langle\langle \bar{u}_f \rangle\rangle}{1 - \langle\bar{\alpha}\rangle} \right) + \frac{\rho_g \langle\langle \bar{u}_g \rangle\rangle^2}{\langle\bar{\alpha}\rangle} + \frac{\rho_f \langle\langle \bar{u}_f \rangle\rangle^2}{1 - \langle\bar{\alpha}\rangle} \right] \frac{\partial^2 \langle\alpha\rangle'}{\partial x^2} \\
 & + \left[\frac{a_3}{\langle\bar{\alpha}\rangle} + \frac{a_4}{1 - \langle\bar{\alpha}\rangle} + 2 \left(\frac{\rho_g \langle\langle \bar{u}_g \rangle\rangle}{\langle\bar{\alpha}\rangle} + \frac{\rho_f \langle\langle \bar{u}_f \rangle\rangle}{1 - \langle\bar{\alpha}\rangle} \right) \right] \frac{\partial^2 \langle\alpha\rangle'}{\partial x \partial t} + \left(\frac{\rho_g}{\langle\bar{\alpha}\rangle} + \frac{\rho_f}{1 - \langle\bar{\alpha}\rangle} \right) \frac{\partial^2 \langle\alpha\rangle'}{\partial t^2} \\
 & + \left(\frac{a_6}{\langle\bar{\alpha}\rangle} + \frac{a_7}{1 - \langle\bar{\alpha}\rangle} \right) \frac{\partial \langle\alpha\rangle'}{\partial t} = 0
 \end{aligned} \tag{2.44}$$

This differential equation is the characteristic equation from which stability of the system can be found. To determine the stability, one must determine whether a disturbance amplifies or decays for a given mean flow condition. To determine flow regime transition, one must find the point for a given flow condition where a small disturbance of the surface, which is directly related to $\langle\alpha\rangle'$, will amplify with time. This interfacial instability will instigate growth of the wave crest to reach the top of the pipe. The flow then transitions from the stratified wavy flow regime into the slug/intermittent flow regime under these conditions.

2.4.2 Numerical stability

Another important concept to consider when modeling two-phase flow is to account for the numerical stability of the model. If the resultant model is not numerically stable under typical flow conditions, the model will be of little use since it cannot be properly solved. Many of the numerical instabilities come about from using

assumptions that oversimplify the model and remove some of the important physical characteristics of the model in the process.

The one-dimensional two-fluid model equations have been shown to be unstable for unequal phase velocities by several authors (Lyczkowski et al., 1978; Song and Ishii, 2001; Gidaspow, 1974). This instability results in complex characteristics which creates increased difficulty in solving the equations because the equations become elliptic instead of hyperbolic. The difficulty with having complex characteristics is that the first order set of partial differential equations is ill-posed as an initial value problem. Given a set of initial conditions and proper boundary conditions, a stable numerical method for solving such a set of equations has yet to be determined. It is important to determine a correct way to model typical two-phase flow conditions without becoming ill-posed.

Since it is common for the gas phase and liquid phase velocity to differ, it is important for properly modeling two-phase flow systems that restriction of the two velocities being equal must be eliminated. Many researchers have tried various methods in order to try to increase the numerical stability of such a system (Song and Ishii, 2001; Song and Ishii, 2000; Song, 2003; Trapp, 1986, Gidaspow, 1983, Lyczkowski et al., 1978). Methods of improving the averaged two-fluid model have ranged from adding a virtual mass term, to accounting for surface tension effects, to adding fluctuating velocity components (Trapp, 1986) as well as other methods in an attempt to create a realistic and stable one-dimensional two-fluid model for horizontal flow.

One of the causes for the instability for unequal phase velocities is the use of incompressible assumption for both phases (Lyczkowski et al., 1978; Song and Ishii, 2001; Gidaspow, 1974). With the incompressible condition, perturbations are allowed to travel anywhere in the system at an infinite velocity. That is to say, a disturbance is felt everywhere in the system at the instance that the disturbance is created. One

method of increasing the stability of the model is by accounting for the compressibility of the fluids. The system is stabilized due to the disturbances being limited to finite velocities, the speed of sound in each phase, but increased computational requirements are added.

In Gidaspow (Gidaspow, 1974), the method of determining complex characteristic is shown for a simplified separated flow two-fluid model. The well-posedness of the governing differential equation as an initial value problem can be analyzed by performing a characteristic analysis (Lyczkowski et al., 1978; Song and Ishii, 2001; Gidaspow, 1974; Gidaspow, 1983). To determine the stability of the two-fluid model though the use of characteristic analysis, first the governing differential equations are written. In the case of Gidaspow (Gidaspow, 1974) it was assumed that the flow was incompressible, potential flow, with no body forces, etc. The simplified case is written as:

continuity equation:

$$\frac{\partial \alpha_k}{\partial t} + \frac{\partial \alpha_k u_k}{\partial x} = 0 \quad (2.45)$$

momentum equation:

$$\rho_k \frac{\partial u_k}{\partial t} + \rho_k u_k \frac{\partial u_k}{\partial x} - \frac{\partial P_k}{\partial x} = 0 \quad (2.46)$$

Now define the vector \mathbf{x} :

$$\mathbf{x} = \begin{bmatrix} \alpha \\ u_g \\ u_f \\ P \end{bmatrix} \quad (2.47)$$

The governing differential equation can now be expressed in matrix form.

$$[A] \frac{\partial}{\partial t} \mathbf{x} + [B] \frac{\partial}{\partial x} \mathbf{x} = [C] \quad (2.48)$$

The dependence of the solution based upon a prescribed set of initial data can be reduced to an investigation of the roots of the following determinant:

$$\text{Det} \{ [A] \lambda - [B] \} = 0 \quad (2.49)$$

In this particular case, the value of $[A] \lambda - [B]$ is:

$$\begin{bmatrix} \lambda - u_g & -\alpha & 0 & 0 \\ -\lambda + u_f & 0 & -(1-\alpha) & 0 \\ 0 & \rho_g \lambda - \rho_g u_g & 0 & -1 \\ 0 & 0 & \rho_f \lambda - \rho_f u_f & -1 \end{bmatrix} \quad (2.50)$$

While the $\text{Det} \{ [A] \lambda - [B] \}$ is equal to:

$$-\alpha(1-\alpha) \left[(1-\alpha) \rho_g (\lambda - u_g)^2 + \alpha \rho_f (\lambda - u_f)^2 \right] \quad (2.51)$$

In order for the determinant to be equal to zero, and keeping the solution nontrivial, the condition $\lambda = u_g = u_f$ must be met. This implies that the liquid and gas velocities must be equal for the problem to remain hyperbolic and be well-posed as an initial value problem.

Song and Ishii (Song and Ishii, 2001; Song and Ishii, 2000) performed a characteristic analysis, similar to Gidaspow (Gidaspow, 1974), on the stability of the governing differential equation for an incompressible, one-dimensional, two-fluid model. Song and Ishii proposes the use of the gas and liquid momentum flux parameters, which incorporate the effect of velocity and void profiles, to improve the stability of the governing differential equations. Song and Ishii used a simplified two-phase model by using existing correlation for the volumetric distribution parameter

and experimentally correlated velocity profiles to determine the validity of the proposed theory. After taking the determinant and the discriminate of the resulting matrix with the use of the momentum flux parameters, for λ to have real roots and therefore the differential equation to be hyperbolic, the following criteria must be met:

$$\begin{aligned}
 &F(\alpha, C_{vg}, C_{vf}, u_g, u_f, \rho_f, \rho_g) \\
 &= \left[(1-\alpha)\rho_g C_{vg} u_g + \alpha\rho_f C_{vf} u_f \right] \left[(1-\alpha)\rho_g C_{vg} u_g + \alpha\rho_f C_{vf} u_f \right] \\
 &\quad - \left[(1-\alpha)\rho_g + \alpha\rho_f \right] \left[(1-\alpha)\rho_g C_{vg} u_g u_g + \alpha\rho_f C_{vf} u_f u_f \right] \geq 0
 \end{aligned} \tag{2.52}$$

This equation demonstrates that the inclusion of the momentum flux parameters can make the two-fluid model have real roots without imposing the unrealistic condition that the gas velocity should equal the liquid velocity. This indicates that the momentum flux parameters have a stabilizing effect. As long as equation (2.52) remains positive, two real characteristic roots will exist. If the momentum flux parameters behave in such a way that the inequality in equation (2.52) is always met, the two-fluid model with the momentum flux parameters becomes well-posed.

In Song (Song, 2003), the work of Ishii and Song (Song and Ishii, 2001; Song and Ishii, 2000) was taken one step further by completing a linear stability analysis for two-phase flow in order to determine the feasibility of using momentum flux parameters to improve the stability of the one-dimensional two-fluid model. Through the use of the linear stability analysis, for a finite value of ω/k and letting the wave number, k , approach infinity, the characteristic equation was obtained. The characteristic equation obtained using the linear stability analysis produced the same result for the criterion for stability as was found by Song and Ishii (Song and Ishii, 2001; Song and Ishii, 2000) using a characteristic analysis. In addition, Song (Song, 2003) was able to find the stability criterion for whether the flow model with the momentum flux parameters would be stable to small perturbations with the use of the linear perturbation analysis. It was found that the mathematical model was well-posed and can describe the propagation of the void fraction wave in both bubbly flow and slug flow within a wide range of void fraction and density ratios. The model was

found to be consistent with real world bubbly and slug flow cases while neglecting the influence of the momentum flux parameter causes an unphysical instability.

Another attempt at increasing numerical stability for the one-dimensional two-fluid model with unequal phasic velocities was proposed by Trapp (Trapp, 1986). Trapp conjectured that the unstable growth in streaming two-phase flow with unequal phasic velocities is due to a failure to model the fluctuating velocity components, $\overline{u'_k u'_k}$, in the momentum equations. In single-phase turbulent counterpart, these are known as the Reynolds stress terms. In single-phase flow, appropriate closure models for the Reynolds stress terms is the essence of the problem of obtaining a realistic mean motion description of the turbulent flows. One could use the comparison that if the Reynolds stress terms were neglected in the mean flow equations, then the mean flow equations would exhibit the same instability as was present in the laminar flow cases. Because of this issue, Trapp believes that similar terms should also exist in the two-phase flow equations in order to properly model the mean motions of the flow and to improve the one-dimensional two-fluid model stability. Trapp derived a general form of the equations to include the fluctuating components of velocity and was shown that this particular model lead to a stable mean motion description for the cases studied. The continuity and momentum equations proposed by Trapp for one-dimensional, horizontal, incompressible, stratified flow by neglecting the viscous forces and the thermal processes are as follows:

continuity:

$$\frac{\partial \langle \alpha_g \rangle}{\partial t} + \frac{\partial}{\partial x} [\langle \alpha_g \rangle \langle \langle u_g \rangle \rangle] = 0 \quad (2.53)$$

$$\frac{\partial \langle \alpha_f \rangle}{\partial t} + \frac{\partial}{\partial x} [\langle \alpha_f \rangle \langle \langle u_f \rangle \rangle] = 0 \quad (2.54)$$

momentum:

$$\langle \alpha_g \rangle \rho_g \left(\frac{\partial \langle u_g \rangle}{\partial t} + \langle u_g \rangle \frac{\partial \langle u_g \rangle}{\partial x} \right) + \frac{\partial \langle \alpha_g \rangle \rho_g \overline{u'_g u'_g}}{\partial x} = - \frac{\partial \langle \alpha_g \rangle \langle P_g \rangle}{\partial x} + \langle P_{gi} \rangle \frac{\partial \langle \alpha_g \rangle}{\partial x} \quad (2.55)$$

$$\langle \alpha_f \rangle \rho_f \left(\frac{\partial \langle u_f \rangle}{\partial t} + \langle u_f \rangle \frac{\partial \langle u_f \rangle}{\partial x} \right) + \frac{\partial \langle \alpha_f \rangle \rho_f \overline{u'_f u'_f}}{\partial x} = - \frac{\partial \langle \alpha_f \rangle \langle P_f \rangle}{\partial x} + \langle P_{fi} \rangle \frac{\partial \langle \alpha_f \rangle}{\partial x} \quad (2.56)$$

Trapp used the Helmholtz instability as a basis for speculative closure model for the fluctuating velocity components, $\overline{u'_k u'_k}$. The Helmholtz instability is the shear induced instability that occurs between two stratified layers of fluid. The Helmholtz instability is commonly analyzed by considering the basic flow of incompressible inviscid fluids in two horizontal parallel infinite streams of different velocities, u_g and u_f , and densities, ρ_g and ρ_f , with the faster stream above the other. The two fluids are considered to be immiscible.

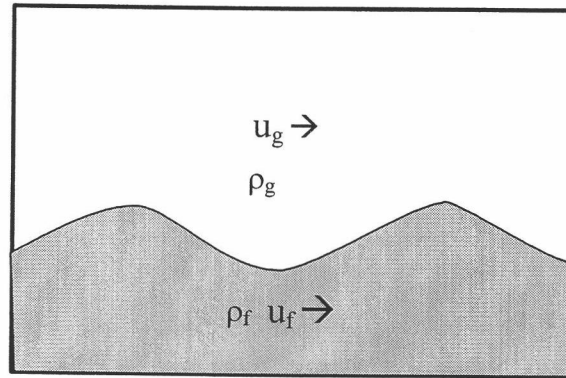


Figure 2.5: Kelvin-Helmholtz problem

In the shear layer, vorticity is approximately uniform while it is equal to zero each side outside of the layer as velocities are uniform. The shearing layer appears as a vortex sheet inside an irrotational flow. It is assumed that the lower fluid is stationary, while the upper fluid moves at the steady and uniform velocity, as the difference in

velocities is what is important, not the absolute velocities. The general Helmholtz problem, given in Article 232 of Lamb (Lamb, 1932), assumes both streams to have infinite depth and considers the stabilizing effect of gravity, but neglects the surface tension forces. The dispersion relationship for these conditions is given as:

$$\frac{\omega}{k} = -\left(\frac{\rho_g u_g + \rho_f u_f}{\rho_g + \rho_f}\right) \pm \sqrt{-\frac{\rho_g \rho_f (u_g - u_f)^2}{(\rho_g + \rho_f)^2} + \frac{g}{k} \frac{\rho_f - \rho_g}{\rho_g + \rho_f}} \quad (2.57)$$

From this equation, it can be noted that ω has a real part and a complex part. The \pm term indicates that the waves can move in both the upstream and downstream directions. During condition in which ω has an imaginary part, the Helmholtz instability occurs. In equation (2.57) it can be noted that if the two fluids have the same density or if gravity is not considered, the equation can be reduced to:

$$\frac{\omega}{k} = -\left(\frac{\rho_g u_g + \rho_f u_f}{\rho_g + \rho_f}\right) \pm \sqrt{-\frac{\rho_g \rho_f (u_g - u_f)^2}{(\rho_g + \rho_f)^2}} \quad (2.58)$$

Under these conditions, the interface instability will occur for any wave number if the two velocities are not identical. If surface tension and gravity are considered, the dispersion relation becomes:

$$\frac{\omega}{k} = -\left(\frac{\rho_g u_g + \rho_f u_f}{\rho_g + \rho_f}\right) \pm \sqrt{-\frac{\rho_g \rho_f (u_g - u_f)^2}{(\rho_g + \rho_f)^2} + \frac{g}{k} \frac{\rho_f - \rho_g}{\rho_g + \rho_f} + \frac{\sigma k}{\rho_g + \rho_f}} \quad (2.59)$$

It can be seen from this equation that the surface tension and gravity forces add a restoring force that dampens out perturbations to stabilize the interface. It can be noted that the surface tension term is related to the wave number, k , so that as k increases (wave length decreases) the surface tension term becomes more important and helps to damp out short wavelength phenomena.

2.5 VOID DISTRIBUTION MEASUREMENT (HORIZONTAL FLOW)

Kocamustafaogullari et al. (Kocamustafaogullari et al., 1994a) used three double-sensor conductivity probes at different locations along a 50.3 mm diameter horizontal pipe to study the profiles of void fraction, interfacial area, and velocity for horizontal two-phase flow. Each of the probes was placed in a custom instrumentation mount that allowed for traversing the probe across the diameter of the pipe as well as allowing for rotation of the probe. These two abilities allow for the creation of cross sectional mapping of important two-phase flow parameters. The ability for the probe mount to be able to rotate is especially important in horizontal flow since the parameters such as void fraction are highly asymmetric due to buoyancy allowing the migration of the bubble towards the top of the pipe. Kocamustafaogullari et al. measured 23 points along the pipe diameter for each rotation of 22.5° of the probe with respect to the pipe. This resulted in 108 measurement points for each probe location for each flow rate tested. Data was sampled for 1 second at 20 kHz for each probe location. Kocamustafaogullari et al. presented the data as three-dimensional plots for each flow condition and each axial measurement location. One can see from these plots the development of void fraction, interfacial area concentration, and interfacial velocity along the length of the pipe.

Iskandrani and Kojasoy (Iskandrani and Kojasoy, 2001) employed the use of hot-film anemometry to investigate the internal phase distribution of concurrent air-water bubbly flow in a 50.3 mm i.d. horizontal pipe. The hot-film anemometry technique was able to measure time-averaged local values of void fraction, bubble passing frequency, mean liquid velocity, as well as the liquid turbulent fluctuations. The range of liquid and gas superficial velocities for which data was gathered were 3.8 to 5.0 m/s and 0.25 to 0.8 m/s respectively. The experimental results indicated that both the local time-averaged void fraction and the bubble passing frequency have a local maximum near the upper wall ($r/R \approx 0.8 - 0.9$) under all test conditions. It was also discovered that the local void fraction for horizontal bubbly flow never exceeded 65%. The data

also shows a flattening of the void distribution with increasing liquid velocity due to the impact of increased liquid turbulent fluctuations, however, the relative position of the void fraction peak was relatively unaffected by changes in the gas or liquid superficial velocities. The mean liquid velocity was found to follow the same $1/7^{\text{th}}$ power law as would be found as in the case of single phase turbulent flow. The mean velocity profiles indicate an asymmetric distribution with the velocity peak at the bottom of the pipe. The degree of asymmetry was shown to decrease with increasing liquid flow or decreasing gas flow. The turbulent intensity was found to be the greatest near the walls of the pipe with velocity fluctuations around 10 to 15% of the local mean velocity. It was also discovered that at a very low void fraction, the turbulent fluctuations could be less than those of single phase flow. However, as the void fraction increased, the turbulent fluctuations became much greater than the single phase case. It was determined that the void fraction distribution plays the greatest role in influencing the local turbulence intensity.

Fukano and Ousaka (Fukano and Ousaka, 1989) constructed a theoretical model to predict the circumferential liquid film thickness distribution for horizontal and near-horizontal annular flow. The theoretical model was then compared to experimental results. The film thickness distribution for horizontal and near-horizontal annular flows is said to be controlled by the following four mechanisms:

- (1) Spreading of the film by a wave action.
- (2) Transfer of liquid by entrainment and deposition of droplets.
- (3) Spreading by circumferential shear forces due to secondary gas flow.
- (4) Spreading by surface tension forces.

Fukano and Ousaka assumed that for the modeling of the annular film that:

- (1) The liquid in the film is fully developed.
- (2) The film is thin compared to the diameter of the flow channel

- (3) The velocity of the liquid film in the axial direction is much greater than that in the circumferential direction.
- (4) The eddy viscosity in the liquid film is isotropic and is governed by the axial flow of the liquid.
- (5) The distribution of the eddy viscosity is the same as that for single-phase flow in a tube.

It was found that the pumping action of the disturbance wave tends to be the most important factor in transferring liquid to the upper portion of the tube, while previous models ignored this transfer mechanism (Fukano and Ousaka, 1989). The model presented by Fukano and Ousaka was found to be much more accurate than previous models as well as having the ability to cover a wider range of flow rates to get solutions in regions where previous models had no solution (Fukano and Ousaka, 1989).

Andreussi et al. (Andreussi et al., 1993) characterized air-water horizontal slug flow at atmospheric conditions in 31 and 53 mm i.d. pipes experimentally. Both local void fraction measurement, with the use of optical probes, and area-averaged void measurement, using ring type conductance probes, was obtained. The intention of Andreussi et al. was to use the measured data to improve the description of horizontal slug flow and the closure relations required in the mean kinematic slug flow models. The optical probe was used to determine the radial void fraction profile as well as the size of the smaller dispersed bubbles within the liquid slug as well as those within the aeration layer underneath the vapor slug. The ring type conductance probe was used to measure the area-averaged void fraction, slug lengths and frequencies, and the length of the aerated mixing region that occurs just in front of the slug bubble. Andreussi et al. found that the measured slug lengths are independent of flow rates and are within the range of lengths reported by other authors. The dispersed bubbles were found to be less than 5 mm in diameter shown by bubble size distribution chart given. A few void

fraction profiles are also given to compare the void fraction distribution at the leading edge of the slug bubble with the void distribution at the trailing edge.

Shi and Kocamustafaogullari (Shi and Kocamustafaogullari, 1994) used a set of parallel wire conductance probes to experimentally determine the interfacial characteristic parameters of horizontal wavy flow patterns. The experiments were performed in a 15.4 m long Pyrex glass horizontal loop of 50.3 mm internal diameter. The gas and liquid superficial velocities varied from 0.85 to 31.67 m/s and 0.014 to 0.127 m/s, respectively. The interfacial wave patterns were characterized by wave height, most dominant frequency, mean propagation velocity and mean wavelength. The interfacial shear stress calculated from the experimental results was used to evaluate several widely used interfacial shear models.

2.6 INTERFACIAL PRESSURE MODELING

For the case of bubbly/slug flow, the impact of interfacial pressure is typically ignored. The reasoning behind this assumption is that the local gas phase pressure should equal to the local liquid pressure as long as surface tension can be ignored. This means that the interfacial pressure is also equal to both the liquid and the gas phase pressures under this condition. Due to this assumption, the term accounting for the pressure difference between the interface and either the gas or liquid phases in the two-fluid model momentum equation is usually ignored. The stratified flow case has a similar term in the momentum equation with the exception that the definition of the interface pressure is slightly different in the case of stratified flow as there is only a single interface versus the many interfaces that would be found in bubbly flow. For the case of stratified flow, this term should always remain due to the difference in hydrostatic head both above and below the interface.

$$\left(\langle \langle P_{ki} \rangle \rangle - \langle \langle P_k \rangle \rangle \right) \frac{\partial \alpha}{\partial x} \quad (2.60)$$

According to several papers, (Chung et al., 2004; Chung et al., 2001) the interfacial pressure term can be accounted for in the bubbly flow regime by assuming the interface has a thickness to it. Chung et al. (Chung et al., 2001) analyzed the interfacial pressure jump term based on the physics of the phasic interface and bubble dynamics into the two-fluid model momentum equations. The pressure discontinuity due to the surface tension of the bubble was expressed in terms of the fluid bulk moduli and the bubble radius. By incorporating the interfacial pressure terms, the system of equations was found to have real eigenvalues representing the void fraction propagation and pressure wave speed in terms of bubble radius. The numerical stability was found to improve significantly with the inclusion of the interfacial pressure jump terms over the case of using virtual mass terms.

In Chung et al. (Chung et al., 2004), the two-dimensional numerical calculation performed existed within the bubbly flow regime at very low void fractions. It was also assumed that the bubble were small so the shape of the bubbly can be considered perfectly spherical. Chung et al. (Chung et al. 2004, Chung et al., 2001) considered the compressibility of both phases in order to determine the sound speed propagated in the two-phase mixture. The result of the calculated values of speed of sound in the mixture was compared to experimental data and a good agreement was found. A two-phase shock tube analysis was performed as a benchmark problem to study the wave propagation characteristics and interaction between the liquid and gas phases. In addition to the shock tube problem, additional calculations for a sedimentation problem and cavity growth in a duct with a bend were also performed.

2.7 INTERFACIAL AREA TRANSPORT EQUATION

As discussed in previous sections, interfacial area or the interfacial area concentration is vital to the development of two-phase flow modeling. Several researchers have published papers on one and two group interfacial area transport equations (Hibiki and Ishii, 1999; Hibiki and Ishii, 2000; Hibiki et al., 2001b; Morel et

al., 1999; Wu et al., 1998). Typically, the interfacial area transport equations are based on a particle number densities model. The bubbles are broken up into two groups, the spherical/distorted bubble group and the cap/slug bubble group. Lafi and Reyes (Lafi and Reyes, 1991) incorporated a population balance approach as well as a Monte Carlo approach in determining bubble and droplet breakage and coalescence criteria. This would be a good basis on which one could develop conceptually how a bubble size distribution may change from containing only group one bubbles to a distribution which contains both group one and group two bubbles. The idea behind having an interfacial area transport equation is that with proper modeling one could determine the interfacial area concentration at the inlet of the section of interest and predict what the interfacial area concentration would be at different times and at different axial and radial positions. The transport equation consists of both source and sink terms for interfacial area for each of the two groups. Examples of a source term would be bubble break up or a phase change from the liquid phase to the vapor phase. Examples of a sink term would be bubble coalescence or bubble collapse. In order to properly characterize the interfacial area transport equation, all of the source and sink terms must be fully understood and modeled correctly. The interfacial area sink terms that need to be properly described are coalescence due to random collision and the wake-entrainment process. For the interfacial area source terms, one can have bubble breakup due to turbulence impact, shearing off small bubbles from a larger bubble, or bubble breakup due to a surface instability. In addition to these source and sink terms, one could also have phase change as an additional source or sink term. Separate experiments as well as additional theoretical investigation are needed to identify and model the entire set of possible source and sink terms in the interfacial area transport equation. Once these tasks are performed, this information can be combined with experimental results for interfacial area concentration to provide additional insight into the behavior of multiphase flow as well as allowing computer codes which model multiphase flow to become more accurate. Hibiki et al. (Hibiki et al., 2001b) created an interfacial area transport equation for bubbly flow in a small diameter pipe. They

modeled the sink terms by just using wake entrainment. Hibiki et al. believed that since the bubble diameter is close to the pipe diameter, the lateral motion of the bubble would be restricted by the pipe wall and therefore coalescence due to random collision may be neglected. The interfacial area concentration source terms were neglected since at low liquid velocities, the amount of bubble breakup would be negligible. There was no phase change to deal with since this was an adiabatic air/water system. In addition, since only bubble flow was being studied, the two-group interfacial area concentration transport equation could be reduced to a one-group equation since cap or slug bubbles did not exist. The one group interfacial area transport equation may be given as (Hibiki et al., 2001b):

$$\begin{aligned} \frac{\partial a_i}{\partial t} + \frac{d}{dz}(a_i v_g) &= \frac{1}{3\psi} \left(\frac{\alpha}{a_i} \right)^2 (\phi_B - \phi_C + \phi_P) + \left(\frac{2a_i}{3\alpha} \right) \left\{ \frac{\partial \alpha}{\partial t} + \frac{d}{dz}(\alpha v_g) \right\} \\ &= \Phi_B - \Phi_C + \Phi_P + \Phi_V \end{aligned} \quad (2.61)$$

where

$$\begin{aligned} \Phi_B &\equiv \frac{1}{3\psi} \left(\frac{\alpha}{a_i} \right)^2 \phi_B \\ \Phi_C &\equiv \frac{1}{3\psi} \left(\frac{\alpha}{a_i} \right)^2 \phi_C \\ \Phi_P &\equiv \frac{1}{3\psi} \left(\frac{\alpha}{a_i} \right)^2 \phi_P \\ \Phi_V &\equiv \left(\frac{2a_i}{3\alpha} \right) \left\{ \frac{\partial \alpha}{\partial t} + \frac{d}{dz}(\alpha v_g) \right\} \end{aligned}$$

The terms a_i , t , v_g , z , ψ , and α denote the interfacial area concentration, time, gas velocity, axial position, bubble shape factor ($\psi = 1/(36\pi)$ for spherical bubbles), and the void fraction respectively. The terms ϕ_B , ϕ_C , and ϕ_P are the rates of change of the bubble number density due to bubble breakup, bubble coalescence, and phase change. The terms Φ_B , Φ_C , Φ_P , and Φ_V are the rates of change of the interfacial

area concentration due to bubble breakup, bubble coalescence, phase change, and void transport respectively.

With all of the simplifications that Hibiki et al. used, the transport equation can be greatly simplified since many of the terms reduce to zero. Hibiki et al. found that the modeled interfacial area concentration transport equation could reproduce the axial interfacial area transport within an error of 11.1% for a 9.0 mm diameter tube with a superficial gas velocity of 0.013-0.052 m/s and a superficial liquid velocity ranging from 0.58 to 1.0 m/s.

Wu et al. (Wu et al, 1998) did some development with the interfacial area transport equation and then compared the one group theoretical equations to the experimental results for vertical bubbly flow. Wu et al. analyzed various methods of bubble breakup and bubble coalescence. They analyzed the important mechanisms for one group interfacial area transport. These mechanisms include: wake-entrainment induced bubble coalescence, bubble breakup due to turbulent impact, and random collision induced bubble coalescence. For two-group interfacial area transport, one must also include the shearing of small bubbles from large bubbles as well as the breakup of large bubbles due to surface instabilities. Wu et al. found that the proposed models for bubble breakup and bubble coalescences compared well to the experimental data and that the adjustable parameters used in the theoretical modeling were within the range of expected physical values. However, since the data set that was compared only had measurements at three axial locations, more data will need to be gathered in order to finely tune the theoretical model's adjustable parameters.

Several researchers have used the information gained using the theoretical development of the interfacial area transport equation and have compared the theoretical results with experimental results (Hibiki et al., 2001a; Hibiki and Ishii, 1999; Hibiki and Ishii, 2000). This sort of comparison could reveal missing areas within the theoretical result and could help to determine the rate of change of the

bubble number density within the pipe as well as to characterize the transfer rates between the two bubble groups.

Leung et al. (Leung et al., 1995) performed several experiments to determine the axial development of interfacial area and void concentration profiles in a vertical bubble column. This produces a data set for one to compare the experimental results with the one group interfacial area transport equation. By employing a double-sensor conductivity probe, Leung et al. was able to measure the radial profiles of the void fraction, interfacial area concentration, Sauter mean diameter, bubble velocity, and bubble frequency at each axial location. Leung et al., unfortunately only took measurements at two different axial locations: one at the entrance to the test section ($L/D=8$) the other at a position far away from the entrance ($L/D=60$). This makes it difficult to determine how the interfacial area concentration is actually changing along the flow direction. Leung et al. found that the void fraction peak is near the wall in the entrance region for all of the test cases ran. Leung et al. also found that in most of the flow rates that were used, the void profile remained saddle shaped even at $L/D=60$, but in one case the void fraction profile developed from saddle shaped at the entrance to a parabolic shape in the fully developed region. Leung et al. also compared their results to the drift flux model and found the distribution parameter, C_o , to be 0.7. This value is consistent with a near wall void peak profile.

Hibiki et al. (Hibiki et al., 2001a) also performed experiments to examine axial interfacial area transport in vertical bubbly flows. Hibiki et al. used three double-sensor conductivity probes located at $L/D=6.00$, 30.3 , and 53.5 to determine the axial interfacial area transport. The probes were also set up to traverse the pipe in the radial direction and data was taken at fifteen different radial locations for each flow condition specified. This allows for the creation of radial profiles for void fraction, interfacial velocity, and local interfacial area concentration. Hibiki et al. also employed the use of a hot-film anemometer to measure local liquid velocity and turbulence. Hibiki et al. also observed some of the same phenomena as Leung et al.

(Leung et al., 1995) such as the saddle shaped void profiles in the developed region. However, Hibiki et al. also observed situations in the transitional regime in where the void profile exhibited a near wall peak as well as a centerline peak. These transitional regions occur as the flow is transferring from a saddle shaped void profile into a void profile that is parabolic in shape.

Hibiki and Ishii (Hibiki and Ishii, 2000) provided involved theoretical development of the two-group interfacial area transport equation. They then applied this theoretical formulation and performed a comparison with experimental results. The experimental setup is essentially identical to that used in Hibiki et al. (Hibiki et al., 2001a). The difference between this particular set of experiments for the axial development of interfacial area concentration is that flow rates which contained cap/slug bubbles were used in order for comparison against their theoretical development of the two-group interfacial area concentration transport equation. Hibiki and Ishii observed that for low void fractions, the one-group interfacial area concentration transport equation could be applied within an average deviation of $\pm 9.51\%$. On the other hand, for higher void fractions, one may apply the two-group interfacial area concentration transport equation within an average deviation of $\pm 3.61\%$ for the flow cases studied.

2.8 INTERFACIAL AREA MEASUREMENT

Typically, one is interested in the measurement of local interfacial area concentration. However, most of the interfacial area data is an average over a section of pipe and is typically measured via a chemical technique. Thus, researchers are trying to develop a database of local interfacial area measurements so one will be able to improve the modeling of the terms in the interfacial area transport equation as well as to be able to compare the current one or two group interfacial area transport equations with experimental data. Currently, the most popular method in acquisition of local interfacial area is the multi-sensor conductivity/impedance probe. The multi-

sensor probes that are used are usually either double sensor or four sensor probes. The four-sensor probes give better interfacial area measurement results since one does not have to make assumptions on the actual shape of the bubble. However, the four sensor probes are more difficult to construct and since the probe area is relatively large, one experiences many cases in which bubbles miss one or more of the probe tips. This can make data processing very difficult and can lead to inaccuracies in interfacial area measurement. However, this problem is currently being combated with researchers such as Kim et al. (Kim et al., 2001) with the development of the miniaturized four-sensor conductivity probe. By reducing the size of these probes, one will have fewer problems with missing bubbles and be able to get a more accurate measurement of local interfacial area concentration. This reduction in size, however, is not without its drawbacks. By reducing the size of the probe tips, one needs to determine the spacing between the probe tips with greater precision as well as accounting for the fact that some of the probe tips have more area exposed to the surrounding fluid. This increased precision of the probe tip spacing must also be matched with an increased data-sampling rate for good temporal resolution. Revankar and Ishii (Revankar and Ishii, 1993) produced a theoretical foundation for the measurement of the time averaged local interfacial area concentration using a four-sensor conductivity probe. They then used this theoretical formulation to determine interfacial velocity, local interfacial area concentration, and void fraction in a vertical air-water cap bubbly flow. Revankar and Ishii then compared the four-sensor probe results to differential pressure measurements and to theoretical predictions of the interfacial area concentration profiles and found good agreement between theory and measurement. At the present stage of research in the field of two-phase flow, there is some debate on which type of probe, double sensor or four-sensor, is better for local interfacial area measurement. This will continue until the four sensor probes can be built easily with a small measurement area and with good precision. Until that time many researchers will still rely on the more simplistic and smaller double sensor probe.

In addition to the theoretical development of the local volumetric interfacial area transport equation, Morel et al. (Morel et al., 1999) also performed numerical simulations of simple upward bubble flows and compared the results to the theoretical calculations. Morel et al. also analyzed the effect that the spacing of the probe tips has on the measurement of interfacial area concentration as well as the vertical velocity component measurement numerically. It was discovered that if the probe tip spacing was less than 50 times smaller than the bubble diameter, one would achieve excellent measurement of the interfacial area concentration. However, if the spacing of the probe tips is greater than one fifth of the bubble radius, the measurement error for interfacial area concentration will be at least 20%. Morel et al. also found that the error in the vertical velocity component measurement was not sensitively affected by the probe spacing. These numerical results were obtained with the assumption that the bubbles are spherical, monodispersed, with the same radius and velocity. Morel et al. also ran simulations with varying bubble sizes to see the effect of the bubble interfaces missing one or more of the sensors. They found good agreement with the actual value of the interfacial area and the vertical velocity component. However, these results are somewhat artificial since in the simulation, it was assumed that the flow consisted of a uniform distribution in bubble sizes with no lateral velocity components. In the case of real two-phase flow, bubbles tend to exhibit size distributions which are not uniform and do indeed have lateral velocity components.

Another work by Kocamustafaogullari et al. (Kocamustafaogullari et al., 1994b) is similar to the work in Kocamustafaogullari et al., 1994a except for the fact that in this paper Kocamustafaogullari et al. concentrated on just traversing the double-sensor conductivity probe across the pipe with no rotation of the probe with respect to the pipe. The local and are-averaged void fractions and interfacial area concentrations were analyzed as a function of gas and liquid superficial velocities in the 50.3 mm internal diameter horizontal test section. These particular parameters were found to increase with decreased liquid flows and increase gas flows. It was also found that the

void fraction and interfacial area concentration were a stronger function of the gas flow rate than the liquid flow rate. In addition, Kocamustafaogullari et al. provided plots of the radial distribution of void fraction and interfacial area concentration showing the influence of these profiles with various superficial gas velocities while the superficial liquid velocity was kept nearly constant. Kocamustafaogullari et al. provided a theoretical model for mean bubble size and interfacial area concentration based upon the competing forces of surface tension and turbulent liquid fluctuations have on the shape of the bubble. The theoretical model was found to agree reasonably well with that obtained from experimental data. Kocamustafaogullari et al. plotted the experimental results using the drift flux model (Zuber and Finley, 1965). It was found that, although there was a linear relation between the average gas velocity, \bar{u}_g , and the area-averaged superficial velocity, $\langle j \rangle$, for a given superficial liquid velocity, the values of the drift velocity, $\langle \langle v_{gj} \rangle \rangle$, and the distribution parameter, C_o , were found to differ substantially depending on the liquid flow rates used. It was found that a better way to collapse all of the data would be to plot the data on the $\langle \alpha \rangle - \langle \beta \rangle$ plane, where $\langle \alpha \rangle$ and $\langle \beta \rangle$ are defined as:

$$\langle \alpha \rangle = \frac{\langle \beta \rangle}{C_o + \langle \langle v_{gj} \rangle \rangle / \langle j \rangle} \equiv K \langle \beta \rangle \quad (2.62)$$

$$\langle \beta \rangle \equiv \frac{\langle j_g \rangle}{\langle j_f \rangle + \langle j_g \rangle} \quad (2.63)$$

It was found that the all of the data gathered collapsed well to a linear relation with a value of K equal to 1.03, independent of the flow rate. It was determined that the constant value of K stems from the fact that horizontal bubbly flow occurs at relatively high mass flow rates. Due to this fact, the local relative velocities tend to be small and therefore the effect of $\langle \langle v_{gj} \rangle \rangle$ is negligible under these conditions.

2.9 LITERATURE REVIEW SUMMARY

Several attempts have been made to overcome the non-hyperbolic nature of the one-dimensional two-fluid model. Although these attempts have shown to add stability to the problem, some of the methods are not well justified from a physical point of view. This section will summarize some of the other methods that other researchers have tried in order to overcome the non-hyperbolic nature of the one-dimensional two-fluid model for unequal velocities. Many of the techniques either work for limited cases or lack some physical insight.

Table 2.1: Summary of previous work in improving two-fluid model stability

Author	Year	Method	Result	Comment
Gidaspow Lyczkowski et al. Gidaspow et al.	1974 1978 1983	Add influence of compressibility for both phases	Creates an improvement of stability by forcing a finite propagation speed	Generally, if $Ma < 0.3$, the flow should be incompressible. Compressibility should not be relied upon for stability.
Ransom and Hicks	1984 1988	Two-pressure model	Shows how the pressure difference between the phases add stability	Only developed for stratified flow
Trapp	1986	Fluctuating velocity components, $\overline{u'_k u'_k}$	Compares the instability to that between laminar and turbulent single phase flows	
Park et al. Lahey	1990 1991	Virtual mass term	Includes mass of liquid near the outer edge of bubbles	Requires knowledge of virtual mass coefficient May not work for stratified flows
Song and Ishii Song and Ishii Song	2000 2001 2003	Use of momentum covariance term	Uses information from the void and velocity distribution to help stabilize flow	Tries to account for both void and velocity distributions May not work well for horizontal flows
Chung et al.	2001 2004	Finite interface thickness Modifies interfacial pressure	Modifies the interfacial pressure term to enhance stability	Used for bubbly flows Requires knowledge of interface thickness
Guo et al.	2002	Liner and non-linear stability analysis Surface tension and viscosity included	The non-linear analysis confirms the linear analysis results	Circular pipe Created a set of non-linear hyperbolic equations
Ansari	2004	Two-pressure model	Well-posed over a wide range	Numerically calculated Only used for stratified flow

It is seen that previous authors have tried a wide range of techniques in order to overcome the deficiency of the non-hyperbolic nature of the one-dimensional two-fluid model for unequal gas and liquid velocities. The various techniques have had varying degrees of success. Many techniques only work for limited cases or include things such as compressibility that shouldn't be a factor for low speed flows. Some of the methods require knowledge of coefficients that are not well known, such as the virtual mass coefficient. It is desired to create a physical method that will work for a wide range of flow conditions. The model should not rely on things like compressibility, surface tension, or viscosity to create stability. Instead, if a model can be found to be stable without these terms, accounting for these terms will just increase the stability further.

3 TWO-PRESSURE TWO-FLUID MODEL DEVELOPMENT

In the one-dimensional two-fluid model, the momentum equations for intermittent flow and stratified flow in horizontal flow channels are different due to different considerations of the transverse gravity term. In the case of stratified flow, the pressure difference between the two phases caused by the gravitational head is modeled, which is the main mechanism responsible for phase separation. By definition, the average pressure for each phase should be:

$$\langle\langle P_g \rangle\rangle = \frac{\int_A P \alpha dA}{\int_A \alpha dA}, \quad \text{and} \quad \langle\langle P_f \rangle\rangle = \frac{\int_A P (1-\alpha) dA}{\int_A (1-\alpha) dA} \quad (3.1)$$

With the effect of gravity considered, the phase-averaged pressures in incompressible stratified flow are given by:

$$\langle\langle P_g \rangle\rangle = \frac{1}{A_g} \int_{A_g} (P_r + \rho_g g y) dA = P_r + \frac{\rho_g g}{A_g} \int_{A_g} y dA \quad (3.2)$$

$$\langle\langle P_f \rangle\rangle = \frac{1}{A_f} \int_{A_f} (P_r + \rho_g g y_i + \rho_f g (y - y_i)) dA = P_r - \Delta \rho g y_i + \frac{\rho_f g}{A_f} \int_{A_f} y dA \quad (3.3)$$

The reference pressure, P_r , is the pressure at the top of the pipe. The value of y is the vertical distance measured from the top of the pipe, in the downward direction. The value y_i is the location of the interface in stratified flow. The area integration is dependent on the shape of the pipe cross-section. For a rectangular pipe cross-section, the integration can be greatly simplified.

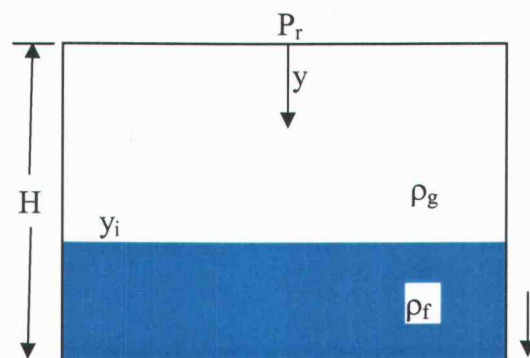


Figure 3.1: Stratified flow channel definitions

However, for intermittent or bubbly types of flow in horizontal pipes, the one-dimensional two-fluid model that is currently employed does not consider the gravity head effect on the two phases. This model assumes that the liquid and gas phases are in equilibrium with the average gas phase pressure equal to that of the average liquid phase pressure for the case when surface tension is neglected. Because of this assumption, this model is similar to the one-dimensional two-fluid model for vertical flows with an axisymmetric phase distribution. Due to this equilibrium pressure assumption, there is no mechanism to allow the phases to separate back into a stratified flow regime.

It is desired to incorporate a phase distribution parameter that allows for unification of the stratified flow and intermittent flow two-fluid models for the case of horizontal flow. By unifying the equations, only one set of equations will need to be solved for any flow regime. This phase distribution parameter will also allow accounting for flows in between the fully mixed bubbly type flows and the stratified type of flows. By incorporating this feature, a smoothing of the flow regime maps are possible and will reduce or eliminate the numerical oscillations brought on by sudden changes in flow regime.

3.1 FULLY-MIXED FLOW VS. SEPARATED FLOW EQUATIONS

The general one-dimensional two-fluid is shown for the two primary flow assumptions; stratified/annular flow and for bubbly/intermittent flow. The two models are then simplified using various assumptions and then compared. This way, the similarities of the two models can be shown and the typical assumptions analyzed in order to create a unified two-fluid model for one-dimensional flow that can match these two flow models as well as others that may be encountered.

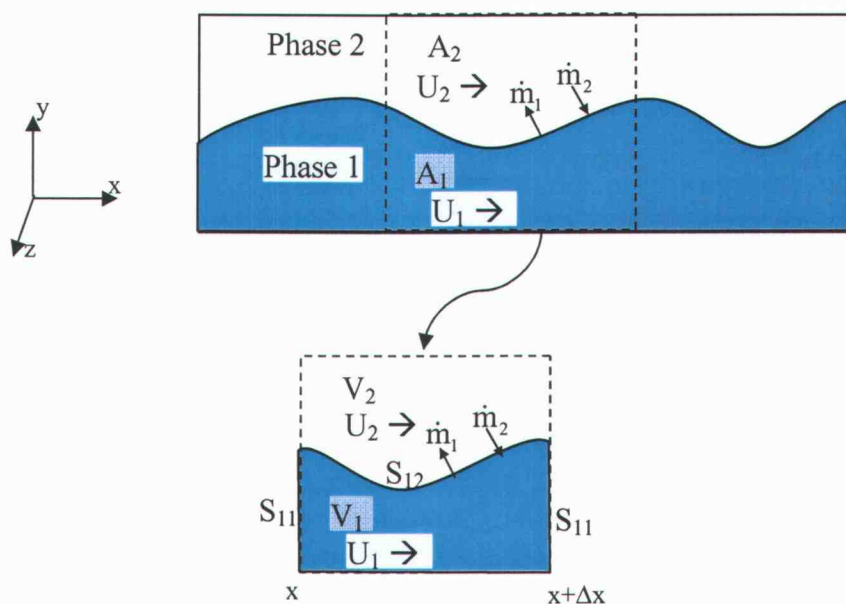


Figure 3.2: Control volume for continuity equation

$S_{ff}(x, t)$ – liquid-liquid interface area

$S_{fg}(x, t)$ – liquid-gas interface area

$S_{fw}(x, t)$ – surface bounded by the wall

$V_f(x, t)$ – volume of liquid in control volume

$V_g(x, t)$ – volume of gas in control volume

Assumptions

- flow is incompressible
- 1-D flow
- at the wall, assume no-slip condition (i.e. $u_f = u_i = 0$)
- at S_{ff} (liquid-liquid interface) $u_i = 0$
- at S_{fg} , $\iint_{S_{fg}} \rho_f (u_f - u_i) \cdot n \, dS = \iint_{S_{fg}} \dot{m}_{fi} \, dS$
- assume that \dot{m}_{fi} is constant over the interface of the control volume

Now for the one-dimensional control volume for the momentum equation:

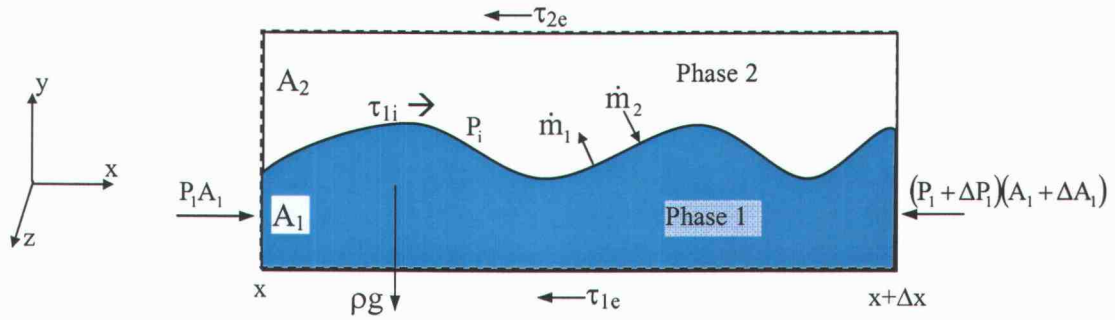


Figure 3.3: Control volume for momentum equation

Continuity (stratified) – Given in Kocamustafaogullari (1985)

$$\frac{\partial \rho_1 \langle 1 - \alpha \rangle}{\partial t} + \frac{\partial}{\partial x} [\langle 1 - \alpha \rangle \rho_1 \langle u_1 \rangle] = -\dot{m}_{li} \left(\frac{\xi_i}{A} \right) \quad (3.4)$$

$$\frac{\partial \rho_2 \langle \alpha \rangle}{\partial t} + \frac{\partial}{\partial x} [\langle \alpha \rangle \rho_2 \langle u_2 \rangle] = -\dot{m}_{2i} \left(\frac{\xi_i}{A} \right) \quad (3.5)$$

Momentum (stratified) – Given in Kocamustafaogullari (1985)

$$\left(\frac{\partial \langle 1-\alpha \rangle \rho_1 \langle \langle u_1 \rangle \rangle}{\partial t} + \frac{\partial \langle 1-\alpha \rangle \rho_1 \langle \langle u_1 \rangle \rangle^2}{\partial x} \right) = -\langle 1-\alpha \rangle \frac{\partial \langle \langle P_1 \rangle \rangle}{\partial x} + \langle 1-\alpha \rangle \rho_1 g \cos \varphi - \left(P_{1i} - \langle \langle P_1 \rangle \rangle \right) \frac{\partial \alpha}{\partial x} \quad (3.6)$$

$$- m_{1i} u_{1i} \left(\frac{\xi_i}{A} \right) + \tau_{1i} \left(\frac{\xi_i}{A} \right) - \tau_{1e} \left(\frac{\xi_{1e}}{A} \right) - \frac{\partial}{\partial x} \left[\langle 1-\alpha \rangle \rho_1 \text{Cov}(u_1^2) \right]$$

$$\left(\frac{\partial \langle \alpha \rangle \rho_2 \langle \langle u_2 \rangle \rangle}{\partial t} + \frac{\partial \langle \alpha \rangle \rho_2 \langle \langle u_2 \rangle \rangle^2}{\partial x} \right) = -\langle \alpha \rangle \frac{\partial \langle \langle P_2 \rangle \rangle}{\partial x} + \langle \alpha \rangle \rho_2 g \cos \varphi + \left(P_{2i} - \langle \langle P_2 \rangle \rangle \right) \frac{\partial \alpha}{\partial x} \quad (3.7)$$

$$- m_{2i} u_{2i} \left(\frac{\xi_i}{A} \right) - \tau_{2i} \left(\frac{\xi_i}{A} \right) - \tau_{2e} \left(\frac{\xi_{2e}}{A} \right) - \frac{\partial}{\partial x} \left[\langle \alpha \rangle \rho_2 \text{Cov}(u_2^2) \right]$$

Continuity (homogeneous) – Given in Song and Ishii (2001)

$$\frac{\partial \rho_1 \langle 1-\alpha \rangle}{\partial t} + \frac{\partial}{\partial x} \left[\rho_1 \langle 1-\alpha \rangle \langle \langle u_1 \rangle \rangle \right] = \langle \Gamma_1 \rangle \quad (3.8)$$

$$\frac{\partial \rho_2 \langle \alpha \rangle}{\partial t} + \frac{\partial}{\partial x} \left[\rho_2 \langle \alpha \rangle \langle \langle u_2 \rangle \rangle \right] = \langle \Gamma_2 \rangle \quad (3.9)$$

Momentum (homogeneous) – Given in Song and Ishii (2001)

$$\left(\frac{\partial \langle 1-\alpha \rangle \rho_1 \langle \langle u_1 \rangle \rangle}{\partial t} + \frac{\partial \langle 1-\alpha \rangle \rho_1 C_{v1} \langle \langle u_1 \rangle \rangle^2}{\partial x} \right) = -\langle 1-\alpha \rangle \frac{\partial \langle \langle P_1 \rangle \rangle}{\partial x} + \langle 1-\alpha \rangle \rho_1 g \cos \varphi - \left(P_{1i} - \langle \langle P_1 \rangle \rangle \right) \frac{\partial \alpha}{\partial x} \quad (3.10)$$

$$- \langle \Gamma_1 \rangle \langle \langle v_{1i} \rangle \rangle - \frac{4\alpha_{1w} \tau_{1w}}{D} + \frac{\partial \langle 1-\alpha \rangle \langle \langle \tau_{1xx} + \tau_{1xx}^T \rangle \rangle}{\partial x} - \langle M_{1i} \rangle$$

$$\left(\frac{\partial \langle \alpha \rangle \rho_2 \langle \langle u_2 \rangle \rangle}{\partial t} + \frac{\partial \langle \alpha \rangle \rho_2 C_{v2} \langle \langle u_2 \rangle \rangle^2}{\partial x} \right) = -\langle \alpha \rangle \frac{\partial \langle \langle P_2 \rangle \rangle}{\partial x} + \langle \alpha \rangle \rho_2 g \cos \varphi + \left(P_{2i} - \langle \langle P_2 \rangle \rangle \right) \frac{\partial \alpha}{\partial x} \quad (3.11)$$

$$- \langle \Gamma_2 \rangle \langle \langle v_{2i} \rangle \rangle - \frac{4\alpha_{2w} \tau_{2w}}{D} + \frac{\partial \langle \alpha \rangle \langle \langle \tau_{2xx} + \tau_{2xx}^T \rangle \rangle}{\partial x} - \langle M_{12} \rangle$$

Assuming

- no phase change
- incompressible
- neglect Covariance term
- neglect surface tension effects

So the final form of the equations with the assumptions made is:

Continuity (stratified)

$$\frac{\partial \rho_1 \langle 1 - \alpha \rangle}{\partial t} + \frac{\partial}{\partial x} [\langle 1 - \alpha \rangle \rho_1 \langle \langle u_1 \rangle \rangle] = 0 \quad (3.12)$$

$$\frac{\partial \rho_2 \langle \alpha \rangle}{\partial t} + \frac{\partial}{\partial x} [\langle \alpha \rangle \rho_2 \langle \langle u_2 \rangle \rangle] = 0 \quad (3.13)$$

Momentum (stratified)

$$\left(\frac{\partial \langle 1 - \alpha \rangle \rho_1 \langle \langle u_1 \rangle \rangle}{\partial t} + \frac{\partial \langle 1 - \alpha \rangle \rho_1 \langle \langle u_1 \rangle \rangle^2}{\partial x} \right) = -\langle 1 - \alpha \rangle \frac{\partial \langle \langle P_1 \rangle \rangle}{\partial x} + \langle 1 - \alpha \rangle \rho_1 g \cos \varphi \\ - (\mathbf{P}_{1i} - \langle \langle P_1 \rangle \rangle) \frac{\partial \alpha}{\partial x} + \tau_{1i} \left(\frac{\xi_i}{A} \right) - \tau_{1e} \left(\frac{\xi_{1e}}{A} \right) \quad (3.14)$$

$$\left(\frac{\partial \langle \alpha \rangle \rho_2 \langle \langle u_2 \rangle \rangle}{\partial t} + \frac{\partial \langle \alpha \rangle \rho_2 \langle \langle u_2 \rangle \rangle^2}{\partial x} \right) = -\langle \alpha \rangle \frac{\partial \langle \langle P_2 \rangle \rangle}{\partial x} + \langle \alpha \rangle \rho_2 g \cos \varphi \\ + (\mathbf{P}_{2i} - \langle \langle P_2 \rangle \rangle) \frac{\partial \alpha}{\partial x} - \tau_{2i} \left(\frac{\xi_i}{A} \right) - \tau_{2e} \left(\frac{\xi_{2e}}{A} \right) \quad (3.15)$$

Continuity (homogeneous)

$$\frac{\partial \rho_1 \langle 1 - \alpha \rangle}{\partial t} + \frac{\partial}{\partial x} [\rho_1 \langle 1 - \alpha \rangle \langle \langle u_1 \rangle \rangle] = 0 \quad (3.16)$$

$$\frac{\partial \rho_2 \langle \alpha \rangle}{\partial t} + \frac{\partial}{\partial x} [\rho_2 \langle \alpha \rangle \langle \langle u_2 \rangle \rangle] = 0 \quad (3.17)$$

Momentum (homogeneous)

$$\left(\frac{\partial \langle 1 - \alpha \rangle \rho_1 \langle \langle u_1 \rangle \rangle}{\partial t} + \frac{\partial \langle 1 - \alpha \rangle \rho_1 \langle \langle u_1 \rangle \rangle^2}{\partial x} \right) = -\langle 1 - \alpha \rangle \frac{\partial \langle \langle P_1 \rangle \rangle}{\partial x} + \langle 1 - \alpha \rangle \rho_1 g \cos \varphi - (\mathbf{P}_{1i} - \langle \langle P_1 \rangle \rangle) \frac{\partial \alpha}{\partial x} \\ - \frac{4\alpha_{1w} \tau_{1w}}{D} + \frac{\partial \langle 1 - \alpha \rangle \langle \langle \tau_{1xx} + \tau_{1xx}^T \rangle \rangle}{\partial x} - \langle M_{1i} \rangle \quad (3.18)$$

$$\begin{aligned}
\left(\frac{\partial \langle \alpha \rangle p_2 \langle \langle u_2 \rangle \rangle}{\partial t} + \frac{\partial \langle \alpha \rangle p_2 \langle \langle u_2 \rangle \rangle^2}{\partial x} \right) = & -\langle \alpha \rangle \frac{\partial \langle \langle P_2 \rangle \rangle}{\partial x} + \langle \alpha \rangle p_2 g \cos \varphi + \left(p_{2i} - \langle \langle P_2 \rangle \rangle \right) \frac{\partial \alpha}{\partial x} \\
& - \frac{4\alpha_{2w} \tau_{2w}}{D} + \frac{\partial \langle \alpha \rangle \langle \langle \tau_{2xx} + \tau_{2xx}^T \rangle \rangle}{\partial x} - \langle M_{12} \rangle
\end{aligned} \quad (3.19)$$

So the differences between the two sets of equations with the given assumptions lie in the shear terms as well as having the drag term in the homogenous case. This indicates with proper modeling of the drag and shear terms, the separated flow equation could be unified with the fully-mixed flow equations to account for both of these flows and any flow regime in between these limits. Additional work will need to be performed to link these cases together with a unified set of governing equations. Work will need to be performed with the drag and shear terms as well as any mass, momentum, and energy exchange terms not shown above due to the simplifying assumptions made.

3.2 INTERFACIAL PRESSURE TERM

In order to develop a unified two-fluid model for horizontal flow, the interfacial pressure term in each of the equations must be compared and combined in some manner so that as the flow transitions from one flow regime to another, the two-fluid model equation are consistent with those currently used in each flow regime. The pressure terms for the momentum equations will be developed and compared in the following sections. A distribution parameter, similar to what will be used to unify the phasic pressure terms, will be proposed in order to unify the interfacial pressure term for each given flow regime.

3.2.1 Stratified flow - pressure terms

For the case of stratified/annular types of flows, the pressure term in the momentum equation is derived as follows:

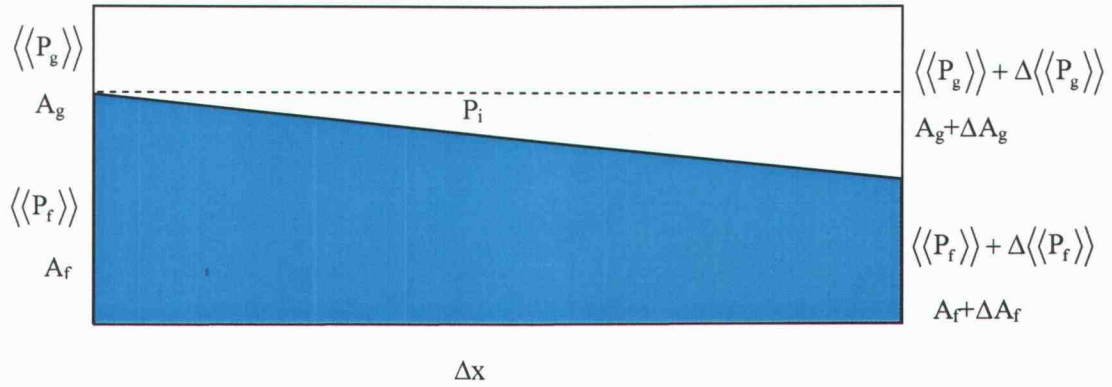


Figure 3.4: Stratified flow pressure development

The net force acting on the gas phase is:

$$\begin{aligned}
 & -\left(\langle P_g \rangle + \Delta \langle P_g \rangle\right)(A_g + \Delta A_g) + A_g \langle P_g \rangle + P_i \Delta A_g \\
 & \quad \Delta x \\
 \rightarrow & \frac{-A_g \langle P_g \rangle - A_g \Delta \langle P_g \rangle - \Delta A_g \langle P_g \rangle - \Delta A_g \Delta \langle P_g \rangle + A_g \langle P_g \rangle + P_i \Delta A_g}{\Delta x} \quad (3.20) \\
 \rightarrow & \frac{-A_g \Delta \langle P_g \rangle - \Delta A_g \langle P_g \rangle - \Delta A_g \Delta \langle P_g \rangle + P_i \Delta A_g}{\Delta x}
 \end{aligned}$$

Divide through by A and take the limit as $\Delta x \rightarrow 0$

$$\begin{aligned}
 & \frac{1}{\Delta x} \left[-\langle \alpha \rangle \Delta \langle P_g \rangle - \Delta \langle \alpha \rangle \langle P_g \rangle - \Delta \langle \alpha \rangle \Delta \langle P_g \rangle + P_i \Delta \langle \alpha \rangle \right] \\
 \rightarrow & -\langle \alpha \rangle \frac{\partial \langle P_g \rangle}{\partial x} - \langle P_g \rangle \frac{\partial \langle \alpha \rangle}{\partial x} - \frac{\partial \langle \alpha \rangle \partial \langle P_g \rangle}{\partial x} + P_i \frac{\partial \langle \alpha \rangle}{\partial x} \quad (3.21)
 \end{aligned}$$

Assume that the term $-\frac{\partial \langle \alpha \rangle \partial \langle P_g \rangle}{\partial x}$ is small, the equation for the gas phase becomes:

$$-\langle \alpha \rangle \frac{\partial \langle P_g \rangle}{\partial x} + (P_i - \langle P_g \rangle) \frac{\partial \langle \alpha \rangle}{\partial x} \quad (3.22)$$

Using the same process for the liquid phase, we get:

$$\begin{aligned}
 & \frac{-\langle\langle P_f \rangle\rangle + \Delta\langle P_f \rangle\rangle(A_f + \Delta A_f) + A_f\langle\langle P_f \rangle\rangle + P_i\Delta A_f}{\Delta x} \\
 \rightarrow & \frac{-A_f\langle\langle P_f \rangle\rangle - A_f\Delta\langle P_f \rangle\rangle - \Delta A_f\langle\langle P_f \rangle\rangle - \Delta A_f\Delta\langle P_f \rangle\rangle + A_f\langle\langle P_f \rangle\rangle + P_i\Delta A_f}{\Delta x} \\
 \rightarrow & \frac{-A_f\Delta\langle P_f \rangle\rangle - \Delta A_f\langle\langle P_f \rangle\rangle - \Delta A_f\Delta\langle P_f \rangle\rangle + P_i\Delta A_f}{\Delta x}
 \end{aligned} \tag{3.23}$$

Divide through by A and take the limit as $\Delta x \rightarrow 0$

$$\begin{aligned}
 & \frac{1}{\Delta x} \left[-\langle\alpha_f\rangle\Delta\langle P_f \rangle\rangle - \Delta\langle\alpha_f\rangle\langle\langle P_f \rangle\rangle - \Delta\langle\alpha_f\rangle\Delta\langle\langle P_f \rangle\rangle + P_i\Delta\langle\alpha_f\rangle \right] \\
 \rightarrow & -\langle\alpha_f\rangle\frac{\partial\langle\langle P_f \rangle\rangle}{\partial x} - \langle\langle P_f \rangle\rangle\frac{\partial\langle\alpha_f\rangle}{\partial x} - \frac{\partial\langle\alpha_f\rangle}{\partial x}\Delta\langle\langle P_f \rangle\rangle + P_i\frac{\partial\langle\alpha_f\rangle}{\partial x}
 \end{aligned} \tag{3.24}$$

Assume that $-\frac{\partial\langle\alpha_f\rangle}{\partial x}\Delta\langle\langle P_f \rangle\rangle$ is small, the equation for the liquid phase becomes:

$$-\langle 1 - \alpha \rangle \frac{\partial\langle\langle P_f \rangle\rangle}{\partial x} - (P_i - \langle\langle P_f \rangle\rangle) \frac{\partial\langle\alpha\rangle}{\partial x} \tag{3.25}$$

3.2.2 Bubbly flow - pressure terms

Using a similar approach, the pressure terms may be found for the case of a well mixed bubbly/intermittent type of flow. Since there are multiple interfaces in this case, a summation will have to be used in order to include all of the individual interface pressures.

First, the interface pressure term needs to be defined for a single bubble. The interface values are defined in Figure 3.5.

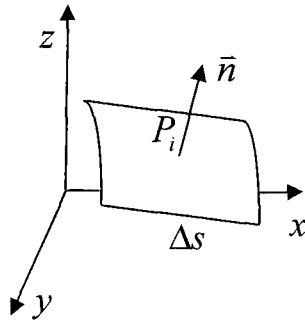


Figure 3.5: Interface definitions

The outward force in the direction normal to the interface is defined as:

$$\vec{F} = P_i \Delta s \vec{n} \quad (3.26)$$

where the term, $\Delta s \vec{n}$, is can be defined in terms of individual components as:

$$\Delta s \vec{n} = \vec{i} \Delta s_x + \vec{j} \Delta s_y + \vec{k} \Delta s_z \quad (3.27)$$

The pressure force acting in the x-direction on the element Δs becomes:

$$F_{x,i} = (P_i \Delta s \vec{n}) \cdot \vec{i} = P_i \Delta s_x \quad (3.28)$$

A slice of the flow channel is shown in Figure 3.6 to show the force in the x-direction acting on a single bubble due to the interfacial pressure force.

The force in the x-direction acting on a single bubble:

$$(P_i A_i)_x = P_i (A_{g_{x+\Delta x}} - A_{g_x}) \quad (3.29)$$

The total force in the x-direction due to interfacial pressure:

$$\sum_j P_{ij} (A_{g_{j_{x+\Delta x}}} - A_{g_{j_x}}) \quad (3.30)$$

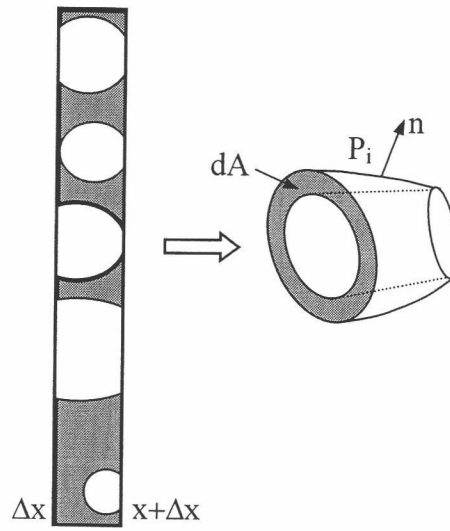


Figure 3.6: Pressure force on bubbly flow

Take the limit as $\Delta x \rightarrow 0$ and divide through by total area, A :

$$\frac{1}{A} \sum_j P_{ij} \frac{\partial A_{gj}}{\partial x} \quad (3.31)$$

Rewriting the summation in integral form, the interfacial term becomes:

$$\frac{1}{A} \int_A P_i \frac{\partial A_g}{\partial x} dA \rightarrow \int_A P_i \frac{\partial \alpha}{\partial x} dA \rightarrow \langle \langle P_i \rangle \rangle \frac{\partial \langle \alpha \rangle}{\partial x} \quad (3.32)$$

For the case when no surface tension is present, the interface pressure is equal to the gas and liquid pressure.

$$P_i = P_g = P_f \quad (3.33)$$

The interfacial pressure term becomes:

$$\langle \langle P_i \rangle \rangle \frac{\partial \langle \alpha \rangle}{\partial x} = \langle \langle P_g \rangle \rangle \frac{\partial \langle \alpha \rangle}{\partial x} = \langle \langle P_f \rangle \rangle \frac{\partial \langle 1 - \alpha \rangle}{\partial x} \quad (3.34)$$

Now that the interfacial pressure term is developed for the bubbly flow case, the remaining pressure terms for the bubbly flow limit may be developed. Figure 3.7 shows the pressures and area definitions related to the development of the fully-mixed bubbly flow model pressure terms.

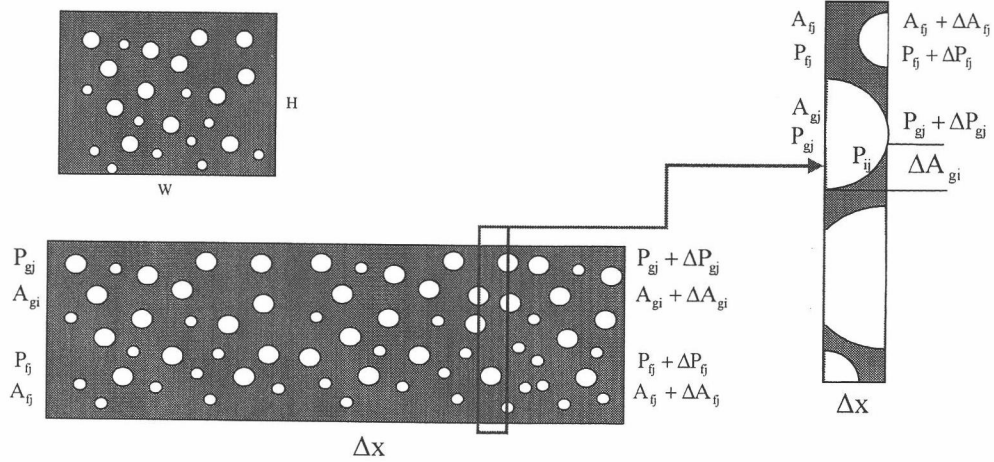


Figure 3.7: Fully-mixed flow pressure development

The net force acting on the gas phase for a slice of the flow channel can be determined by taking the difference in pressures acting the gas phase multiplied by the gas phase area across the slice while accounting for the interfacial pressure term.

$$\frac{-\sum_{j=1}^m [(P_{2j} + \Delta P_{2j})(A_{gj} + \Delta A_{gj})] + \sum_{j=1}^n [P_{2j} A_{gj}]}{\Delta x} + \sum_{j=1}^n \frac{P_{ij} \Delta A_{gj}}{\Delta x} \quad (3.35)$$

Breaking up into the individual terms, one gets:

$$\frac{-\sum_{j=1}^m P_{2j} A_{gj} - \sum_{j=1}^m \Delta P_{2j} A_{gj} - \sum_{j=1}^m P_{2j} \Delta A_{gj} - \sum_{j=1}^m \Delta P_{2j} \Delta A_{gj} + \sum_{j=1}^n P_{2j} A_{gj}}{\Delta x} + \sum_{j=1}^n \frac{P_{ij} \Delta A_{gj}}{\Delta x} \quad (3.36)$$

Dividing through by the flow area, A:

$$-\sum_{j=1}^m \frac{P_{2j} A_{gj}}{\Delta x A} - \sum_{j=1}^m \frac{\Delta P_{2j} A_{gj}}{\Delta x A} - \sum_{j=1}^m \frac{P_{2j} \Delta A_{gj}}{\Delta x A} - \sum_{j=1}^m \frac{\Delta P_{2j} \Delta A_{gj}}{\Delta x A} + \sum_{j=1}^n \frac{\Delta P_{2j} A_{gj}}{\Delta x A} + \frac{1}{A} \sum_{j=1}^n \frac{P_{ij} \Delta A_{gj}}{\Delta x} \quad (3.37)$$

Taking the limit as $\Delta x \rightarrow 0$ and assuming that the #n bubbles = #m bubbles:

$$-\sum_{j=1}^m \frac{\Delta P_{2j} A_{gj}}{\Delta x A} - \sum_{j=1}^m \frac{P_{2j} \Delta A_{gj}}{\Delta x A} - \sum_{j=1}^m \frac{\Delta P_{2j} \Delta A_{gj}}{\Delta x A} + \sum_{j=1}^m \frac{P_{ij} \Delta A_{gj}}{\Delta x A} \quad (3.38)$$

Which then becomes:

$$-\sum_{j=1}^m \left[\frac{A_{gj}}{A} \frac{\partial P_{2j}}{\partial x} \right] - \sum_{j=1}^m P_{2j} \frac{\partial A_{gj}}{A \partial x} - \sum_{j=1}^m \frac{\partial P_{2j}}{\partial x} \frac{\partial A_{gj}}{\partial x A} + \sum_{j=1}^m \frac{P_{ij}}{A} \frac{\partial A_{gj}}{\partial x} \quad (3.39)$$

Assuming a large population of bubbles averaged over time, the summation form can then be converted into an integral form.

$$-\frac{1}{A} \int_A \frac{A_g}{A} \frac{\partial P_2}{\partial x} dA - \frac{1}{A} \int_A P_2 \frac{\partial A_g}{A \partial x} dA - \frac{1}{A} \int_A \frac{\partial P_2}{\partial x} \frac{\partial A_g}{\partial x A} dA + \frac{1}{A} \int_A P_i \frac{\partial A_g}{A \partial x} dA \quad (3.40)$$

Using the definition of void fraction, the pressure terms become:

$$-\frac{1}{A} \int_A \alpha \frac{\partial P_2}{\partial x} dA - \frac{1}{A} \int_A P_2 \frac{\partial \alpha}{\partial x} dA - \frac{1}{A} \int_A \frac{\partial P_2}{\partial x} \frac{\partial \alpha}{\partial x} dA + \frac{1}{A} \int_A P_i \frac{\partial \alpha}{\partial x} dA \quad (3.41)$$

Using the definition of the area averaged void fraction, $\langle \alpha \rangle$, the integrals in the pressure term of the gas phase momentum equation can be eliminated with the addition of the void fraction weighted pressure, $\langle \langle P_2 \rangle \rangle$.

$$\langle \alpha \rangle \equiv \frac{1}{A} \int_A \alpha dA, \quad \text{which lets} \quad \langle \langle P_2 \rangle \rangle = \frac{\int_A \alpha P_2 dA}{\int_A \alpha dA} \quad (3.42)$$

The equation then becomes:

$$-\langle\alpha\rangle\frac{\partial\langle P_2\rangle}{\partial x}-\langle P_2\rangle\frac{\partial\langle\alpha\rangle}{\partial x}-\frac{\partial\langle P_2\rangle}{\partial x}\frac{\partial\langle\alpha\rangle}{\partial x}+\frac{1}{A}\int_A P_i\frac{\partial\alpha}{\partial x}dA \quad (3.43)$$

From the above equation, it can be seen that the interfacial pressure, P_i , could be defined in terms of a void weighted averaged interfacial pressure as:

$$\langle P_i \rangle = \frac{\int_A \alpha P_i dA}{\int_A \alpha dA} \quad (3.44)$$

Using this definition of interfacial pressure, the pressure term of the gas phase momentum equation becomes:

$$\rightarrow -\langle\alpha\rangle\frac{\partial\langle P_2\rangle}{\partial x}-\langle P_2\rangle\frac{\partial\langle\alpha\rangle}{\partial x}-\frac{\partial\langle P_2\rangle}{\partial x}\frac{\partial\langle\alpha\rangle}{\partial x}+\langle P_i\rangle\frac{\partial\langle\alpha\rangle}{\partial x} \quad (3.45)$$

Assuming that $-\frac{\partial\langle P_2\rangle}{\partial x}\frac{\partial\langle\alpha\rangle}{\partial x}$ is negligible, the pressure term of the momentum equation for the gas phase becomes:

$$-\langle\alpha\rangle\frac{\partial\langle P_2\rangle}{\partial x}+(\langle P_i\rangle-\langle P_2\rangle)\frac{\partial\langle\alpha\rangle}{\partial x} \quad (3.46)$$

One can see that this result is very similar to that found for the stratified flow case. A comparison between the two will be discussed in the next section.

3.2.3 Interfacial pressure term unification

It is noted from the previous two subsections (3.2.1 and 3.2.2) that although the general form of the pressure terms are similar between the two cases, there are some differences between how the interfacial pressure term is defined in the two models. The difference comes from the fact that for the stratified two-fluid model, the interface

only exists at one location for a given position and time. However, in the case of the well mixed bubbly flow two-fluid model, multiple interfaces do exist. This is the reason that a void weighted interfacial pressure term is used. The void weighted term assumes that interfaces occur wherever gas is present with an equal probability being at any vertical location. In order to develop a unified one-dimensional two-fluid model, this interfacial pressure term will also need to be unified so that one obtains the stratified definition if the flow is stratified or annular, but also can obtain the void fraction weighted pressure term as in the well mixed flow case. There should also be intermediate points for the interfacial pressure term for when the flow is somewhere in between the stratified flow case and the well mixed bubbly flow case. The difficulty in unifying the interfacial term lies in the fact that the interfacial pressure is only defined on the surface on the gas-liquid interface.

It would physically make sense to define the interfacial pressure in terms of an interfacial area concentration profile. This way, multiple interfaces could be accounted for as well as the single interfaced found in the stratified flow case. Going back to the definition of the average interfacial pressure for the well-mixed flow case:

$$\langle\langle P_i \rangle\rangle = \frac{\int_A \alpha P_i dA}{\int_A \alpha dA} \quad (3.47)$$

If the bubbles are spherical, the void fraction can be related to the interfacial area concentration as:

$$a_i = \frac{6\alpha}{d_{sm}} \quad (3.48)$$

Where a_i is the interfacial area concentration (interfacial area per volume) and d_{sm} is known as the Sauter mean diameter.

Substituting into the previous equation, we get:

$$\langle\langle P_i \rangle\rangle = \frac{\int_A P_i \frac{d_{sm} a_i}{6} dA}{\int_A \frac{d_{sm} a_i}{6} dA} \rightarrow \frac{\int_A P_i d_{sm} a_i dA}{\int_A d_{sm} a_i dA} \quad (3.49)$$

This shows that the average interface pressure can be expressed in terms of local pressure, interfacial area concentration, and Sauter mean diameter. This type of expression makes more sense to use than using local void fraction because the interface pressure is a surface quantity instead of a volume quantity. In this definition, only pressures where interfaces exist are accounted for. This way multiple interfaces can be accounted for, such as the bubbly flow case, or a single interface can be properly modeled such as in the stratified flow limit.

3.3 PHASE DISTRIBUTION PARAMETER

The following section will discuss the development of the phase distribution parameter. The use of this parameter will account for the pressure differences between the two phases based on hydrostatic head. The value of the distribution parameter is dependent on the void fraction profile along the vertical direction (transverse to the flow direction). The use of this parameter is suggested to aid in improving the stability of the one-dimensional two-fluid model as well as possibly allowing for unification between the typical stratified flow model and the model that is typically incorporated for the bubbly type flow assumption.

3.3.1 Development of the phase distribution parameters

The phase distribution parameters can be derived starting with the work of Kocamustafaogullari and Ishii for stratified flows. By neglecting surface tension and phase change, Equation (3.1) can be generalized for the derivation of the phase-averaged pressures to incorporate the influence of the vertical phase distribution.

$$\langle\langle P_g \rangle\rangle = \frac{\frac{1}{A} \int_A (P_R + P_{grav}) \alpha dA}{\frac{1}{A} \int_A \alpha dA} = P_r + \frac{\frac{1}{A} \int_A \int_0^y \rho_m g dy' \alpha dA}{\frac{1}{A} \int_A \alpha dA} \quad (3.50)$$

$$\langle\langle P_f \rangle\rangle = \frac{\frac{1}{A} \int_A (P_R + P_{grav}) (1-\alpha) dA}{\frac{1}{A} \int_A (1-\alpha) dA} = P_r + \frac{\frac{1}{A} \int_A \int_0^y \rho_m g dy' (1-\alpha) dA}{\frac{1}{A} \int_A (1-\alpha) dA} \quad (3.51)$$

$$P_{grav} = \int_0^y \rho_m g dy' \quad (3.52)$$

The equations can be further simplified by using the definition of the mixture density, ρ_m , and assuming that the pressure variation due to gravitational head is only a function of the vertical distance, y . The phase-averaged pressures now become:

$$\langle\langle P_g \rangle\rangle = P_r + \frac{\frac{1}{H} \int_H \int_0^y [\rho_g \alpha + \rho_f (1-\alpha)] g dy' \alpha dy}{\bar{\alpha}^L} \quad (3.53)$$

$$\langle\langle P_f \rangle\rangle = P_r + \frac{\frac{1}{H} \int_H \int_0^y [\rho_g \alpha + \rho_f (1-\alpha)] g dy' (1-\alpha) dy}{\bar{\alpha}^L} \quad (3.54)$$

Where $\bar{\alpha}^L$ is the line-averaged void fraction and is defined as follows:

$$\bar{\alpha}^L \equiv \frac{1}{H} \int_H \alpha dy \quad (3.55)$$

$$\begin{aligned}
\langle\langle P_g \rangle\rangle - P_r &= g \frac{\int_H \left[\int_0^y \rho_g \alpha dy' + \int_0^y \rho_f (1-\alpha) dy' \right] \alpha dy}{\int_H \alpha dy} \rightarrow g \frac{\int_H \left[\rho_g \int_0^y \alpha dy' + \rho_f \int_0^y (1-\alpha) dy' \right] \alpha dy}{\int_H \alpha dy} \\
\langle\langle P_g \rangle\rangle - P_r &= g \frac{\int_H \left[\rho_g \int_0^y \alpha dy' + \rho_f \left[y - \int_0^y \alpha dy' \right] \right] \alpha dy}{\int_H \alpha dy}
\end{aligned} \tag{3.56}$$

$$\langle\langle P_g \rangle\rangle - P_r = \rho_g g \frac{\int_H \int_0^y \alpha dy' \alpha dy}{\int_H \alpha dy} + \rho_f g \frac{\int_H \left[y - \int_0^y \alpha dy' \right] \alpha dy}{\int_H \alpha dy} \tag{3.57}$$

Dividing through by the channel height:

$$\langle\langle P_g \rangle\rangle - P_r = \rho_g g H \frac{\frac{1}{H} \int_H \int_0^y \alpha dy' \alpha dy}{\int_H \alpha dy} + \rho_f g H \left[\frac{\int_H \frac{y}{H} \alpha dy}{\int_H \alpha dy} - \frac{\frac{1}{H} \int_H \int_0^y \alpha dy' \alpha dy}{\int_H \alpha dy} \right] \tag{3.58}$$

Using the definition of the line-averaged void fraction:

$$\langle\langle P_g \rangle\rangle - P_r = \rho_g g H \left[\frac{\int_H \int_0^y \alpha dy' \alpha dy}{H^2 \bar{\alpha}^L} \right] + \rho_f g H \left[\frac{\int_H \frac{y}{H} \alpha dy}{H \bar{\alpha}^L} - \frac{\int_H \int_0^y \alpha dy' \alpha dy}{H^2 \bar{\alpha}^L} \right] \tag{3.59}$$

The gas phase pressure can then be reduced to:

$$\langle\langle P_g \rangle\rangle - P_r = \rho_g g H \theta_2 + \rho_f g H [\theta_0 - \theta_2] \tag{3.60}$$

If the local void fraction distribution in the vertical direction is known, the gravity effects can be modeled through the difference in the phase-averaged pressures. By following this approach, the intermittent and stratified flow models are able to be unified. The different two-fluid models will be unified with the use of two distribution

parameters with H as the maximum vertical dimension of a horizontal pipe. A more detailed development of the phase distribution parameters are shown in Appendix B. Some common values of the distribution parameters are shown in Figure 3.8.

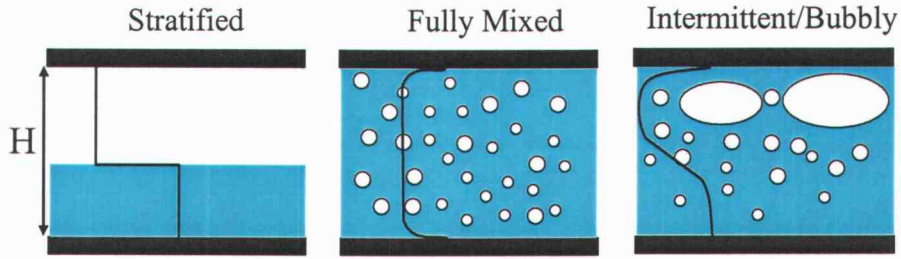


Figure 3.8: Phase distribution for different flow regimes

3.3.2 Comparison of the phase distribution parameters

Now that three phase-distribution parameters are developed to describe the void-weighted pressures of both the gas and liquid phases in a horizontal pipe, it is important to find what the values of these parameters are in the limit of stratified flow and fully mixed flow. For the case of stratified flow, the three distribution parameters can be found as follows:

$$\theta_0 = \frac{\int_H^y \alpha dy}{H \bar{\alpha}^L} = \frac{\int_{H_g}^y \frac{y}{H} dy}{H \bar{\alpha}^L} = \frac{\frac{H_g^2}{2H}}{H \bar{\alpha}^L} = \frac{H_g^2}{2HH \bar{\alpha}^L} = \frac{\bar{\alpha}^{L^2}}{2 \bar{\alpha}^L} = \frac{\bar{\alpha}^L}{2} \quad (3.61)$$

$$\begin{aligned}\theta_1 &= \frac{\int_0^y \int \alpha dy' dy}{H^2 \bar{\alpha}^L} = \frac{\int_0^H \alpha y dy}{H^2 \bar{\alpha}^L} = \frac{\int_0^{H_g} y dy + \int_{H_g}^H y_g dy}{H^2 \bar{\alpha}^L} \\ &\rightarrow \frac{\int_0^{H_g} y dy + y_g \int_{H_g}^H dy}{H^2 \bar{\alpha}^L} = \frac{\frac{H_g^2}{2} + H_g(H - H_g)}{H^2 \bar{\alpha}^L} = \frac{\frac{\bar{\alpha}^{L^2}}{2} + \bar{\alpha}^L(1 - \bar{\alpha}^L)}{\bar{\alpha}^L} = \frac{\bar{\alpha}^L}{2} + (1 - \bar{\alpha}^L)\end{aligned}\quad (3.62)$$

$$\theta_2 = \frac{\int_0^y \int \alpha dy' \alpha dy}{H^2 \bar{\alpha}^L} = \frac{\int_0^{H_g} \alpha y dy}{H^2 \bar{\alpha}^L} = \frac{H_g^2}{2H^2 \bar{\alpha}^L} = \frac{\bar{\alpha}^{L^2}}{2\bar{\alpha}^L} = \frac{\bar{\alpha}^L}{2}\quad (3.63)$$

$$\langle\langle P_g \rangle\rangle - P_r = \rho_g g H \theta_2 + \rho_f g H [\theta_0 - \theta_2]\quad (3.64)$$

The average pressure for the gas phase for the stratified flow regime becomes:

$$\langle\langle P_g \rangle\rangle - P_r = \rho_g g H \frac{\bar{\alpha}^L}{2} + \rho_f g H \left[\frac{\bar{\alpha}^L}{2} - \frac{\bar{\alpha}^L}{2} \right] = \frac{\rho_g g H \bar{\alpha}^L}{2}\quad (3.65)$$

Now for the liquid phase.

$$\begin{aligned}\langle\langle P_f \rangle\rangle - P_r &= \frac{\rho_g g H}{(1 - \bar{\alpha}^L)} [\bar{\alpha}^L \theta_1 - \bar{\alpha}^L \theta_2] + \frac{\rho_f g H}{(1 - \bar{\alpha}^L)} \left[\frac{1}{2} - \bar{\alpha}^L \theta_0 - \bar{\alpha}^L \theta_1 + \bar{\alpha}^L \theta_2 \right] \\ &= \frac{\rho_g g H}{(1 - \bar{\alpha}^L)} \left[\bar{\alpha}^L \left[\frac{\bar{\alpha}^L}{2} + (1 - \bar{\alpha}^L) \right] - \bar{\alpha}^L \frac{\bar{\alpha}^L}{2} \right] + \frac{\rho_f g H}{(1 - \bar{\alpha}^L)} \left[\frac{1}{2} - \bar{\alpha}^L \frac{\bar{\alpha}^L}{2} - \bar{\alpha}^L \left[\frac{\bar{\alpha}^L}{2} + (1 - \bar{\alpha}^L) \right] + \bar{\alpha}^L \frac{\bar{\alpha}^L}{2} \right] \\ &= \frac{\bar{\alpha}^L \rho_g g H}{(1 - \bar{\alpha}^L)} \left[\frac{\bar{\alpha}^L}{2} + (1 - \bar{\alpha}^L) - \frac{\bar{\alpha}^L}{2} \right] + \frac{\rho_f g H}{2(1 - \bar{\alpha}^L)} [1 - \bar{\alpha}^L \bar{\alpha}^L - 2\bar{\alpha}^L + 2\bar{\alpha}^L \bar{\alpha}^L] \\ &= \frac{\bar{\alpha}^L \rho_g g H}{(1 - \bar{\alpha}^L)} (1 - \bar{\alpha}^L) + \frac{\rho_f g H}{2(1 - \bar{\alpha}^L)} [1 - \bar{\alpha}^L] [1 - \bar{\alpha}^L]\end{aligned}\quad (3.66)$$

The average pressure for the liquid phase for the stratified flow regime becomes:

$$\langle\langle P_f \rangle\rangle - P_r = \bar{\alpha}^L \rho_g g H + \frac{\rho_f g H}{2} [1 - \bar{\alpha}^L]\quad (3.67)$$

Now, the fully mixed flow condition will be tested. For the fully mixed case, it is assumed that the local void fraction is equal to the area-averaged void fraction or, $\alpha(y) = \bar{\alpha}^L$.

$$\theta_0 = \frac{\int_0^H \frac{y}{H} \alpha dy}{H \bar{\alpha}^L} = -\frac{\bar{\alpha}^L \int_0^H \frac{y}{H} dy}{H \bar{\alpha}^L} = -\frac{\int_0^H \frac{y}{H} dy}{H} = -\frac{H^2}{2HH} = -\frac{1}{2} \quad (3.68)$$

$$\theta_1 = \frac{\int_0^H \int_0^y \alpha dy' dy}{H^2 \bar{\alpha}^L} = -\frac{\bar{\alpha}^L \int_0^H \int_0^y dy' dy}{H^2 \bar{\alpha}^L} = -\frac{\int_0^H y dy}{H^2} = -\frac{H^2}{2H^2} = -\frac{1}{2} \quad (3.69)$$

$$\theta_2 = \frac{\int_0^H \int_0^y \alpha dy' \alpha dy}{H^2 \bar{\alpha}^L} = -\frac{\bar{\alpha}^L \int_0^H \int_0^y dy' \alpha dy}{H^2 \bar{\alpha}^L} = -\frac{\bar{\alpha}^L \int_0^H y \alpha dy}{H^2 \bar{\alpha}^L} = -\frac{\int_0^H y \alpha dy}{H^2} = -\frac{\bar{\alpha}^L \int_0^H y dy}{H^2} = -\frac{\bar{\alpha}^L H^2}{2H^2} = -\frac{\bar{\alpha}^L}{2} \quad (3.70)$$

$$\langle\langle P_g \rangle\rangle - P_r = \rho_g g H \theta_2 + \rho_f g H [\theta_0 - \theta_2] \quad (3.71)$$

The average pressure for the gas phase for the fully mixed case becomes:

$$\langle\langle P_g \rangle\rangle - P_r = \rho_g g H \frac{\bar{\alpha}^L}{2} + \rho_f g H \left[\frac{1}{2} - \frac{\bar{\alpha}^L}{2} \right] = \frac{\rho_g g H \bar{\alpha}^L}{2} + \frac{\rho_f g H (1 - \bar{\alpha}^L)}{2} \quad (3.72)$$

Now for the liquid phase:

$$\begin{aligned} \langle\langle P_f \rangle\rangle - P_r &= \frac{\rho_g g H}{(1 - \bar{\alpha}^L)} [\bar{\alpha}^L \theta_1 - \bar{\alpha}^L \theta_2] + \frac{\rho_f g H}{(1 - \bar{\alpha}^L)} \left[\frac{1}{2} - \bar{\alpha}^L \theta_0 - \bar{\alpha}^L \theta_1 + \bar{\alpha}^L \theta_2 \right] \\ &= \frac{\rho_g g H}{(1 - \bar{\alpha}^L)} \left[\bar{\alpha}^L \frac{1}{2} - \bar{\alpha}^L \frac{\bar{\alpha}^L}{2} \right] + \frac{\rho_f g H}{(1 - \bar{\alpha}^L)} \left[\frac{1}{2} - \bar{\alpha}^L \frac{1}{2} - \bar{\alpha}^L \frac{1}{2} + \bar{\alpha}^L \frac{\bar{\alpha}^L}{2} \right] \\ &= \frac{\bar{\alpha}^L \rho_g g H}{2(1 - \bar{\alpha}^L)} [1 - \bar{\alpha}^L] + \frac{\rho_f g H}{2(1 - \bar{\alpha}^L)} [1 - 2\bar{\alpha}^L + \bar{\alpha}^L \bar{\alpha}^L] \\ &= \frac{\bar{\alpha}^L \rho_g g H}{2} + \frac{\rho_f g H}{2(1 - \bar{\alpha}^L)} [1 - \bar{\alpha}^L] [1 - \bar{\alpha}^L] \end{aligned} \quad (3.73)$$

The average pressure for the liquid phase for the fully mixed case becomes:

$$\langle\langle P_f \rangle\rangle - P_r = \frac{\bar{\alpha}^L \rho_g g H}{2} + \frac{\rho_f g H}{2} (1 - \bar{\alpha}^L) \quad (3.74)$$

It is seen that for the gas and liquid phase pressure are equal in the fully mixed case, as expected.

A table of the theoretical values found for the various distribution parameters the stratified flow case and the fully-mixed condition are given in Table 3.1. The theoretical limits for the distribution parameters for are shown in graphical form in Figures 3.9 through 3.11. The theoretical values for the distribution parameters for the intermittent/bubbly flow condition are not known in general at this point.

Table 3.1: Comparison of theoretical values of the phase distribution parameters

	Stratified Flow	Fully Mixed	Intermittent / Bubbly Flow
θ_0	$\bar{\alpha}^L/2$	$1/2$?
θ_1	$1 - \bar{\alpha}^L/2$	$1/2$?
θ_2	$\bar{\alpha}^L/2$	$\bar{\alpha}^L/2$?

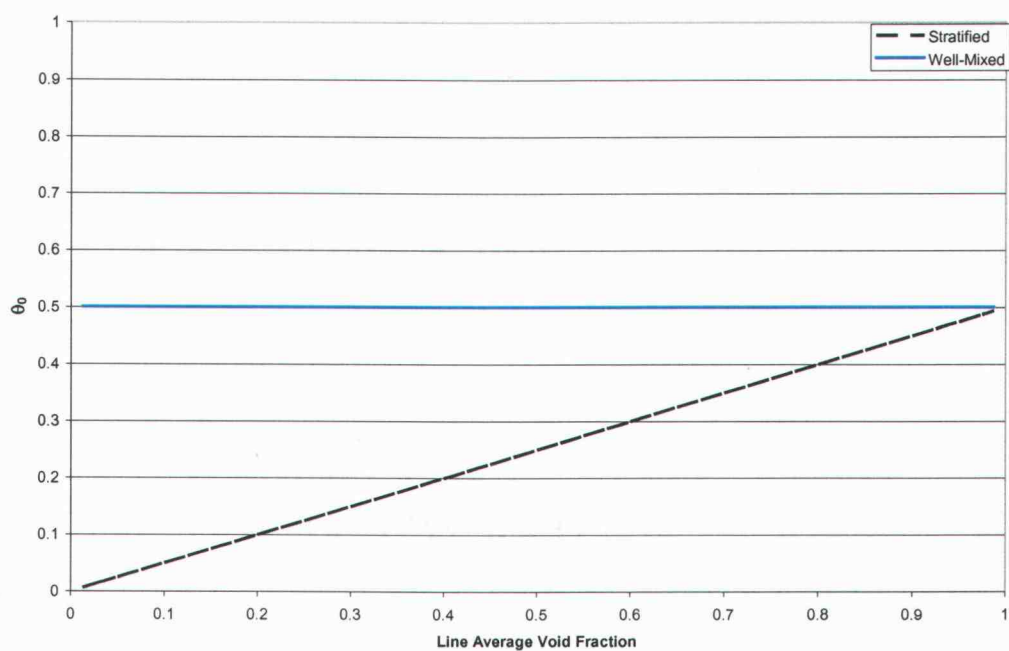


Figure 3.9: Comparison of the theoretical limits of the θ_0 distribution parameter

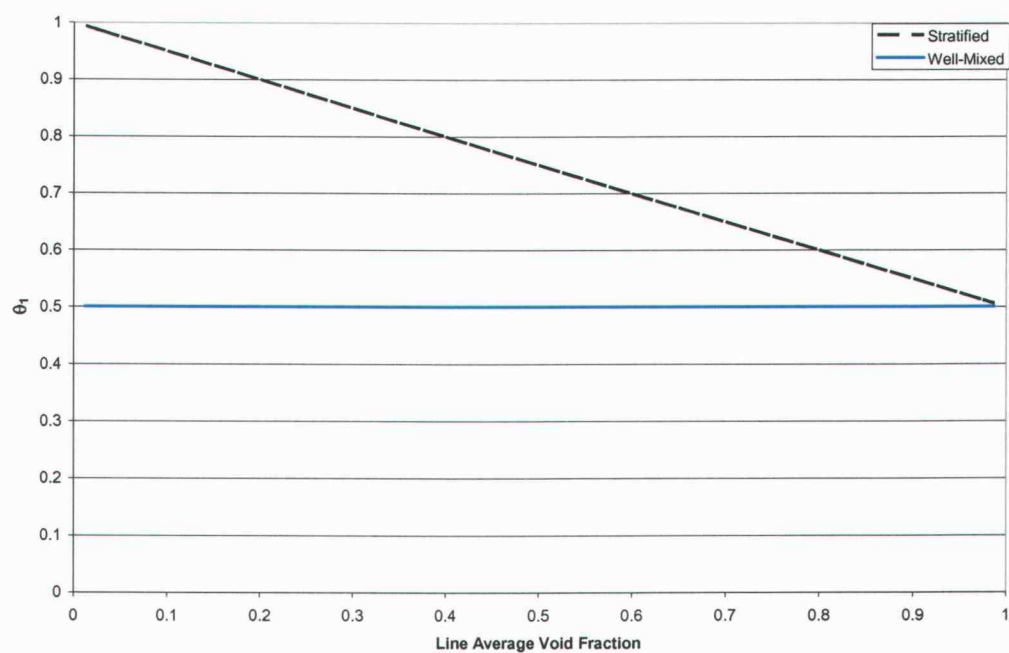


Figure 3.10: Comparison of the theoretical limits of the θ_1 distribution parameter

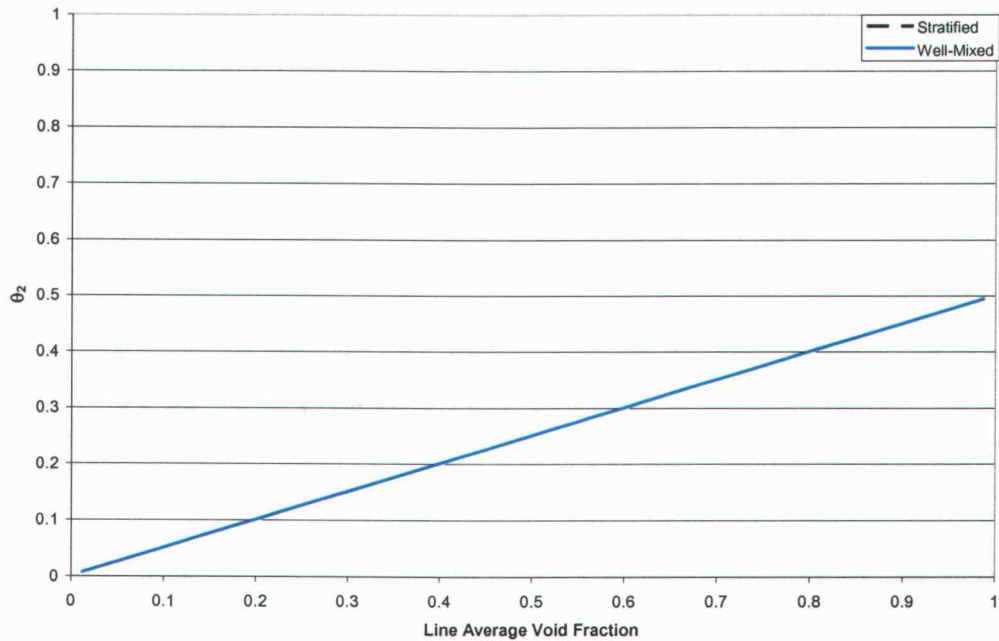


Figure 3.11: Comparison of the theoretical limits of the θ_2 distribution parameter

3.3.3 Simplification of the phase distribution parameters

From the previous section, one can see some possible connection between the various phase distribution parameters. It appears that θ_0 and θ_1 are mirror images of one another with the reflection about the 0.5 value of the distribution parameter. One will also note that the third distribution parameter, θ_2 , appears to be equal to $\bar{\alpha}^L/2$ for stratified flow and fully mixed flow. Since, there appears to be a direct relationship between θ_0 and θ_1 , and that θ_2 seems to equal a fixed value, perhaps a single phase distribution parameter can be found that will describe the phase-averaged pressure for horizontal flow.

From the previous section, the distribution parameters are defined as:

$$\theta_0 = \frac{\int_0^y \frac{y}{H} \alpha dy}{H \bar{\alpha}^L} \quad \theta_1 = \frac{\int_0^y \int_0^y \alpha dy' dy}{H^2 \bar{\alpha}^L} \quad \theta_2 = \frac{\int_0^y \int_0^y \alpha dy' \alpha dy}{H^2 \bar{\alpha}^L} \quad (3.75)$$

Using $\eta = \frac{y}{H}$, the distribution parameters become:

$$\theta_0 = \frac{\int_0^1 \eta \alpha d\eta}{\bar{\alpha}^L} \quad \theta_1 = \frac{\int_0^1 \int_0^\eta \alpha d\eta' d\eta}{\bar{\alpha}^L} \quad \theta_2 = \frac{\int_0^1 \int_0^\eta \alpha d\eta' \alpha d\eta}{\bar{\alpha}^L} \quad (3.76)$$

To obtain a relationship between θ_0 and θ_1 , we first evaluate θ_0 using integration by parts.

Let:

$$u = \eta \quad du = d\eta$$

$$dv = \alpha d\eta \quad v = \int_0^\eta \alpha d\eta' \quad (3.77)$$

$$\int u dv = u v - \int v du \quad (3.78)$$

$$\int_0^1 \eta \alpha d\eta = \eta \int_0^\eta \alpha d\eta' - \int_0^1 \int_0^\eta \alpha d\eta' d\eta \quad (3.79)$$

We note that the last term in the equation is equal to $\bar{\alpha}^L \theta_1$, the two quantities are related by:

$$\bar{\alpha}^L \theta_0 = \int_0^1 \eta \alpha d\eta = \eta \int_0^\eta \alpha d\eta' - \bar{\alpha}^L \theta_1 \quad (3.80)$$

So,

$$\theta_0 = \frac{\eta}{\bar{\alpha}^L} \int_0^\eta \alpha d\eta' \Big|_{\eta=0}^1 - \theta_1 \quad (3.81)$$

Which leads to:

$$\theta_0 = \frac{1}{\bar{\alpha}^L} \int_0^1 \alpha d\eta' - \theta_1 \quad (3.82)$$

Note that $\bar{\alpha}^L = \int_0^1 \alpha d\eta'$, so the relation becomes:

$$\theta_0 = \frac{\bar{\alpha}^L}{\bar{\alpha}^L} - \theta_1 \rightarrow 1 - \theta_1 \quad (3.83)$$

$$\theta_0 = 1 - \theta_1$$

Now to simplify the θ_2 void distribution parameter. First the θ_2 void distribution parameter is defined as:

$$\theta_2 = \frac{\int_0^y \int_0^y \alpha dy' \alpha dy}{H^2 \bar{\alpha}^L} \quad (3.84)$$

Substituting $\eta = \frac{y}{H}$, the distribution parameter becomes:

$$\theta_2 = \frac{\int_0^1 \int_0^\eta \alpha d\eta' \alpha d\eta}{\bar{\alpha}^L} \quad (3.85)$$

Now to solve by using the method of u-substitution.

$$u = \int_0^\eta \alpha d\eta' \quad (3.86)$$

$$du = \alpha d\eta$$

$$\int_0^1 \int_0^\eta \alpha d\eta' \alpha d\eta = \int_0^1 u du \rightarrow \frac{u^2}{2} \Big|_0^1 \quad (3.87)$$

This is then simplified to:

$$\begin{aligned}
 &\rightarrow \frac{1}{2} [u]^2 \Big|_0^1 \rightarrow \frac{1}{2} \left[\int_0^1 \alpha d\eta' \right]^2 \Big|_0^1 \\
 &\rightarrow \frac{1}{2} \left[\int_0^1 \alpha d\eta' \right]^2 - \frac{1}{2} \left[\int_0^0 \alpha d\eta' \right]^2 = \frac{1}{2} \left[\int_0^1 \alpha d\eta' \right]^2
 \end{aligned} \tag{3.88}$$

The θ_2 phase distribution parameter reduces to:

$$\theta_2 = \frac{\frac{1}{2} \left[\int_0^1 \alpha d\eta' \right]^2}{\bar{\alpha}^L} = \frac{\frac{1}{2} [\bar{\alpha}^L]^2}{\bar{\alpha}^L} = \frac{\bar{\alpha}^L}{2} \tag{3.89}$$

The following relationships between the distribution parameters were found:

$$\theta_0 = 1 - \theta_1 \tag{3.90}$$

$$\theta_2 = \frac{\bar{\alpha}^L}{2} \tag{3.91}$$

Substituting into the pressure equations, we get:

$$\begin{aligned}
 \langle \langle P_g \rangle \rangle - P_r &= \rho_g g H \theta_2 + \rho_f g H [\theta_0 - \theta_2] \\
 &= \rho_g g H \frac{\bar{\alpha}^L}{2} + \rho_f g H \left[\theta_0 - \frac{\bar{\alpha}^L}{2} \right]
 \end{aligned} \tag{3.92}$$

The gas phase pressure becomes:

$$\langle \langle P_g \rangle \rangle - P_r = \frac{\rho_g g H \bar{\alpha}^L}{2} + \rho_f g H \left[\theta - \frac{\bar{\alpha}^L}{2} \right] \tag{3.93}$$

Now for the liquid phase.

$$\begin{aligned} \langle\langle P_f \rangle\rangle - P_r &= \frac{\rho_g g H}{(1 - \bar{\alpha}^L)} [\bar{\alpha}^L \theta_1 - \bar{\alpha}^L \theta_2] + \frac{\rho_f g H}{(1 - \bar{\alpha}^L)} \left[\frac{1}{2} - \bar{\alpha}^L \theta_0 - \bar{\alpha}^L \theta_1 + \bar{\alpha}^L \theta_2 \right] \\ &= \frac{\rho_g g H}{(1 - \bar{\alpha}^L)} \left[\bar{\alpha}^L (1 - \theta_0) - \frac{\bar{\alpha}^L \bar{\alpha}^L}{2} \right] + \frac{\rho_f g H}{(1 - \bar{\alpha}^L)} \left[\frac{1}{2} - \bar{\alpha}^L \theta_0 - \bar{\alpha}^L + \bar{\alpha}^L \theta_0 + \frac{\bar{\alpha}^L \bar{\alpha}^L}{2} \right] \end{aligned} \quad (3.94)$$

Which simplifies to:

$$\langle\langle P_f \rangle\rangle - P_r = \frac{\rho_g g H}{(1 - \bar{\alpha}^L)} \left[\bar{\alpha}^L (1 - \theta) - \frac{\bar{\alpha}^L \bar{\alpha}^L}{2} \right] + \frac{\rho_f g H}{2} [1 - \bar{\alpha}^L] \quad (3.95)$$

One can see from the preceding equations that the gas phase pressure contains the collapsed gas pressure plus a term for the liquid phase that depends on the distribution parameter, while the liquid phase pressure contains the collapsed liquid pressure plus a term due to the presence of the gas phase. This physically makes sense as the pressure due to the hydrostatic head for a given phase cannot be less than the value of that phase alone.

The distribution parameter, θ , has a possible range of values of:

$$\frac{\bar{\alpha}^L}{2} \leq \theta \leq \frac{1}{2} \quad (3.96)$$

where $\theta = \frac{\bar{\alpha}^L}{2}$ corresponds to stratified flow while, in the other extreme where $\theta = \frac{1}{2}$, corresponds to the fully mixed flow condition.

4 MODEL RESULTS AND COMPARISON

4.1 AVERAGE PHASE PRESSURE BASED ON EXPERIMENTAL DATA

The theoretical values for the distribution parameters for both stratified and well mixed flow are plotted and compared to experimental data by Kocamustafaogullari (later known as Kojasoy), and his coworkers (Kocamustafaogullari and Wang, 1991; Kocamustafaogullari and Huang, 1994; Kocamustafaogullari et al., 1994; Riznic et al., 1996; Iskandrani and Kojasoy, 2001; Lewis et al., 2002) for horizontal two-phase flow. Data was obtained by scanning the various data plots and using the commercial program DigitizeIt ver. 1.5 to digitize the image and collect the data points from the graphs. The test conditions for the various authors are summarized in Table 4.1. Void fraction based on the area-averaged quantities given, the area-averaged void fraction calculated based on the homogenous flow assumption, and the calculated line-averaged void fraction along the vertical direction are also given within Table 4.1. The majority of the data is just within the bubbly flow regime based on the horizontal flow regime map of Mandhane (Mandhane et al., 1974). Only a couple of the data points given exist within the plug or slug flow regimes. Additional experimental data under different conditions would be beneficial.

Table 4.1: Experimental data test conditions

Author	Year	j_g	j_r	$\langle \alpha \rangle$ Reported	$\langle \alpha \rangle$ Calculated*	$\overline{\alpha}^L$ Calculated	Measurement Method
Kocamustafaogullari & Wang	1991	0.24	5.10	0.043	0.045	0.0382	Double Sensor Resistivity Probe
		0.25	3.74	0.057	0.063	0.067	
		0.53	4.67	0.087	0.102	0.093	
		0.51	3.77	0.105	0.119	0.115	
		0.71	3.83	0.151	0.156	0.160	
		1.03	3.74	0.183	0.216	0.186	
		1.34	4.98	0.204	0.212	0.188	
		1.59	4.36	0.226	0.267	0.220	
Kocamustafaogullari & Huang	1994	0.213	4.67	0.044	0.044	0.0469	Double Sensor Resistivity Probe
		0.419	4.67	0.085	0.082	0.0941	
		0.788	4.67	0.146	0.144	0.1479	
		1.21	4.67	0.2048	0.206	0.2030	
Kocamustafaogullari et al.	1994	0.22	5.00	0.042	0.042	0.025	Double Sensor Resistivity Probe
		0.43	4.98	0.080	0.080	0.079	
		0.61	4.98	0.111	0.109	0.115	
		1.00	4.98	0.167	0.167	0.168	
		1.25	5.01	0.204	0.200	0.207	
Riznic et al.	1996	0.55	1.65	-	0.25	0.247	Four Sensor Resistivity Probe
		1.10	1.65	-	0.4	0.401	
		2.20	1.65	-	0.571	0.480	
Iskandrani and Kojasoy	2001	0.25	3.8	-	0.062	0.069	Hot-Film Anemometry
		0.50	3.8	-	0.116	0.131	
		0.80	3.8	-	0.174	0.174	
		0.25	4.4	-	0.054	0.060	
		0.25	5.0	-	0.048	0.046	
		0.50	5.0	-	0.091	0.100	
		0.80	5.0	-	0.138	0.142	
Lewis et al. [†]	2002	0.55	1.65	-	0.25	-	Hot-Film Anemometry
		1.10	1.65	-	0.4	-	
		2.20	1.65	-	0.571	-	

* - Calculated based on the homogeneous flow assumption

† - Data is similar to Riznic et al. (1996). Used for verification of the hot-film anemometry technique

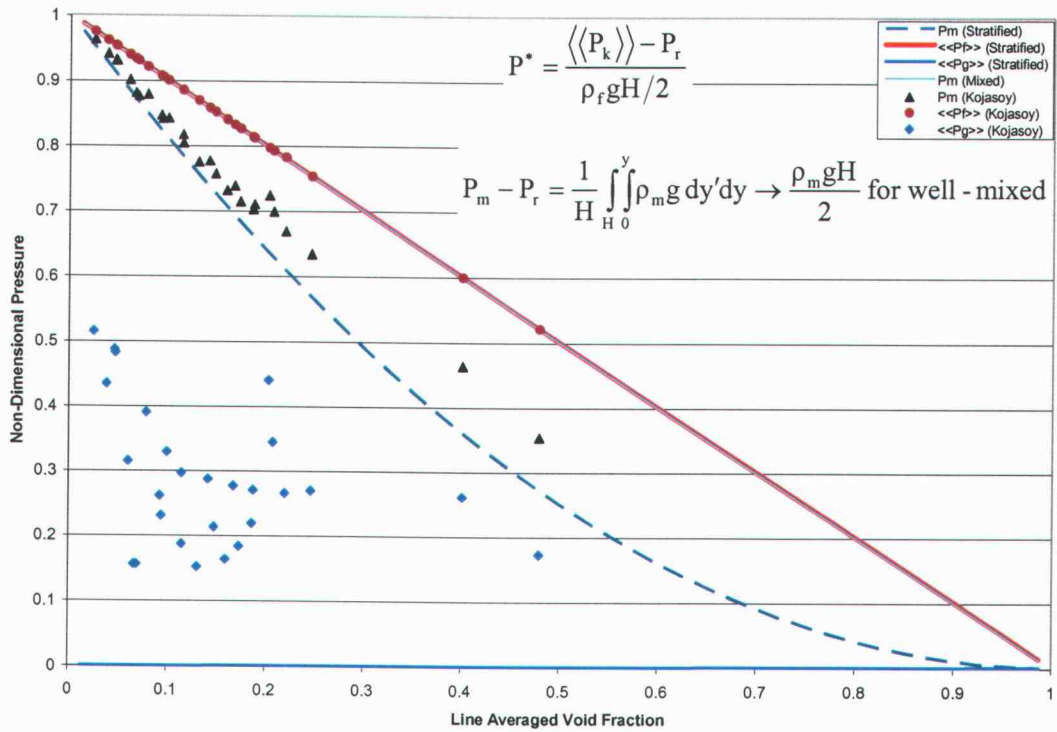


Figure 4.1: Comparison of theoretical vs. experimental pressure due to gravity force

From Figure 4.1, one can see the influence that the transverse gravity has on individual phase pressures. It can be seen that the liquid phase pressure for stratified flow is nearly equal to the pressure in the well-mixed flow case. This is because the density of the liquid phase is typically dominant so the majority of the head comes for the liquid phase. One will also note how the gas phase transverse pressure head is nearly zero. This is due to the fact that the gas sits on top on the liquid and has a very small density. This means that the pressure at the bottom of the gas layer is nearly the same as the top of the gas layer. Included in this figure is the phase pressure based upon the void fraction distribution measured by Kojasoy and his coworkers for horizontal bubbly and slug air-water flows. Typically these types of flows are assumed to be well-mixed ($\langle\langle P_g \rangle\rangle = \langle\langle P_f \rangle\rangle = \langle\langle P_m \rangle\rangle$). One can clearly see from the above figure that

this is not the case. If it were true that $\langle\langle P_g \rangle\rangle = \langle\langle P_f \rangle\rangle = \langle\langle P_m \rangle\rangle$, all of the data points would be on the P_m line. One can see that instead there is a distinct separation in pressures between the gas and liquid phases. This is due to the fact that buoyancy causes the bubbles to rise to near the top of the pipe. Because of this, the pressure difference is almost that of stratified flow, with all pressure are bounded between the stratified flow limit and the well-mixed flow condition. Because of this difference in pressures between the two phases, it is the goal of this dissertation to determine the impact that this pressure difference has on the stability of the one-dimensional two-fluid model for horizontal flows.

It is also beneficial to look at the pressure differences between the gas and the liquid phase to compare how the experimental data compares to the stratified and fully-mixed theoretical limits. The relative pressure difference between the two phases for stratified flow, experimental data, and the fully-mixed flow condition are shown in Figure 4.2. The pressure difference is scaled by the area-averaged liquid pressure in order to get a relative magnitude instead of an absolute pressure difference. This helps to compare data of different sized pipes and for different fluids directly. The plot shows that the pressure difference is always zero for the fully-mixed flow condition, as is expected. The stratified flow condition has a relative pressure difference of nearly one until high values of void fraction. This means that the gas pressure is small compared to the liquid pressure in this case. This is primarily due to the fact that water has a density that is nearly one-thousand times greater than that of air at atmospheric pressure and near room temperature. The pressure for the experimental data was based on local void fraction measurements and assuming constant densities of both fluids. It is seen that the pressure difference between the two phases is between forty percent and eighty-three percent of the pressure difference that would be seen for stratified flow (data mostly bubbly flow). This shows that accounting for the pressure difference between the two phases may improve the stability of the problem as it does in the case of stratified flow.

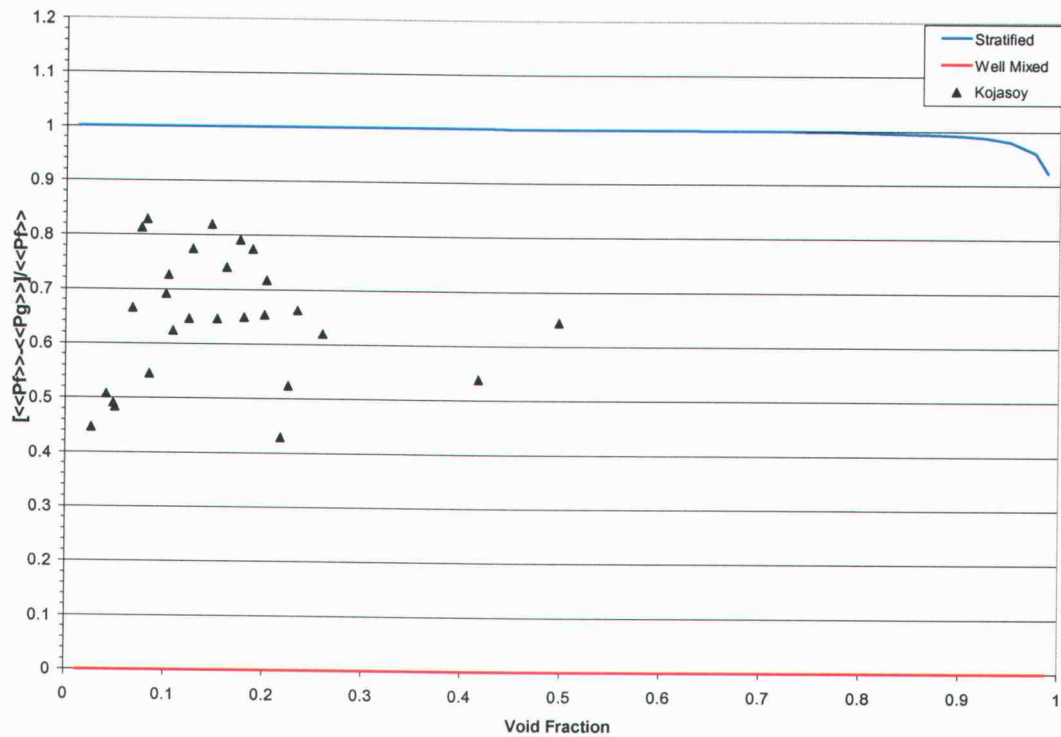


Figure 4.2: Relative pressure difference between two phases

4.2 DISTRIBUTION PARAMETER BASED ON EXPERIMENTAL DATA

In order to determine what value the phase distribution parameters may be under real types of flow, experimental data from other researchers will be used and the resultant phase distribution parameters will be calculated and compared to those of the stratified flow regime and those of the well-mixed bubbly flow regime. Figures 4.3 though 4.6 show some of the void fraction profiles obtained from Kojasoy and his colleagues (Kocamustafaogullari and Wang, 1991; Kocamustafaogullari and Huang, 1994; Kocamustafaogullari et al., 1994; Riznic et al., 1996; Iskandrani and Kojasoy, 2001; Lewis et al., 2002).

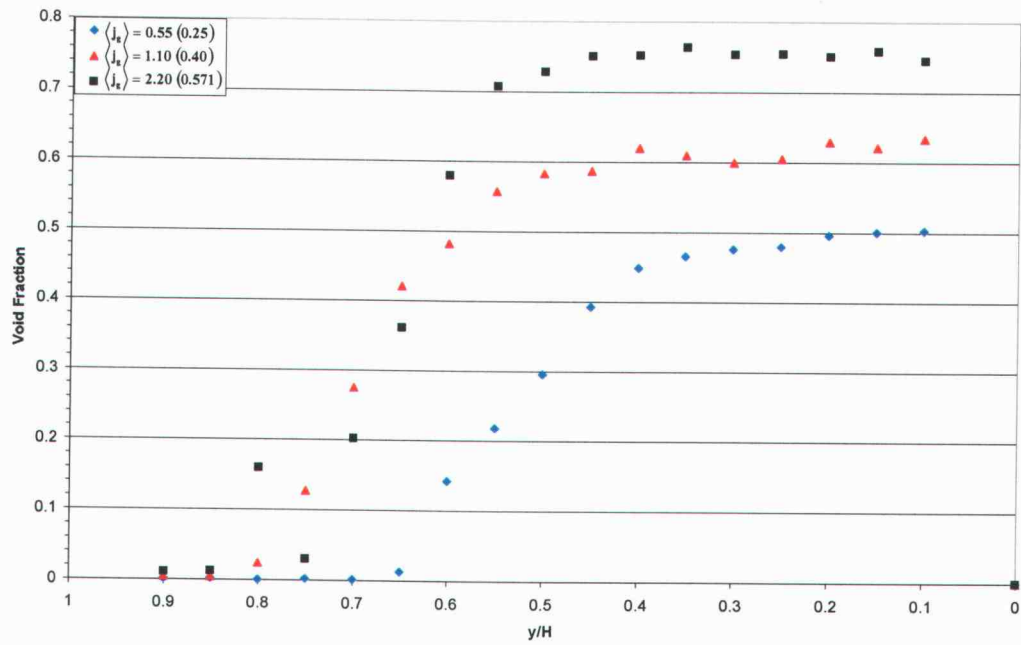


Figure 4.3: Experimental void fraction profiles, $\langle j_f \rangle = 1.65 \text{ m/s}$

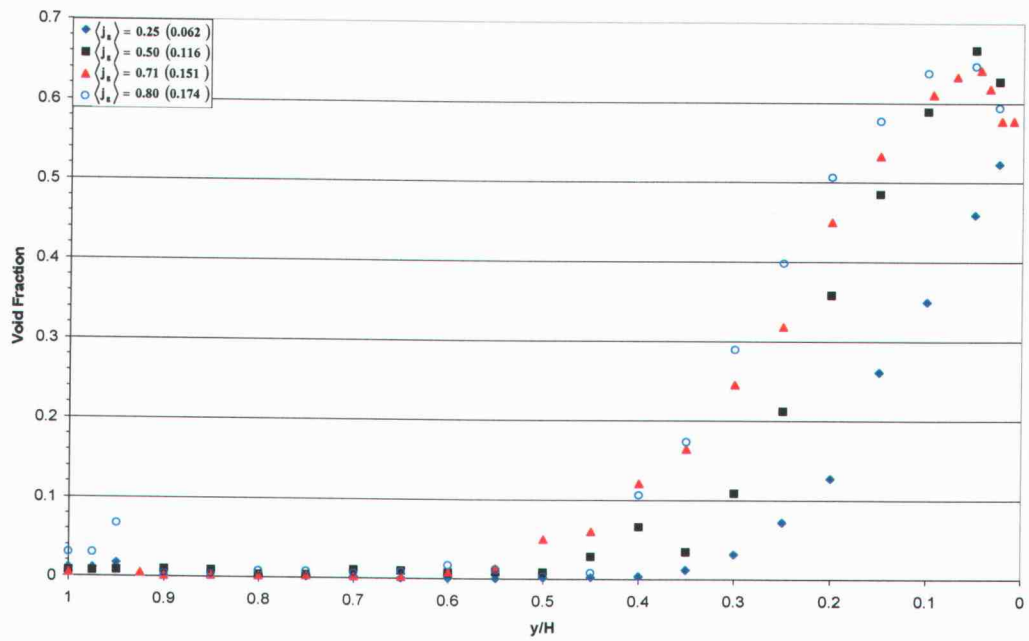


Figure 4.4: Experimental void fraction profiles, $\langle j_f \rangle = 3.8 \text{ m/s}$

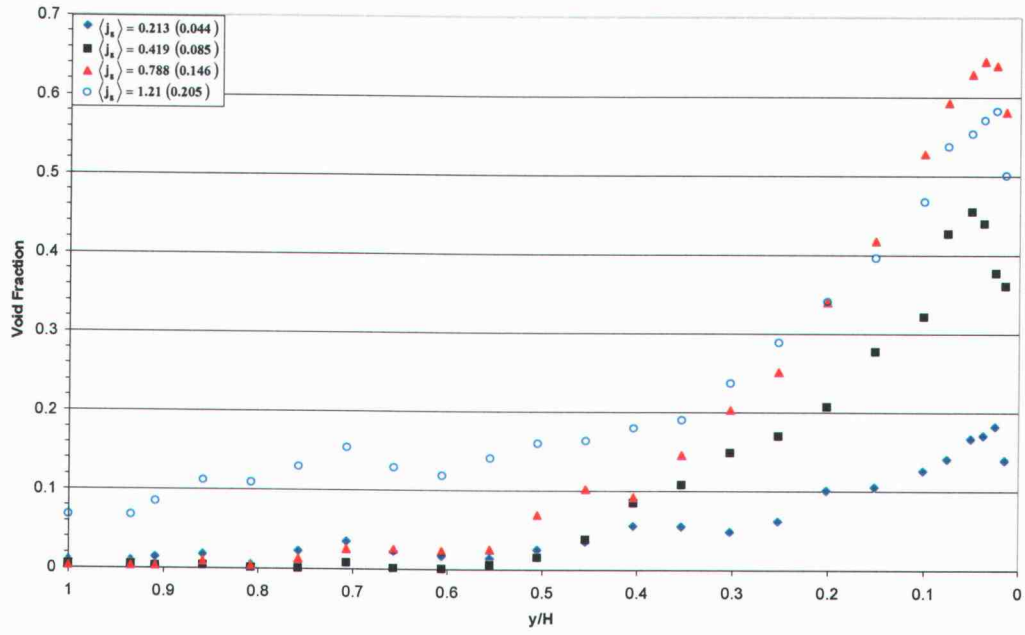


Figure 4.5: Experimental void fraction profiles, $\langle j_f \rangle = 4.67 \text{ m/s}$

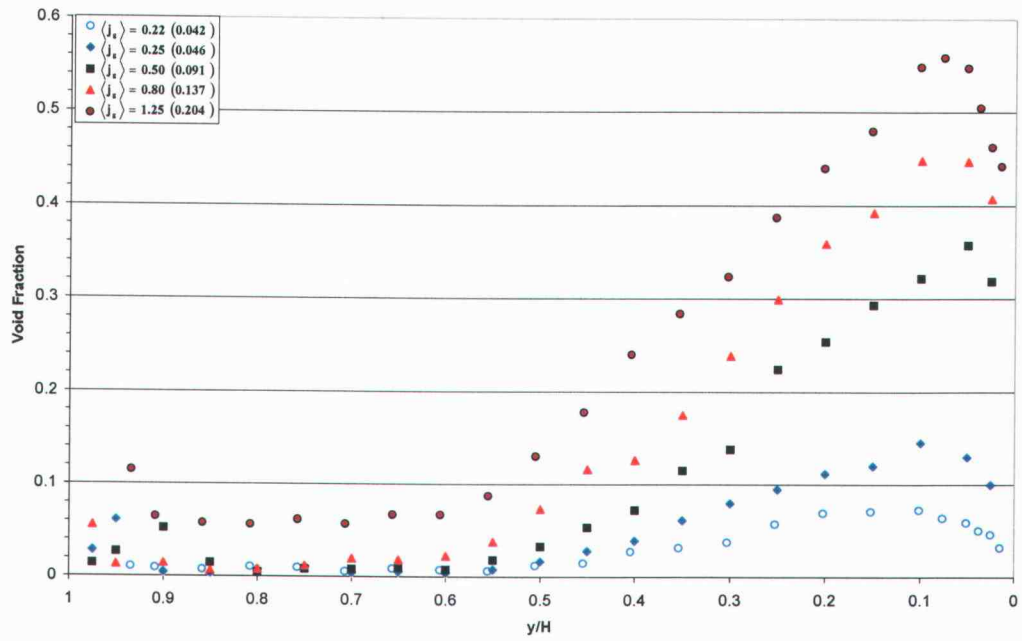


Figure 4.6: Experimental void fraction profiles, $\langle j_f \rangle = 5.0 \text{ m/s}$

One can clearly see how the void fraction profile can evolve in the above figures. In the first case, Figure 4.3, slug and plug flow exists. The profile is similar in shape to the step profile found in the stratified flow case, except the void fraction does not equal one at the top of the pipe and there is a continuous transition from the high void fraction at the top of the pipe to the low transition at the bottom of the pipe. For stratified flow, one would expect the transition from the high void fraction area to the low void fraction region to be very sharp. As the liquid superficial velocity is increased, the large bubbles found in the case of plug and slug flow can no longer exist. This is because the liquid turbulence force overcomes the surface tension force found in the larger bubbles, causing the large bubble to break apart. This occurs above about a liquid superficial velocity of 4 m/s for horizontal air/water flow at atmospheric pressure and room temperature.

When bubbly flow is formed, a sharp peak in the void fraction is seen near the top of the pipe. This peak reaches a maximum value of about 0.65. This can be most clearly seen in Figure 4.4. This corresponds to the maximum packing fraction for nearly spherical bubbles. Once this point is reached, the bubbles are forced more towards the bottom of the pipe, widening the void peak in the process. Once the entire pipe reaches its maximum packing fraction, bubbles are forced to distort and coalesce, eventually creating annular flow.

Table 4.2 shows the average pressure of each phase based on the void fraction profiles given and assuming that the densities are constant for both phases. Columns of non-dimensionalized pressures are also given. This pressure is relative to the pipe completely full of liquid. This way, one can compare relative pressures of each phase for different sized pipes and different density fluids directly.

$$\langle\langle P_k \rangle\rangle^* = \frac{\langle\langle P_k \rangle\rangle - P_r}{\rho_f g H / 2} \quad (4.1)$$

Table 4.2: Pressure of gas and liquid phases based on experimental data

j_g	j_f	$\langle \alpha \rangle$	$\bar{\alpha}^L$	$\langle\langle P_m \rangle\rangle$	$\langle\langle P_f \rangle\rangle$	$\langle\langle P_g \rangle\rangle$	$\langle\langle P_m \rangle\rangle^*$	$\langle\langle P_f \rangle\rangle^*$	$\langle\langle P_g \rangle\rangle^*$
0.22	5	0.042	0.026	236.93	244.03	74.96	0.96	0.99	0.30
0.213	4.67	0.044	0.050	228.92	233.64	126.34	0.93	0.95	0.51
0.24	5.1	0.043	0.041	231.54	237.68	94.69	0.94	0.97	0.39
0.25	5	-	0.048	229.25	234.91	116.01	0.93	0.96	0.47
0.25	4.4	-	0.067	221.75	229.47	86.55	0.90	0.93	0.35
0.25	3.8	-	0.081	215.67	227.03	43.01	0.88	0.92	0.17
0.43	4.98	0.08	0.084	216.19	226.78	94.48	0.88	0.92	0.38
0.53	4.67	0.087	0.101	208.42	221.76	68.40	0.85	0.90	0.28
0.419	4.67	0.085	0.104	207.16	220.57	62.76	0.84	0.90	0.26
0.61	4.98	0.111	0.124	201.10	216.81	75.29	0.82	0.88	0.31
0.5	3.8	-	0.147	190.80	210.33	41.96	0.78	0.86	0.17
0.5	5	-	0.108	207.30	219.14	88.89	0.84	0.89	0.36
0.8	5	-	0.153	191.17	210.15	72.54	0.78	0.85	0.30
0.788	4.67	0.146	0.162	186.31	209.10	53.04	0.76	0.85	0.22
1	4.98	0.167	0.180	181.81	204.63	68.18	0.74	0.83	0.28
0.8	3.8	-	0.188	175.86	203.41	44.99	0.72	0.83	0.18
0.25	3.74	0.057	0.076	216.79	227.19	44.73	0.88	0.92	0.18
0.51	3.77	0.105	0.128	197.99	215.33	50.24	0.81	0.88	0.20
0.71	3.83	0.151	0.176	180.08	204.54	42.55	0.73	0.83	0.17
1.03	3.74	0.183	0.202	172.89	199.34	54.83	0.70	0.81	0.22
1.25	5.01	0.204	0.225	172.08	194.11	86.08	0.70	0.79	0.35
1.21	4.67	0.2048	0.217	178.17	196.45	107.19	0.72	0.80	0.44
1.34	4.98	0.204	0.201	174.78	203.90	61.15	0.71	0.83	0.25
1.59	4.36	0.226	0.234	164.57	194.05	63.58	0.67	0.79	0.26
0.55	1.65	-	0.259	156.01	186.24	65.32	0.63	0.76	0.27
1.1	1.65	-	0.417	114.03	147.19	64.28	0.46	0.60	0.26
2.2	1.65	-	0.498	87.06	155.63	35.63	0.35	0.63	0.14

4.3 DISTRIBUTION PARAMETER SIMPLIFICATION VERIFICATION

In the previous section, it was shown theoretically how the distribution parameters can be related to one another and simplified down to a single parameter. This section will use the void fraction profile data gathered by Kojasoy and his coworkers (Kocamustafaogullari and Wang, 1991; Kocamustafaogullari and Huang, 1994; Kocamustafaogullari et al., 1994; Riznic et al., 1996; Iskandrani and Kojasoy, 2001; Lewis et al., 2002) to calculate what each distribution parameter equals and see how they are related. Data was obtained by scanning the various data plots and using the commercial program DigitizeIt ver. 1.5 to digitize the image and collect the data points from the graphs. The distribution parameters were then calculated by performing a numerical integration technique known as the trapezoidal rule. Since there are not values of void fraction obtained at the walls, it was assumed that the values of void fraction at the wall are the same as the values obtained closest to the wall. The values obtained for the three distribution parameters are plotted in Figures 4.4 through 4.6. One can see that the data is bounded between the stratified and fully mixed flow extremes as expected. One will also note that values of the θ_2 distribution parameter do indeed collapse to the $\theta_2 = \frac{\bar{\alpha}^L}{2}$ value.

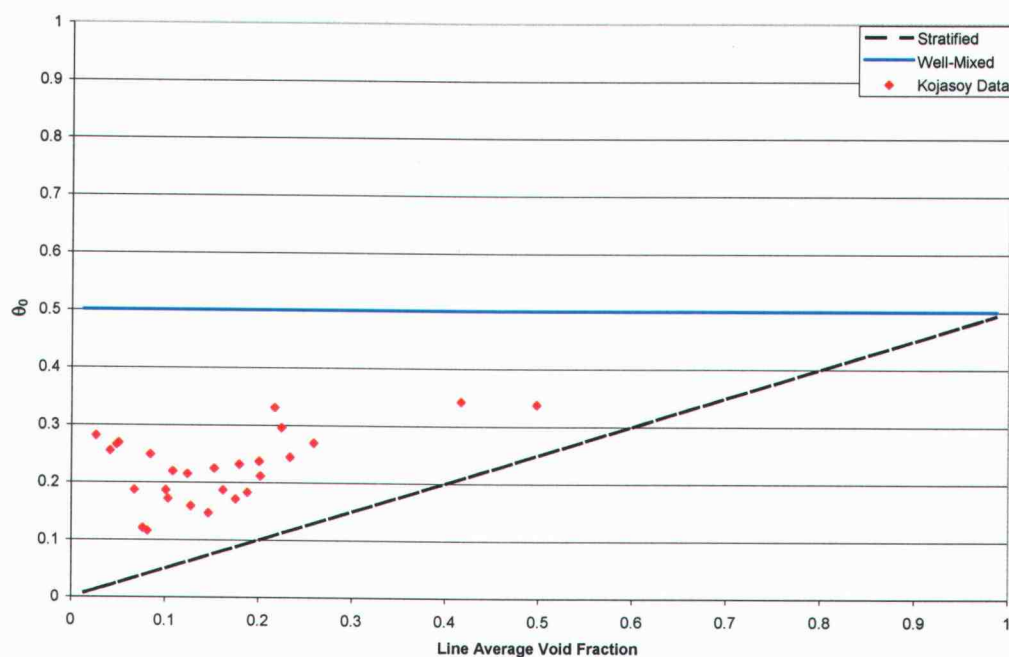


Figure 4.7: Comparison of the θ_0 distribution parameter with experimental data

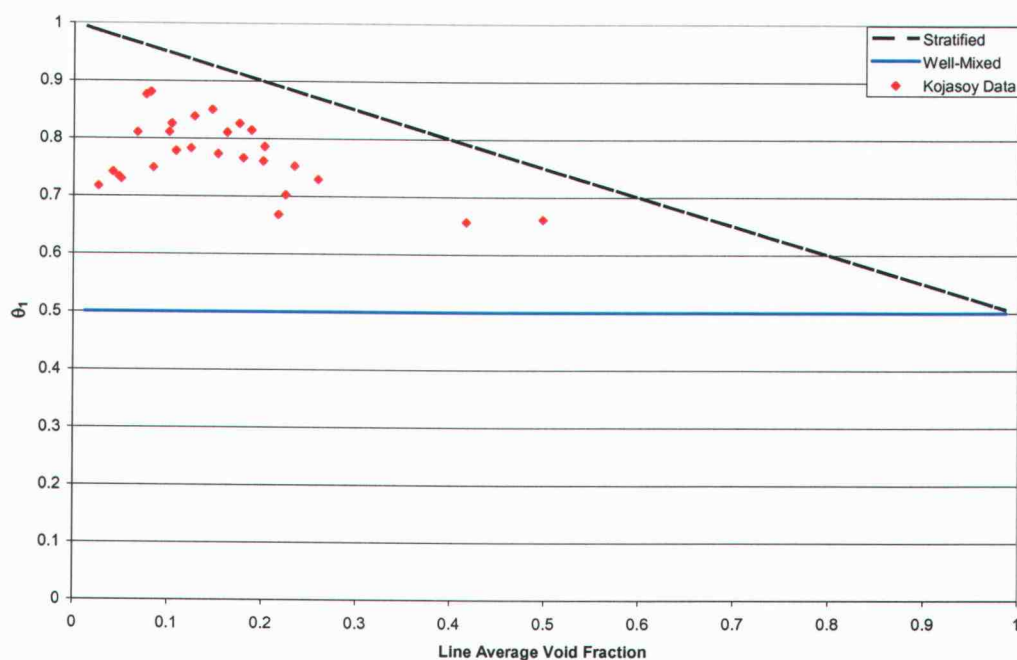


Figure 4.8: Comparison of the θ_1 distribution parameter with experimental data

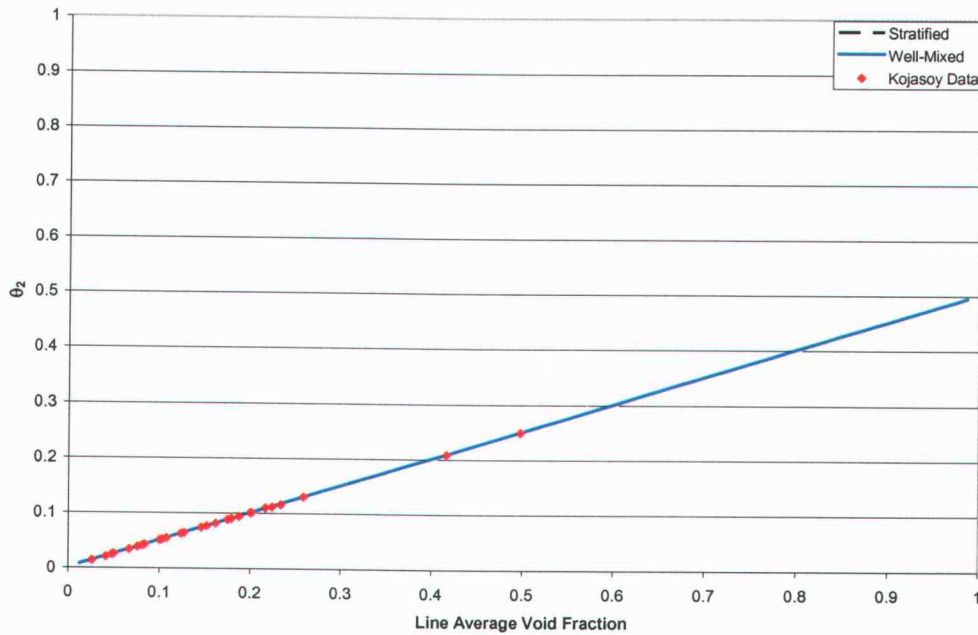


Figure 4.9: Comparison of the θ_2 distribution parameter with experimental data

A comparison between experimentally determined values of the distribution parameters and the theoretical values found from the simplification analysis is shown in Table 4.3. It can be seen that $\theta_0 + \theta_1 = 1$ or $\theta_0 = 1 - \theta_1$ is nearly exact. The slight departure from one can be attributed to round-off error and the limitations of the numerical integration that was performed. The other simplification, $\theta_2 = \frac{\bar{\alpha}^L}{2}$, is also seen to be true. With the number of significant digits shown, it is seen that θ_2 is indeed equal to $\frac{\bar{\alpha}^L}{2}$. This substantiates the theoretical values found during the simplification analysis. Because of this, the model can in fact be reduced to a single distribution parameter. This makes the model more useful and easier to implement as well as allowing one to find ways of modeling the phase distribution parameter with greater ease.

Table 4.3: Comparison of experimentally obtained distribution parameters and their theoretical values

j_g	j_f	$\bar{\alpha}^L$	θ_0	θ_1	$\theta_0 + \theta_1$	θ_2	$\bar{\alpha}^L/2$
0.22	5	0.026	0.281	0.717	0.998	0.013	0.013
0.213	4.67	0.050	0.269	0.730	0.999	0.025	0.025
0.24	5.1	0.041	0.255	0.742	0.997	0.020	0.021
0.25	5	0.048	0.265	0.734	0.999	0.024	0.024
0.25	4.4	0.067	0.187	0.811	0.998	0.034	0.034
0.25	3.8	0.081	0.116	0.881	0.996	0.041	0.041
0.43	4.98	0.084	0.249	0.750	0.999	0.042	0.042
0.53	4.67	0.101	0.187	0.811	0.998	0.050	0.050
0.419	4.67	0.104	0.172	0.826	0.998	0.052	0.052
0.61	4.98	0.124	0.215	0.783	0.998	0.062	0.062
0.5	3.8	0.147	0.147	0.850	0.997	0.073	0.073
0.5	5	0.108	0.220	0.778	0.998	0.054	0.054
0.8	5	0.153	0.225	0.774	0.998	0.076	0.076
0.788	4.67	0.162	0.187	0.811	0.998	0.081	0.081
1	4.98	0.180	0.232	0.766	0.998	0.090	0.090
0.8	3.8	0.188	0.183	0.815	0.998	0.094	0.094
0.25	3.74	0.076	0.121	0.876	0.997	0.038	0.038
0.51	3.77	0.128	0.159	0.838	0.998	0.064	0.064
0.71	3.83	0.176	0.172	0.826	0.998	0.088	0.088
1.03	3.74	0.202	0.212	0.786	0.998	0.101	0.101
1.25	5.01	0.225	0.296	0.703	0.998	0.112	0.112
1.21	4.67	0.217	0.331	0.669	0.999	0.109	0.109
1.34	4.98	0.201	0.237	0.761	0.999	0.101	0.100
1.59	4.36	0.234	0.245	0.753	0.998	0.115	0.117
0.55	1.65	0.259	0.269	0.730	0.999	0.130	0.130
1.1	1.65	0.417	0.342	0.657	0.999	0.208	0.208
2.2	1.65	0.498	0.337	0.662	0.999	0.249	0.249

4.4 EFFECTS OF DISTRIBUTION PARAMETER ON STABILITY

An important part of any two-fluid model development is how the model affects the stability of the problem. First, it is important that the model remains numerically stable and the solution is consistent with the method used to solve the problem (hyperbolic). Another type of stability is known as a flow instability. This is caused when the low pressure area above surface waves becomes low enough due to the Bernoulli effect to overcome the gravity force. When this occurs, the wave crest is pulled towards the top of the pipe and intermittent flow is then created.

4.4.1 Phase transition

A linear perturbation analysis should be performed in order to determine what influence the unified model with its associated phase distribution parameters has upon the transition point from stratified wavy flow to intermittent flow. For the model to be usable, it is important that the predicted transition point agrees with that determined from experimental results. In order to truly determine the influence that the phase distribution parameter has on the transition between stratified wavy and intermittent flow, one must know the distribution parameter and how it changes to perturbations in quantities such as void fraction, superficial liquid velocity, and superficial gas velocity. Since this is unknown at this time, the linear perturbation analysis to determine the transition between stratified flow and intermittent flow will be performed at a later time.

4.4.2 Characteristic analysis

As part of the unified model development and comparison, the numerical stability of the new model will be determined in order to see under what conditions the model remains numerically stable and consistent. This is the main motivation to the work performed within the scope of this dissertation. The goal is to create a version of the

one-dimensional two-fluid model that does not suffer from the ill-posed nature that the standard one-dimensional two-fluid model has for unequal velocities.

Commonly, one may apply the method of characteristics to determine the numerical stability boundary (i.e. hyperbolic, parabolic, or elliptic) for a set of governing differential equations. Because we are dealing with a convective type problem, we need the set of governing equations to remain hyperbolic in order to properly solve. This is where a problem is created using the one-dimensional two-fluid model in current form. Because of the assumptions placed on the model, the problem is only boarder line stable (parabolic) when the gas and liquid velocities are equal. In the case of unequal velocities, the problem has complex roots and is therefore an elliptic problem and can no longer be solved as a convection problem. This section will demonstrate how, by including the phase distribution parameter and the resulting difference in void weighted pressures between the two phases, the problem can remain hyperbolic over a wide range of conditions (increased numerical stability). The equations are now simplified for the characteristic analysis with brackets dropped to make equations more clear.

Continuity

$$\begin{aligned} \frac{\partial \alpha}{\partial t} + u_g \frac{\partial \alpha}{\partial x} + \alpha \frac{\partial u_g}{\partial x} &= 0 \\ -\frac{\partial \alpha}{\partial t} - u_f \frac{\partial \alpha}{\partial x} + (1 - \alpha) \frac{\partial u_f}{\partial x} &= 0 \end{aligned} \quad (4.2)$$

Momentum (stratified)

$$\begin{aligned} \alpha \rho_g \frac{\partial u_g}{\partial t} + \rho_g u_g \frac{\partial \alpha}{\partial t} + \rho_g u_g \frac{\partial \alpha}{\partial x} + 2\alpha \rho_g u_g \frac{\partial u_g}{\partial x} + \alpha \frac{\partial P_g}{\partial x} + (P_g - P_f) \frac{\partial \alpha}{\partial x} &= 0 \\ (1 - \alpha) \rho_f \frac{\partial u_f}{\partial t} - \rho_f u_f \frac{\partial \alpha}{\partial t} - \rho_f u_f \frac{\partial \alpha}{\partial x} + 2(1 - \alpha) \rho_f u_f \frac{\partial u_f}{\partial x} + (1 - \alpha) \frac{\partial P_f}{\partial x} - (P_f - P_g) \frac{\partial \alpha}{\partial x} &= 0 \end{aligned} \quad (4.3)$$

Assume that $\frac{\partial P_g}{\partial x} = \frac{\partial P_f}{\partial x} = \frac{\partial P_m}{\partial x}$ in order to reduce the number of unknowns to equal

the number of equations. Now to write the continuity equations and the momentum equations in matrix form.

$$\mathbf{x} = \begin{bmatrix} \alpha \\ u_g \\ u_f \\ P_m \end{bmatrix} \quad (4.4)$$

$$[\mathbf{A}] \frac{\partial}{\partial t} \mathbf{x} + [\mathbf{B}] \frac{\partial}{\partial x} \mathbf{x} = [\mathbf{C}] \quad (4.5)$$

Matrix $[\mathbf{A}]$ becomes:

$$[\mathbf{A}] = \begin{bmatrix} 1 & 0 & 0 & 0 \\ -1 & 0 & 0 & 0 \\ \rho_g u_g & \alpha \rho_g & 0 & 0 \\ -\rho_f u_f & 0 & (1-\alpha)\rho_f & 0 \end{bmatrix} \quad (4.6)$$

while matrix $[\mathbf{B}]$ is:

$$[\mathbf{B}] = \begin{bmatrix} u_g & \alpha & 0 & 0 \\ -u_f & 0 & (1-\alpha) & 0 \\ \rho_g u_g u_g - (P_{gi} - P_g) & 2\alpha \rho_g u_g & 0 & \alpha \\ -\rho_f u_f u_f + (P_{fi} - P_f) & 0 & 2(1-\alpha)\rho_f u_f & (1-\alpha) \end{bmatrix} \quad (4.7)$$

Let the terms $(P_{gi} - P_g)$ and $(P_{fi} - P_f)$ be known as ΔP_1 and ΔP_2 , respectively for simplification purposes. In order to perform the method of characteristics, we write the matrix form of the governing equations as:

$$[\mathbf{A}] \lambda - [\mathbf{B}] \quad (4.8)$$

Where λ contains the eigenvalues of the equations. The problem is solved by taking the determinant and setting it equal to zero.

$$\text{Det}[\mathbf{A}\lambda - \mathbf{B}] = 0 \quad (4.9)$$

For this case, we get:

$$\text{Det} \begin{bmatrix} \lambda - u_g & -\alpha & 0 & 0 \\ -\lambda + u_f & 0 & -(1-\alpha) & 0 \\ \rho_g u_g (\lambda - u_g) - (P_g - P_i) & \alpha \rho_g (\lambda - 2u_g) & 0 & -\alpha \\ -\rho_f u_f (\lambda - u_f) + (P_f - P_i) & 0 & (1-\alpha) \rho_f (\lambda - 2u_f) & -(1-\alpha) \end{bmatrix} = 0 \quad (4.10)$$

$$\text{DET} [\mathbf{A}\lambda - \mathbf{B}] = \alpha(1-\alpha) \left[(\Delta P_1 - \rho_g (u_g - \lambda)^2)(1-\alpha) + (\Delta P_2 - \rho_f (u_f - \lambda)^2)\alpha \right] \quad (4.11)$$

If we assume that the pressures of each phase are equal ($\Delta P_1 = \Delta P_2 = 0$), we get the following relation:

$$\text{DET} [\mathbf{A}\lambda - \mathbf{B}] = -\alpha(1-\alpha) \left[(1-\alpha) \rho_g (u_g - \lambda)^2 + \alpha \rho_f (u_f - \lambda)^2 \right] \quad (4.12)$$

This equation has been shown that it can only have a real solution under the condition that $u_g = u_f$. In the case of stratified flow, the pressure of each phase relative to the interface pressure is shown to be:

$$\Delta P_1 = -\frac{\rho_g g H \alpha}{2} \quad \Delta P_2 = \frac{\rho_f g H (1-\alpha)}{2} \quad (4.13)$$

By accounting for this difference between the two phase pressures, the following relation is obtained:

$$\frac{g H \alpha}{2} [\rho_f - \rho_g] = \rho_g u_g^2 - 2\rho_g \lambda u_g + \rho_g \lambda^2 + \frac{\rho_f \alpha}{(1-\alpha)} [\rho_g u_f^2 - 2\rho_f \lambda u_f + \rho_f \lambda^2] \quad (4.14)$$

or

$$0 = \lambda^2 \left(\rho_g + \frac{\rho_f \alpha}{(1-\alpha)} \right) - \lambda \left(2\rho_g u_g + \frac{2\rho_f u_f \alpha}{(1-\alpha)} \right) + \rho_g u_g^2 + \frac{\alpha \rho_f u_f^2}{(1-\alpha)} - \frac{g H \alpha}{2} [\rho_f - \rho_g] \quad (4.15)$$

The roots of this equation can now be found using the quadratic formula.

$$\lambda = \frac{b \pm \sqrt{b^2 - 4ac}}{2a}$$

$$= \frac{\left(\rho_g u_g + \frac{\rho_f u_f \alpha}{(1-\alpha)} \right) \pm \frac{1}{2} \sqrt{-\frac{4\alpha \rho_g \rho_f}{(1-\alpha)} (u_f - u_g)^2 + 2gH[\rho_f - \rho_g] \left(\rho_g \alpha + \frac{\rho_f \alpha^2}{(1-\alpha)} \right)}}{\left(\rho_g + \frac{\rho_f \alpha}{(1-\alpha)} \right)} \quad (4.16)$$

The primary interest lies in the term under the radical or in other words, $b^2 - 4ac$. This is because it is this term that determines what type of problem it is (hyperbolic, parabolic, or elliptic). These terms are classified as follows:

hyperbolic $b^2 - 4ac > 0$ real distinct roots

parabolic $b^2 - 4ac = 0$ real repeated roots

elliptic $b^2 - 4ac < 0$ imaginary roots

By rearranging the portion under the radical and solving for $(u_g - u_f)^2$, one gets the following relation:

$$(u_g - u_f)^2 = \frac{gH\alpha}{2\rho_g} [\rho_f - \rho_g] \left(\frac{\rho_g}{\rho_f} \frac{(1-\alpha)}{\alpha} + 1 \right) \quad (4.17)$$

if $\rho_g \ll \rho_f$

$$(u_g - u_f) < \pm \sqrt{\frac{gH\alpha}{2\rho_g} [\rho_f - \rho_g]} \quad (4.18)$$

This shows how the gravity term helps to stabilize the flow. This result is similar to that achieved using the Kelvin-Helmholtz instability criterion.

In order to solve the characteristic equation in general for different values of the distribution parameter, we need to know the value of the interface pressure. For well mixed flow with the absence of surface tension, the average interface pressure should

equal the average gas and average liquid pressure or $\langle\langle P_i \rangle\rangle = \langle\langle P_f \rangle\rangle = \langle\langle P_g \rangle\rangle$. In the other extreme, for stratified flow, it is known that $\langle\langle P_i \rangle\rangle = \langle\langle P_g \rangle\rangle + \frac{\rho_g g H \alpha}{2} = \langle\langle P_f \rangle\rangle - \frac{\rho_f g H (1 - \alpha)}{2}$.

Other types of flows should be somewhere between these two limits. Because the interface pressure only occurs where an interface is present, it would make sense that the average interface pressure should be weighted by interfacial area concentration (area of interface per volume). For a uniform distribution of bubbles, the average interfacial pressure can be written as:

$$\langle\langle P_i \rangle\rangle = \frac{\int_H P_i \alpha dy}{\int_H \alpha dy} \quad (4.19)$$

If the bubbles are spherical, the void fraction can be related to the interfacial area concentration as:

$$a_i = \frac{6\alpha}{d_{sm}} \quad (4.20)$$

Substituting into the previous equation, we get:

$$\langle\langle P_i \rangle\rangle = \frac{\int_H P_i \frac{d_{sm} a_i}{6} dy}{\int_H \frac{d_{sm} a_i}{6} dy} \rightarrow \frac{\int_H P_i d_{sm} a_i dy}{\int_H d_{sm} a_i dy} \quad (4.21)$$

This type of expression makes more sense to use than using local void fraction because the interface pressure is a surface quantity instead of a volume quantity.

However, it is difficult to calculate local interfacial area concentration and how interfacial area concentration relates to void fraction for most general two-phase flow conditions. To overcome this difficulty so that the characteristic equation can be solved, an assumption can be made. By examining the relationship between average interfacial pressure and average gas and liquid phase pressures for well-mixed and

stratified flow conditions, one can see that $\langle\langle P_i \rangle\rangle$ can range from $\langle\langle P_i \rangle\rangle = \langle\langle P_g \rangle\rangle$ to $\langle\langle P_i \rangle\rangle = \langle\langle P_g \rangle\rangle + \frac{\rho_g g H \alpha}{2}$, respectively. Because the term, $\frac{\rho_g g H \alpha}{2}$, tends to be small compared to system pressure and to the liquid head, one can assume that $\langle\langle P_i \rangle\rangle = \langle\langle P_g \rangle\rangle$ for simplicity sake. With this assumption in place the characteristic analysis can be performed for general void fraction distributions. The characteristic matrix becomes:

$$\text{Det} \begin{bmatrix} \lambda - u_g & -\alpha & 0 & 0 \\ -\lambda + u_f & 0 & -(1-\alpha) & 0 \\ \rho_g u_g (\lambda - u_g) & \alpha \rho_g (\lambda - 2u_g) & 0 & -\alpha \\ -\rho_f u_f (\lambda - u_f) + (P_f - P_g) & 0 & (1-\alpha) \rho_f (\lambda - 2u_f) & -(1-\alpha) \end{bmatrix} = 0 \quad (4.22)$$

The determinant becomes:

$$\text{DET} [\mathbf{A}\lambda - \mathbf{B}] = -\alpha(1-\alpha) \left[\rho_g (u_g - \lambda)^2 (1-\alpha) - ((P_f - P_g) - \rho_f (u_f - \lambda)^2) \alpha \right] = 0 \quad (4.23)$$

Rearranging, the determinant can be written as:

$$\rightarrow \left[\rho_g (u_g^2 + \lambda^2 - 2\lambda u_g) (1-\alpha) - (P_f - P_g) \alpha + \rho_f (u_f^2 + \lambda^2 - 2\lambda u_f) \alpha \right] = 0 \quad (4.24)$$

$$\rightarrow \left[\rho_g (1-\alpha) + \rho_f \alpha \right] \lambda^2 - \left[2\rho_g u_g (1-\alpha) + 2\rho_f u_f \alpha \right] \lambda - (P_f - P_g) \alpha + \rho_g u_g^2 (1-\alpha) + \rho_f u_f^2 \alpha = 0$$

The term $b^2 - 4ac$, becomes:

$$b^2 - 4ac = \left[2\rho_g u_g (1-\alpha) + 2\rho_f u_f \alpha \right]^2 - 4 \left[\rho_g (1-\alpha) + \rho_f \alpha \right] \left[-(P_f - P_g) \alpha + \rho_g u_g^2 (1-\alpha) + \rho_f u_f^2 \alpha \right] = 0 \quad (4.25)$$

For this problem to remain hyperbolic, the condition $b^2 - 4ac > 0$ must be met. For this case, this means that:

$$\begin{aligned} & \rho_g^2 u_g^2 (1-\alpha)^2 + 2\rho_f u_f \alpha \rho_g u_g (1-\alpha) + \rho_f^2 u_f^2 \alpha^2 \\ & + (P_f - P_g) \rho_g \alpha (1-\alpha) - \rho_g^2 u_g^2 (1-\alpha)^2 - \rho_f u_f^2 \rho_g (1-\alpha) \alpha \\ & + (P_f - P_g) \rho_f \alpha^2 - \rho_g u_g^2 \rho_f \alpha (1-\alpha) - \rho_f u_f^2 \rho_f \alpha^2 > 0 \end{aligned} \quad (4.26)$$

Which reduces to:

$$2\rho_f u_f \alpha \rho_g u_g (1-\alpha) + (P_f - P_g) \rho_g (1-\alpha) \alpha - \rho_f u_f^2 \rho_g (1-\alpha) \alpha + (P_f - P_g) \rho_f \alpha^2 - \rho_g u_g^2 \rho_f \alpha (1-\alpha) > 0 \quad (4.27)$$

Rearranging, the following relation is obtained:

$$(u_g - u_f)^2 \leq (P_f - P_g) \alpha \frac{(\rho_f \alpha + \rho_g (1-\alpha))}{\rho_f \rho_g (1-\alpha) \alpha} \rightarrow (u_g - u_f) \leq \pm \sqrt{(P_f - P_g) \alpha \frac{\rho_f \alpha + \rho_g (1-\alpha)}{\rho_f \rho_g (1-\alpha) \alpha}} \quad (4.28)$$

Substituting in the relations for the phase pressures with the distribution parameter included, the following criterion is found:

$$(u_g - u_f) \leq \pm \sqrt{(P_f - P_g) \alpha \frac{\rho_f \alpha + \rho_g (1-\alpha)}{\rho_f \rho_g (1-\alpha) \alpha}} \quad (4.29)$$

Substituting the definitions for P_f and P_g , the following criterion is found.

$$(u_g - u_f) \leq \pm \sqrt{\left(\left[\frac{\rho_g g H \bar{\alpha}^L}{(1-\bar{\alpha}^L)} \left[(1-\theta) - \frac{\bar{\alpha}^L}{2} \right] + \frac{\rho_f g H}{2} [1 - \bar{\alpha}^L] + P_r \right] - \left[\frac{\rho_g g H \bar{\alpha}^L}{2} + \rho_f g H \left[\theta - \frac{\bar{\alpha}^L}{2} \right] + P_r \right] \right) \alpha \frac{\rho_f \alpha + \rho_g (1-\alpha)}{\rho_f \rho_g (1-\alpha) \alpha}} \quad (4.30)$$

If a rectangular channel is assumed for simplicity, so that it may be assumed that $\bar{\alpha}^L = \langle \alpha \rangle$, the limit for the problem to be hyperbolic is:

$$(u_g - u_f) \leq \pm \sqrt{\frac{g H \alpha}{\rho_g (1-\alpha)} \left(\frac{\rho_g \alpha}{2} \left[\frac{2(1-\theta)}{(1-\alpha)} - \frac{\alpha}{(1-\alpha)} - 1 \right] + \frac{\rho_f [1-\alpha]}{2} \left[1 - \frac{[2\theta - \alpha]}{[1-\alpha]} \right] \right) \left(1 + \frac{\rho_g (1-\alpha)}{\rho_f \alpha} \right)} \quad (4.31)$$

It can be seen that the reference pressure, P_r , drops out of the equation. When $\theta = \frac{\bar{\alpha}^L}{2}$, corresponds to stratified flow while in the other extreme where $\theta = \frac{1}{2}$ corresponds to the fully-mixed flow condition.

$$\begin{aligned}
(u_g - u_f) &\leq \pm \sqrt{\frac{gH\alpha}{\rho_g(1-\alpha)} \left(\frac{\rho_g\alpha}{2} \left[\frac{2\left(1-\frac{1}{2}\right)}{(1-\alpha)} - \frac{\alpha}{(1-\alpha)} - 1 \right] + \frac{\rho_f[1-\alpha]}{2} \left[1 - \frac{[1-\alpha]}{[1-\alpha]} \right] \right) \left(1 + \frac{\rho_g(1-\alpha)}{\rho_f\alpha} \right)} \\
&\rightarrow \pm \sqrt{\frac{gH\alpha}{\rho_g(1-\alpha)} \left(\frac{\rho_g\alpha}{2} \left[\frac{1-\alpha}{(1-\alpha)} - 1 \right] + \frac{\rho_f[1-\alpha]}{2} \left[1 - \frac{[1-\alpha]}{[1-\alpha]} \right] \right) \left(1 + \frac{\rho_g(1-\alpha)}{\rho_f\alpha} \right)} \\
&\rightarrow (u_g - u_f) \leq 0
\end{aligned} \tag{4.32}$$

This result is the same as others have found for the single pressure model. In this limit, any slip between the two phases will make the problem ill-posed as an initial value problem.

Now to check the stratified flow limit, which corresponds to $\theta = \frac{\bar{\alpha}^L}{2}$,

$$(u_g - u_f) \leq \pm \sqrt{\frac{gH\alpha}{\rho_g(1-\alpha)} \left(\frac{\rho_g\alpha}{2} \left[\frac{2\left(1-\frac{\alpha}{2}\right)}{(1-\alpha)} - \frac{\alpha}{(1-\alpha)} - 1 \right] + \frac{\rho_f[1-\alpha]}{2} \left[1 - \frac{[\alpha-\alpha]}{[1-\alpha]} \right] \right) \left(1 + \frac{\rho_g(1-\alpha)}{\rho_f\alpha} \right)} \tag{4.33}$$

the criterion for stratified flow now becomes:

$$(u_g - u_f) \leq \pm \sqrt{\frac{gH\alpha}{2(1-\alpha)} \left(\alpha + \frac{\rho_f}{\rho_g} [1-\alpha] \right) \left(1 + \frac{\rho_g(1-\alpha)}{\rho_f\alpha} \right)} \tag{4.34}$$

This result is different from the previously obtained result for stratified flow. This is due to the assumption that the interface pressure is equal to the gas pressure. To determine the influence of using the interface pressure assumption, we can calculate the relative error for stratified flow. Since stratified flow should be the worst case for this assumption, the relative error for the other types of flow patterns will be less than this value.

If the actual interface pressure for stratified flow is used, the stability boundary is:

$$(u_g - u_f) = \pm \sqrt{\frac{gH\alpha}{2\rho_g} [\rho_f - \rho_g] \left(\frac{\rho_g (1-\alpha)}{\rho_f} + 1 \right)} \quad (4.35)$$

While using the $\langle\langle P_i \rangle\rangle = \langle\langle P_g \rangle\rangle$ assumption, we get:

$$(u_g - u_f) = \pm \sqrt{\frac{gH\alpha}{2(1-\alpha)} \left(\alpha + \frac{\rho_f}{\rho_g} [1-\alpha] \right) \left(1 + \frac{\rho_g (1-\alpha)}{\rho_f} \right)} \quad (4.36)$$

The relative error in the difference in the relative velocity can be found by:

$$\% \text{ diff} = \frac{\text{real} - \text{approximate}}{\text{real}} \times 100 \quad (4.37)$$

In this case, the error is given as:

$$\% \text{ diff} = \frac{\sqrt{\frac{gH\alpha}{2\rho_g} [\rho_f - \rho_g] \left(\frac{\rho_g (1-\alpha)}{\rho_f} + 1 \right)} - \sqrt{\frac{gH\alpha}{2(1-\alpha)} \left(\alpha + \frac{\rho_f}{\rho_g} [1-\alpha] \right) \left(1 + \frac{\rho_g (1-\alpha)}{\rho_f} \right)}}{\sqrt{\frac{gH\alpha}{2\rho_g} [\rho_f - \rho_g] \left(\frac{\rho_g (1-\alpha)}{\rho_f} + 1 \right)}} \times 100 \quad (4.38)$$

Which then reduces to:

$$\% \text{ diff} = \frac{\sqrt{\left[\frac{\rho_f}{\rho_g} - 1 \right]} - \sqrt{\left(\frac{\alpha}{(1-\alpha)} + \frac{\rho_f}{\rho_g} \right)}}{\sqrt{\left[\frac{\rho_f}{\rho_g} - 1 \right]}} \times 100 \quad (4.39)$$

If $\frac{\rho_f}{\rho_g} \gg 1$, the equation for the error in the relative velocity cause by the $\langle\langle P_i \rangle\rangle = \langle\langle P_g \rangle\rangle$

assumption becomes:

$$\% \text{ diff} = \frac{\sqrt{\frac{\rho_f}{\rho_g}} - \sqrt{\left(\frac{\alpha}{(1-\alpha)} + \frac{\rho_f}{\rho_g}\right)}}{\sqrt{\frac{\rho_f}{\rho_g}}} \times 100 \quad (4.40)$$

The amount of error using the approximation increases with increasing void fraction as well as with a decreasing density ratio. The relative error for different density ratios is shown in Figure 4.10.

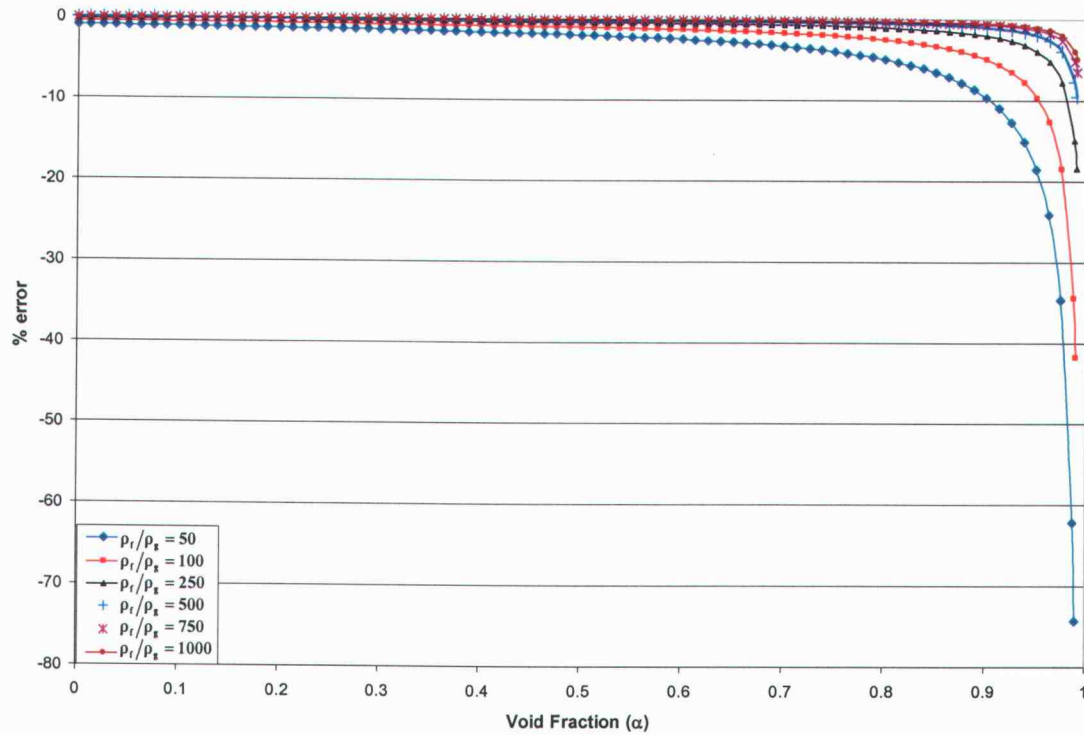


Figure 4.10: Calculation of error in v_r for using the $\langle\langle P_i \rangle\rangle = \langle\langle P_g \rangle\rangle$ approximation

For the range of density ratios shown, the amount of error using the $\langle\langle P_i \rangle\rangle = \langle\langle P_g \rangle\rangle$ approximation is within ten percent up to void fractions near 0.9. This shows that this

approximation may be a good one over the range of void fractions and density ratios of interest.

Figures 4.11 through 4.13 show the relative velocity limit for maintaining a hyperbolic problem for various density ratios and values of the phase distribution parameter. Both the actual stratified limit, using the real interface pressure, as well as the stratified limit, using the $\langle\langle p_i \rangle\rangle = \langle\langle p_g \rangle\rangle$ approximation, is shown. It can be seen that the approximation matches the actual limit over the majority of the range.

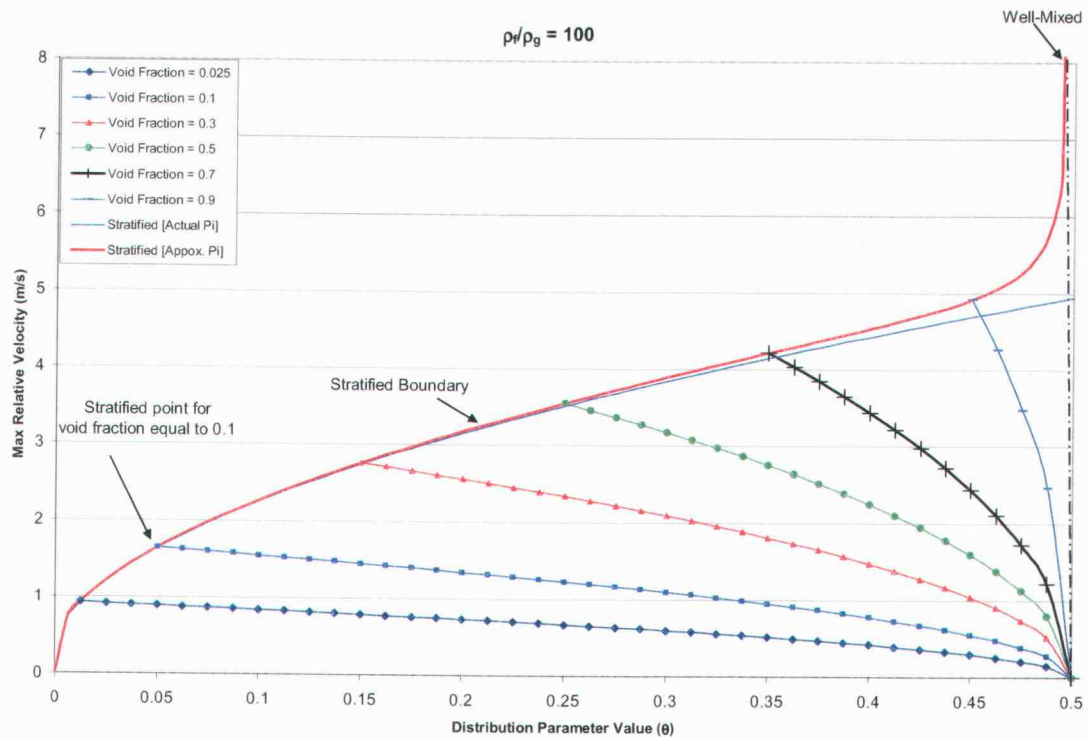


Figure 4.11: Influence of the distribution parameter on stability limit (2'' duct, $\rho_f/\rho_g = 100$)

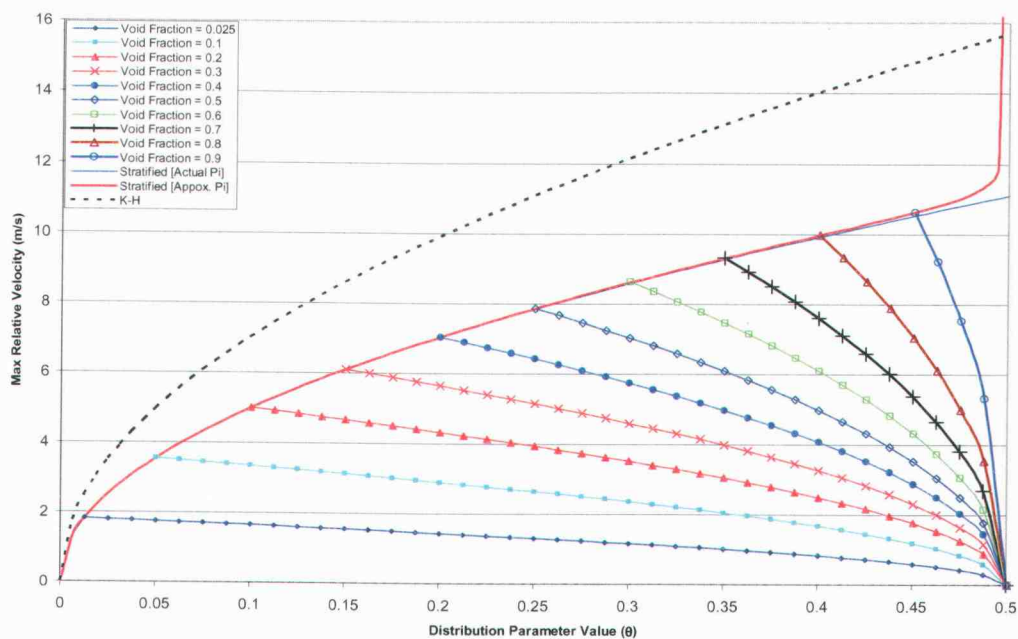


Figure 4.12: Influence of the distribution parameter on stability limit (2" duct, $\rho_f/\rho_g = 500$)

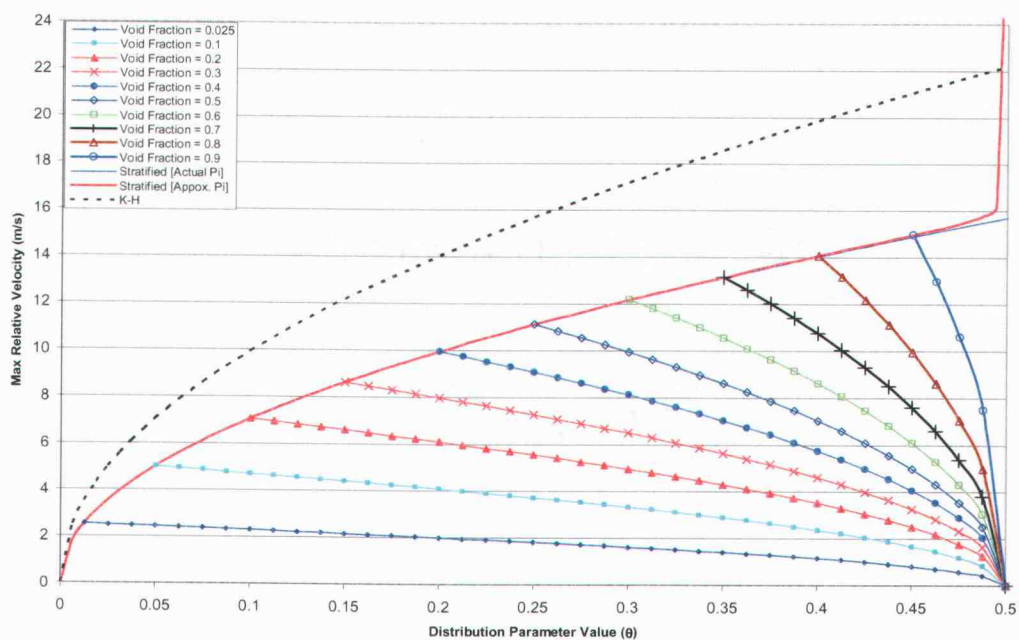


Figure 4.13: Influence of the distribution parameter on stability limit (2" duct, $\rho_f/\rho_g = 1000$)

The above figures show the influence of the distribution parameter for different void fractions and different density ratios. One can see that in all cases where the flow is well-mixed, $\theta = \frac{1}{2}$, the maximum relative velocity is always zero. This is consistent with previous analyses. As the flow diverges from the well-mixed condition, one can see the stabilizing effect that the pressure difference has on the flow. The solid blue line in the figures represents the stability line for stratified flow, $\theta = \frac{\alpha}{2}$, using the characteristic analysis with the real value of the interface pressure. On the other hand, the solid red line shows the predicted stability line for stratified flow using the $\langle\langle P_i \rangle\rangle = \langle\langle P_g \rangle\rangle$ approximation. One can see that the approximation works increasingly well with increased density ratios. In addition, the approximation compares well with the actual value of the relative velocity stability limit except in the case of high void fractions ($\alpha > 0.8$ or 0.9). The solid black line in the above figures represents the stability line predicted by the Kelvin-Helmholtz (K-H) stability analysis. The K-H instability does correspond to a physical flow type instability versus the numerical type of flow instability that we are calculating using the characteristic analysis. This may account for the difference between the values found. Further investigation will have to be performed to determine where the difference comes from and if the difference is physical or not.

4.5 MODELING OF THE DISTRIBUTION PARAMETER

In order to use the void distribution parameter to aid in the computer simulations of two-phase codes, one needs to be able to determine what value the distribution parameter has for a given flow condition. Ideally, this calculation would be performed using some analytical function that is in terms of known parameters such as void fraction, pipe diameter, gravity, and superficial velocities. However, this may be difficult as the physical processes within two-phase flow are still not well understood.

Proper modeling of the void fraction distribution parameter would allow smooth transitions between various flow regimes and eliminate the need for the more subjectively based flow regime maps. This section will explore some of the options that could be used to determine the void distribution parameter.

4.5.1 Using void fraction distribution to calculate parameter

The most ideal way to determine the void distribution parameter is to first determine the actual transverse void fraction profile. Once the void profile is known, it can then be integrated in order to determine the value of the distribution parameter. This method, however, requires a good understanding of the physics which determine the void fraction profile. Possible methods for determining the void fraction profile will be discussed within the following subsections.

4.5.1.1 Determine void distribution using a force balance approach

One method of determining the void fraction distribution would be to perform a momentum balance. If steady state condition were assumed and assumed that there is no net flow in the vertical direction, one may be able to use a two or three-dimensional set of momentum equations to determine where the bubbles will migrate in the vertical direction.

$$\begin{aligned} & \frac{\partial(\alpha_k \rho_k v_{yk})}{\partial t} + \frac{\partial(\alpha_k \rho_k v_{yk} v_{xk})}{\partial x} + \frac{\partial(\alpha_k \rho_k v_{yk}^2)}{\partial y} \\ & = -\alpha_k \frac{\partial P_k}{\partial y} + \alpha_k \rho_k g \cos \varphi + (P_{ki} - P_k) \frac{\partial \alpha_k}{\partial y} - \langle \Gamma_k \rangle \langle v_{ki} \rangle - \frac{4\alpha_{kw} \tau_{kw}}{D} + \frac{\partial \alpha_k \langle \tau_{kxx} + \tau_{kxx}^T \rangle}{\partial x} - \langle M_{ik} \rangle \end{aligned} \quad (4.41)$$

Assume steady state with no velocity in y-direction

$$0 = -\alpha_k \frac{\partial P_k}{\partial y} + \alpha_k \rho_k g \cos \varphi + (P_{ki} - P_k) \frac{\partial \alpha_k}{\partial y} - \langle \Gamma_k \rangle \langle v_{ki} \rangle - \frac{4\alpha_{kw} \tau_{kw}}{D} + \frac{\partial \alpha_k \langle \tau_{kxx} + \tau_{kxx}^T \rangle}{\partial x} - \langle M_{ik} \rangle \quad (4.42)$$

Rearranging:

$$\alpha_k \frac{\partial P_k}{\partial y} + (P_k - P_{ki}) \frac{\partial \alpha_k}{\partial y} = \alpha_k \rho_k g \cos \varphi - \langle \Gamma_k \rangle \langle v_{ki} \rangle - \frac{4\alpha_{kw} \tau_{kw}}{D} + \frac{\partial \alpha_k \langle \tau_{kxx} + \tau_{kxx}^T \rangle}{\partial y} - \langle M_{ik} \rangle \quad (4.43)$$

With no phase change or drag in the y-direction:

$$\frac{\partial P_k}{\partial y} + \frac{(P_k - P_{ki})}{\alpha_k} \frac{\partial \alpha_k}{\partial y} = \rho_k g \cos \varphi \quad (4.44)$$

the phase difference:

$$\frac{\partial P_L}{\partial y} + \frac{(P_L - P_{Li})}{\alpha_L} \frac{\partial \alpha_L}{\partial y} - \frac{\partial P_g}{\partial y} - \frac{(P_g - P_{gi})}{\alpha_g} \frac{\partial \alpha_g}{\partial y} = \rho_L g \cos \varphi - \rho_g g \cos \varphi \quad (4.45)$$

$$\frac{\partial P_L}{\partial y} - \frac{\partial P_g}{\partial y} + \left[-\frac{(P_L - P_{Li})}{(1-\alpha)} - \frac{(P_g - P_{gi})}{\alpha} \right] \frac{\partial \alpha}{\partial y} = [\rho_L - \rho_g] g \cos \varphi \quad (4.46)$$

Assuming that the local pressure gradient and interface pressures are the same for each phase:

$$\left[-\frac{P_L}{(1-\alpha)} - \frac{P_g}{\alpha} + \left[\frac{P_i}{(1-\alpha)} + \frac{P_i}{\alpha} \right] \right] \frac{\partial \alpha}{\partial y} = \Delta \rho g \cos \varphi \quad (4.47)$$

The above analysis neglects the influence of turbulence. It is clear that turbulence, both liquid and bubble-induced, needs to be included in this approach to account for fluctuations in the vertical direction. For this type of approach, one needs to know something about bubble size. The bubble size and relative velocity influences the amount of bubble induced turbulence. The bubble induced turbulence can then influence where the bubbles migrate.

One could perform this type of analysis numerically. Assuming an initial distribution of bubble sizes, one could let the problem run until a steady-state solution is achieved. This would require *a priori* knowledge of the bubble size distribution. In order to obtain this, more experimental data would need to be acquired in conjunction with additional theoretical modeling.

4.5.1.2 Determine void distribution using fits of experimental data

Another approach would be to collect an extensive amount of experimental data where the void fraction distribution is measured along the direction transverse to the direction of flow. By collecting and examining the data and incorporating the needed physics, one could possibly develop a correlation where densities, void fraction, surface tension, and so on are used to determine the profile. This would require extensive measurements as one needs to traverse the pipe and measure the void fraction at several locations for each flow condition. In addition, more experiments would need to be done to determine the effect of density differences, gravity, pipe diameter, and surface tension.

4.5.1.3 Determine void distribution using a physical modeling approach

Based on the experimental results obtained, it appears that the void peak reaches a maximum value of about 0.65. This corresponds to a maximum packing fraction. If the void fraction is increased, the void peak becomes wider. At some point, the void fraction everywhere will reach some maximum packing fraction. Beyond this point, the bubbles are forced to distort to achieve a higher packing fraction. After the bubbles cannot achieve a higher packing fraction through distortion, the bubbles will likely be forced to coalesce. This may be the onset of annular flow. This type of modeling could comprise of a bubble population model in combination with a volume or interfacial area transport model. The bubbles would initially accumulate towards the top of the pipe, assuming that the liquid flow is reasonably slow. As bubbles accumulate, the void peak will become wider. The location of the actual peak is likely due to a balance of surface tension, inertia forces, and buoyancy forces.

4.5.2 Determine distribution parameter in terms of non-dimensional numbers

One could possibly use sets of experimental data along with theoretical limits to determine how the phase distribution parameter may be able to be correlated in terms of meaningful non-dimensional numbers such as the Froude number, Reynolds number or the Weber number. This method would calculate the distribution parameter in terms of some parameters instead of trying to determine the void fraction profile and then calculating the distribution parameter based upon that profile. This method should be easier than calculating the actual profile, but won't contain as much information about the actual profile shape.

4.5.2.1 Discussion of parameters to describe flow regime transition

Moving along the direction of the red arrow in Figure 4.14, there can be a change of both void fraction and liquid velocity. This is because $j_f = v_f(1 - \alpha)$. One can see that moving along this direction will allow for transition between stratified, plug, and bubbly flows or between wavy, slug, and bubbly flows depending on the gas superficial velocity. This assumes that the gas superficial velocity is below that required for annular flow. The annular flow regime will be disregarded in this initial analysis since the annular flow can have droplet existing within the vapor core, which will tend to alter the results of the pressure distribution.

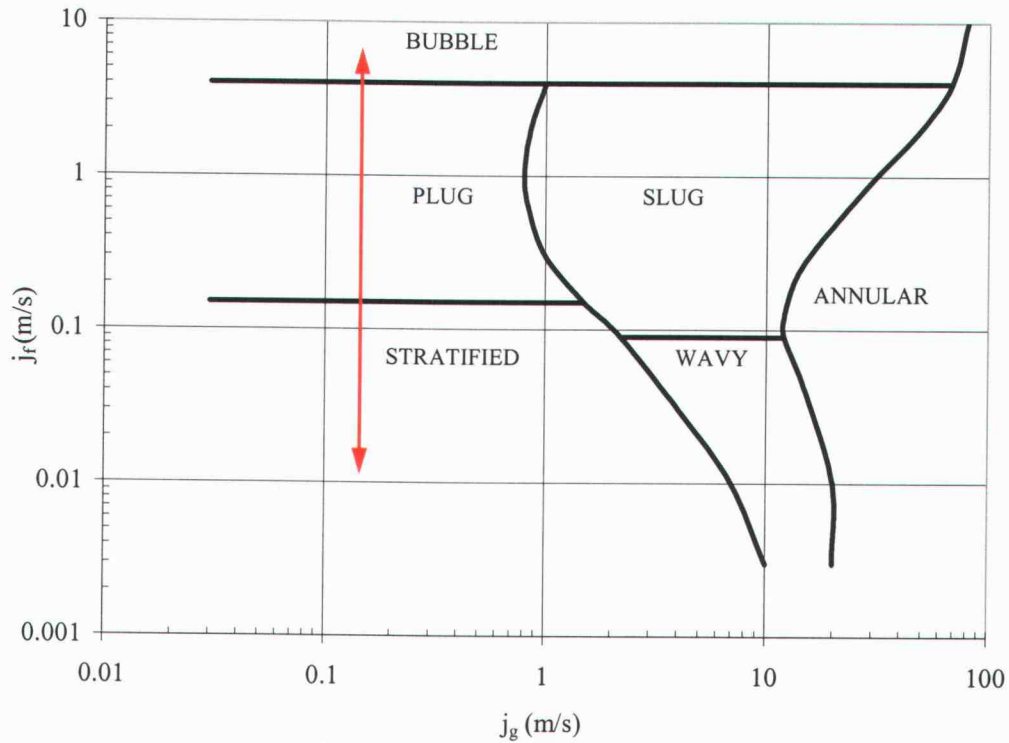


Figure 4.14: Flow regime area of focus for distribution parameter modeling

For the regimes of interest, it is likely that some version of the Froude number is responsible for these flow regime transitions. This is because the Froude number is the ratio of the inertia forces to buoyancy forces. Typically, the Froude number is written as:

$$Fr = \sqrt{\frac{\rho v^2}{\Delta \rho g D}} \quad (4.48)$$

The values of density, ρ , characteristic velocity, v , and characteristic length, D , depend on the problem at hand. It is important to find meaningful values of these parameters based on the physics which govern the problem. Although other forces

may be important such as the Weber number (inertia to surface tension) or the Reynolds number (inertia to viscous force), it is impossible to tell the impact of these other forces since the experimental data that is being analyzed is only for air-water flow. Additional experiments would need to be performed to determine the importance of surface tension and viscous force on the flow regime transitions.

It is known that the stratified flow regime should exist when the buoyancy force dominates over the inertia force used. The fully mixed flow structure should exist well into the bubbly flow regime. In this region, the liquid turbulence force, which is related to the liquid inertia force, dominates over the buoyancy force to create a flat profile. This is region should be similar to the results seen in microgravity conditions at lower flow rates where most flows have profiles that are either flat or symmetric.

There are several definitions of the Froude number that may potentially play a role in these flow regime transitions. For instance, the Froude number may be based on liquid density and velocity or possibly some mixture density and velocity, or maybe a relative velocity and a liquid density. There are several possibilities. One must look at experimental data and theoretical transition boundaries to determine which parameters to use.

1. **Use of Relative Velocity, v_r** – One may consider the use of relative velocity as the characteristic velocity used in the definition of the Froude number. The main factor for using the relative velocity is due to the fact that the onset from stratified wavy flow to slug flow is based on the Kelvin-Helmholtz instability. This instability is based on the relative velocity between the two phases.

$$(v_g - v_f) = v_r < \sqrt{\frac{\Delta \rho g H \alpha}{\rho_g}} \quad (4.49)$$

After the transition from stratified wavy flow to slug or plug flow, the relative velocity between the two phases decreases to the point where the gas phase is typically just slightly faster than the liquid phase.

Data from Kojasoy and his coworkers (Kocamustafaogullari and Wang, 1991; Kocamustafaogullari and Huang, 1994; Kocamustafaogullari et al., 1994; Riznic et al., 1996; Iskandrani and Kojasoy, 2001; Lewis et al., 2002) was again implemented to determine if relative velocity would be a good parameter to describe the phase distribution parameter. The gas and liquid velocities were calculated using:

$$v_g = \frac{j_g}{\langle \alpha \rangle} \quad (4.50)$$

$$v_f = \frac{j_f}{1 - \langle \alpha \rangle} \quad (4.51)$$

The values were calculated for the data sets which listed the area-averaged void fraction. The superficial velocities used were the ones given in the papers.

2. **Use of a Combined Froude Number, Fr_m^2 , $Fr_m^2 = Fr_g^2 + Fr_f^2$** - For stratified concurrent liquid flows, one typically uses a modified Froude number which includes the influence of the gas and liquid Froude numbers. This transition criterion is the point where the inertia forces over take the buoyancy forces. At this point, the fluids begin to mix, transitioning from a stratified flow condition to a well-mixed flow condition. It may be possible to use such a criterion for the gas-liquid flows that this dissertation deals with.

$$Fr_m^2 = Fr_g^2 + Fr_f^2 \quad (4.52)$$

$$Fr_m^2 = \frac{\rho_g V_g^2}{\Delta \rho g H \alpha} + \frac{\rho_f V_f^2}{\Delta \rho g H (1 - \alpha)} \quad (4.53)$$

The transition from stratified flow occurs when:

$$Fr_m^2 \geq 1 \quad (4.54)$$

For this analysis, the distribution parameter should approach the fully-mixed condition at high Froude numbers. The distribution parameter should also approach the stratified condition at low values of Froude number. The problem with using the combined Froude number is that it can approach infinity in a couple different ways. First, high gas or liquid velocities will create a large Froude number as expected. Secondly, if the void fraction approaches zero or one, the Froude number will also approach infinity. The limit where the void fraction approaches one is not a problem. In this limit, annular flow exists. During annular flow, the void profile is flat except for the thin liquid film at the wall. This related to the fully-mixed condition, as one would expect at a high Froude number. The low values of void fraction do create a problem with this definition. One could have a small void fraction and still be stratified; however, the Froude number can be large due to the void fraction being in the denominator. This high Froude number would predict a fully-mixed flow instead of the stratified flow that actually exists. The problem comes from that fact that this dissertation focuses on just the gas phase distribution, whereas one usually cares about the overall mixture with the liquid-liquid stratified flows. Table 4.4 shows a comparison of the various Froude numbers based on experimental data. It can be seen that for these conditions, the liquid Froude number is dominate.

Table 4.4: Comparison of experimental Froude numbers

Author	j_g	j_f	$\langle \alpha \rangle$	Fr_g^2	Fr_f^2	Fr_m^2
Kocamustafaogullari and Wang 1991	0.24	5.1	0.043	1.71	60.21	61.92
	0.25	3.74	0.087	0.22	37.29	37.52
	0.51	3.77	0.057	3.32	34.39	37.71
	0.53	4.67	0.105	0.57	61.72	62.30
	0.71	3.83	0.151	0.35	48.63	48.98
	1.03	3.74	0.183	0.41	52.04	52.45
	1.34	4.98	0.204	0.50	99.77	100.27
	1.59	4.36	0.226	0.52	83.18	83.70
Kocamustafaogullari and Huang 1994	0.213	4.67	0.044	1.26	50.64	51.90
	0.419	4.67	0.085	0.68	57.76	58.44
	0.788	4.67	0.146	0.47	71.04	71.52
	1.21	4.67	0.2048	0.40	88.00	88.40
Kocamustafaogullari et al. 1994	0.22	5.00	0.042	1.55	57.69	59.24
	0.43	4.98	0.08	0.85	64.62	65.47
	0.61	4.98	0.111	0.64	71.62	72.26
	1.00	4.98	0.167	0.51	87.05	87.56
	1.25	5.01	0.204	0.44	100.97	101.41

3. **Use of a Liquid Froude Number, Fr_f^2 or Fr_f** - It appears that perhaps the liquid Froude number should be used for this analysis. It doesn't suffer from the problems that the combined Froude number has at very low void fractions. Physically, the liquid Froude number can be justified by looking at the liquid turbulence. The amount of liquid turbulence is proportional to $\rho_f V_f^2$. The numerator of the liquid Froude number contains this same term. So either the liquid Froude number or the square of the liquid Froude number may be appropriate.

$$Fr_f^2 = \frac{\rho_f V_f^2}{\Delta \rho g H (1 - \alpha)} \quad (4.55)$$

or

$$Fr_f = \sqrt{\frac{\rho_f V_f^2}{\Delta \rho g H (1 - \alpha)}} \quad (4.56)$$

4.5.2.2 Functional relation between θ and non-dimensional numbers

Any functional form that may be used to describe the relation between the distribution parameter, θ , and some non-dimensional number, such as the Froude number, must be able to meet the theoretical limits of the distribution parameter for stratified flow as well as for the fully-mixed flow condition.

As shown previously, the range of the distribution parameter is $\frac{\bar{\alpha}^L}{2} \leq \theta \leq \frac{1}{2}$, with $\theta = \frac{\bar{\alpha}^L}{2}$ being the stratified flow limit and $\theta = \frac{1}{2}$ corresponding to the fully-mixed flow condition. A functional relationship must asymptotically approach these two limits. In the case of using the Froude number to describe the distribution parameter, when the buoyancy force dominates over the inertia force (small Froude number), the function relationship should approach the stratified limit. In the case where the inertia force dominates, the functional relation should approach the fully-mixed flow condition. The hyperbolic tangent would be a good candidate for this since it has two asymptotic limits. One can write the functional relation in general as:

$$\theta = C_1 + C_2 \tanh(C_3 (Fr_m^2 - \delta)) \quad (4.57)$$

Where C_1 , C_2 , C_3 , and δ are constants.

$$\theta(\text{Fr}_m^2 \rightarrow 0) = C_1 + C_2 \tanh(C_3(-\delta)) = \frac{\alpha}{2} \quad (4.58)$$

If δ is large enough, this can be simplified to:

$$\theta(\text{Fr}_m^2 \rightarrow 0) = C_1 - C_2 = \frac{\alpha}{2} \quad (4.59)$$

$$\theta(\text{Fr}_m^2 \rightarrow \infty) = C_1 + C_2 = \frac{1}{2} \quad (4.60)$$

The coefficients for the equation become:

$$C_1 = (1 + \alpha)/4 \quad C_2 = (1 - \alpha)/4$$

The equation reduces to:

$$\theta = \frac{1}{4} \left(1 + \alpha + (1 - \alpha) \tanh(C_3(\text{Fr}_m^2 - \delta)) \right) \quad (4.61)$$

This function is shown in Figure 4.15 for arbitrary values of C_3 and δ and for several values of void fraction.

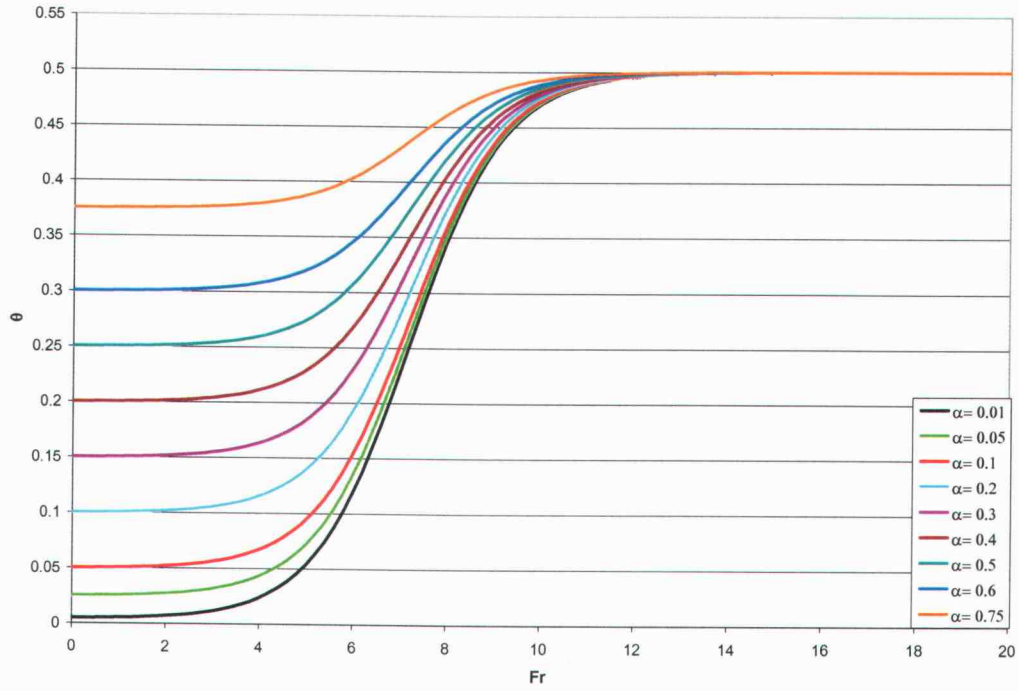


Figure 4.15: Possible function describing the distribution parameter in terms of Fr

One can see from Figure 4.15 that the asymptotic limits are met. Since the upper end of the curve is fixed and the general shape of the curve is the same, but the lower limit changes, it may be beneficial to determine a way to write the function to collapse the curves onto a single line. This can be done by defining a new number, denoted θ^+ . Let θ^+ be defined as:

$$\theta^+ = \frac{\theta - \frac{\alpha}{2}}{\frac{1}{2}(1 - \alpha)} \rightarrow \frac{2\theta - \alpha}{(1 - \alpha)} \quad (4.62)$$

For stratified flow:

$$\theta^+ = 0 \quad (4.63)$$

For the fully-mixed flow condition:

$$\theta^+ = 1 \quad (4.64)$$

The function now becomes:

$$\theta^+ = \frac{\frac{1}{2} \left[1 + \alpha + (1 - \alpha) \tanh(C_3 (Fr_m^2 - \delta)) \right] - \alpha}{(1 - \alpha)} \rightarrow \frac{1}{2} \left[1 + \tanh(C_3 (Fr_m^2 - \delta)) \right] \quad (4.65)$$

The resulting curve for arbitrary values of C_3 and δ is shown in Figure 4.16. It can be seen that this function is always bounded between zero and one. This function is independent of void fraction and may allow one to collapse all data onto a single curve.

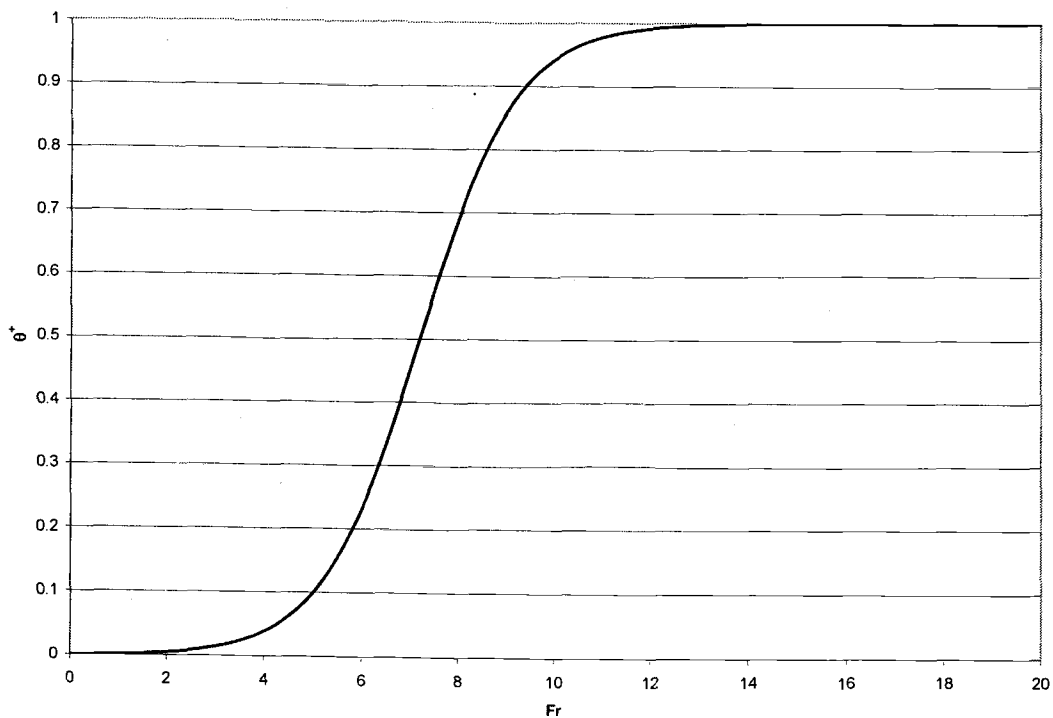


Figure 4.16: The resulting collapsed curve for describing the distribution parameter

Data from Kojasoy and his colleges (Kocamustafaogullari and Wang, 1991; Kocamustafaogullari and Huang, 1994; Kocamustafaogullari et al., 1994) are plotted in terms of liquid Froude number in Figure 4.17 and Figure 4.18 using the average liquid velocity and the liquid superficial velocity, respectively. The curve plotted in Figure 4.17 and Figure 4.18 is generated from equation (4.65) by adjusting the values of the C_3 and δ parameters to best fit the data. It is seen from first glance that the use of liquid superficial velocity provides data points with less scatter and therefore a better fit to the function. The use of a local average liquid velocity does make more sense physically, though. This is because it is a real liquid velocity, unlike the liquid superficial velocity. The amount of scatter in the data may be a combination of error in the experimental data, the different transition criterion for different void fractions, and lack of other important parameters in the model or possibly the use of incorrect characteristic lengths or velocities.

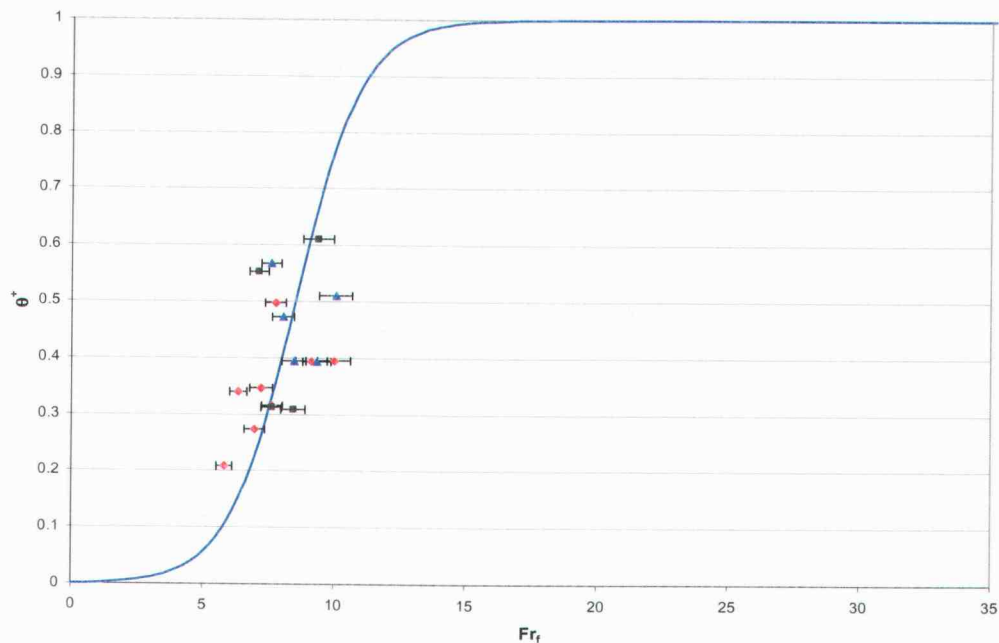


Figure 4.17: Using average liquid velocity for Fr , $v_f = j_f / (1 - \alpha)$

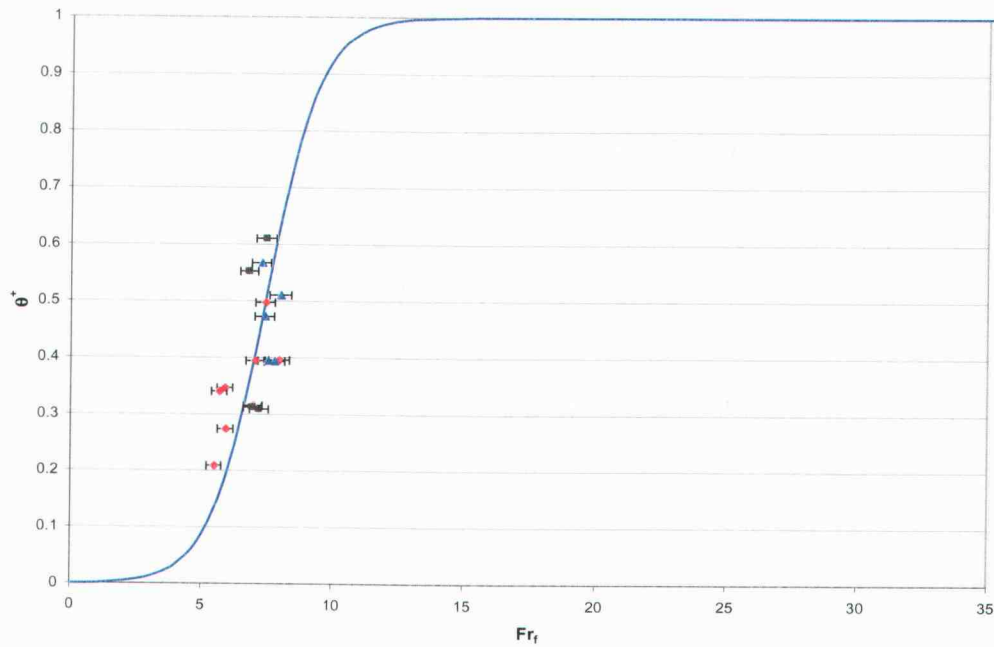


Figure 4.18: Using superficial liquid velocity for Fr

It is important to determine how much of the scatter of the data points is due to possible experimental uncertainty in order to determine how much to the scatter is caused from the experiment and how much is due to possible missing information in the model itself.

In order to determine the uncertainty, we need to know the parameters that the model relies upon and how much error maybe in those measured parameters to determine the overall uncertainty. For this model, it is assumed that the phase distribution parameter is dependent on the liquid Froude number. The liquid Froude number is defined as:

$$Fr_f = \sqrt{\frac{\rho_f V_f^2}{\Delta \rho g H (1 - \alpha)}} \quad (4.66)$$

Which then becomes:

$$Fr_f = \sqrt{\frac{\rho_f \left(\frac{j_f}{(1-\alpha)} \right)^2}{\Delta \rho g H (1-\alpha)}} \quad (4.67)$$

or

$$Fr_f = \sqrt{\frac{\rho_f j_f^2}{\Delta \rho g H (1-\alpha)}} \quad (4.68)$$

depending on the definition of the characteristic liquid velocity that is used. The (Root-Mean-Square) RMS error in the liquid Froude number can be found in general as:

$$\Delta Fr_f = \sqrt{\left(\frac{\partial Fr_f}{\partial \rho_f} \Delta \rho_f \right)^2 + \left(\frac{\partial Fr_f}{\partial j_f} \Delta j_f \right)^2 + \left(\frac{\partial Fr_f}{\partial \alpha} \Delta \alpha \right)^2 + \dots} \quad (4.69)$$

The RMS error is the most probable uncertainty in the liquid Froude number for this case. The RMS error in the liquid Froude number is found by taking the partial derivative of all possible parameters within the liquid Froude number and multiply each term by the uncertainty of that parameter. Each term is squared then summed with the other terms. Finally, the square root of the sum is taken.

For the case where the liquid Froude number is defined as:

$$Fr_f = \sqrt{\frac{\rho_f \left(\frac{j_f}{(1-\alpha)} \right)^2}{\Delta \rho g H (1-\alpha)}} \quad (4.70)$$

The RMS error is found using:

$$\begin{aligned}
Fr_f &= \left(\frac{\rho_f j_f^2}{\Delta \rho g H (1 - \alpha)^3} \right)^{1/2} \\
\rightarrow \frac{\partial Fr_f}{\partial j_f} &= \left(\frac{\rho_f}{\Delta \rho g H (1 - \alpha)^3} \right)^{1/2} \\
\rightarrow \frac{\partial Fr_f}{\partial \alpha} &= \frac{3}{2} \left(\frac{\rho_f}{\Delta \rho g H (1 - \alpha)^5} \right)^{1/2}
\end{aligned} \tag{4.71}$$

For the case where the liquid Froude number is defined as:

$$Fr_f = \sqrt{\frac{\rho_f j_f^2}{\Delta \rho g H (1 - \alpha)}} \tag{4.72}$$

The RMS error is found using:

$$\begin{aligned}
Fr_f &= \left(\frac{\rho_f j_f^2}{\Delta \rho g H (1 - \alpha)} \right)^{1/2} \\
\rightarrow \frac{\partial Fr_f}{\partial j_f} &= \left(\frac{\rho_f}{\Delta \rho g H (1 - \alpha)} \right)^{1/2} \\
\rightarrow \frac{\partial Fr_f}{\partial \alpha} &= \frac{1}{2} \left(\frac{\rho_f}{\Delta \rho g H (1 - \alpha)^3} \right)^{1/2}
\end{aligned} \tag{4.73}$$

The error bars were found assuming an error of 5 percent for the liquid superficial velocity, and 10 percent for void fraction. The actual errors were not given, so reasonable errors were used based on what information was available. It was assumed that densities, gravity, and pipe diameter were all well known and constant. In this case only the error for the liquid flow rate and void fraction come into play in the uncertainty analysis for the liquid Froude number. It is seen that the uncertainty in the experimental data will not account for all of the scatter in the data alone. This is based on that the amount of error assumed in the analysis is correct. A summary of average and maximum relative errors for both definitions of liquid Froude number are shown in Tables 4.5 through 4.8 to get an idea of how the error bars for the data set would change based on the amount of uncertainty in the experimental data.

Table 4.5: Average relative error of Fr_f based on average liquid velocity

$\Delta\alpha(\%) \backslash \Delta j_r(\%)$	0	2.5	5	7.5	10	12.5	15	17.5	20
0	0.0000	0.0250	0.0500	0.0750	0.1000	0.1250	0.1500	0.1750	0.2000
2.5	0.0056	0.0258	0.0504	0.0753	0.1002	0.1252	0.1501	0.1751	0.2001
5	0.0112	0.0280	0.0516	0.0761	0.1008	0.1257	0.1505	0.1755	0.2004
7.5	0.0169	0.0311	0.0535	0.0774	0.1018	0.1265	0.1512	0.1761	0.2009
10	0.0225	0.0349	0.0560	0.0792	0.1032	0.1276	0.1522	0.1769	0.2016
12.5	0.0281	0.0391	0.0589	0.0814	0.1049	0.1290	0.1534	0.1779	0.2025
15	0.0337	0.0436	0.0622	0.0839	0.1070	0.1307	0.1548	0.1792	0.2037
17.5	0.0393	0.0483	0.0659	0.0868	0.1093	0.1327	0.1565	0.1806	0.2049
20	0.0450	0.0531	0.0698	0.0900	0.1119	0.1349	0.1584	0.1823	0.2064

Table 4.6: Maximum relative error of Fr_f based on average liquid velocity

$\Delta\alpha(\%) \backslash \Delta j_r(\%)$	0	2.5	5	7.5	10	12.5	15	17.5	20
0	0.0000	0.0250	0.0500	0.0750	0.1000	0.1250	0.1500	0.1750	0.2000
2.5	0.0109	0.0273	0.0512	0.0758	0.1006	0.1255	0.1504	0.1753	0.2003
5	0.0219	0.0332	0.0546	0.0781	0.1024	0.1269	0.1516	0.1764	0.2012
7.5	0.0328	0.0413	0.0598	0.0819	0.1053	0.1292	0.1536	0.1781	0.2027
10	0.0438	0.0504	0.0665	0.0869	0.1092	0.1325	0.1563	0.1804	0.2047
12.5	0.0547	0.0602	0.0741	0.0929	0.1140	0.1365	0.1597	0.1834	0.2074
15	0.0657	0.0703	0.0826	0.0997	0.1197	0.1412	0.1638	0.1869	0.2105
17.5	0.0766	0.0806	0.0915	0.1072	0.1260	0.1466	0.1684	0.1910	0.2142
20	0.0876	0.0911	0.1009	0.1153	0.1329	0.1526	0.1737	0.1957	0.2183

Table 4.7: Average relative error of Fr_f based on superficial liquid velocity

$\Delta\alpha(\%) \backslash \Delta j_f(\%)$	0	2.5	5	7.5	10	12.5	15	17.5	20
0	0.0000	0.0250	0.0500	0.0750	0.1000	0.1250	0.1500	0.1750	0.2000
2.5	0.0019	0.0251	0.0500	0.0750	0.1000	0.1250	0.1500	0.1750	0.2000
5	0.0037	0.0254	0.0502	0.0751	0.1001	0.1251	0.1501	0.1751	0.2000
7.5	0.0056	0.0258	0.0504	0.0753	0.1002	0.1252	0.1501	0.1751	0.2001
10	0.0075	0.0264	0.0507	0.0755	0.1004	0.1253	0.1502	0.1752	0.2002
12.5	0.0094	0.0271	0.0511	0.0758	0.1006	0.1255	0.1504	0.1753	0.2003
15	0.0112	0.0280	0.0516	0.0761	0.1008	0.1257	0.1505	0.1755	0.2004
17.5	0.0131	0.0289	0.0522	0.0765	0.1011	0.1259	0.1507	0.1756	0.2006
20	0.0150	0.0300	0.0528	0.0769	0.1014	0.1262	0.1510	0.1758	0.2007

Table 4.8: Maximum relative error of Fr_f based on superficial liquid velocity

$\Delta\alpha(\%) \backslash \Delta j_f(\%)$	0	2.5	5	7.5	10	12.5	15	17.5	20
0	0.0000	0.0250	0.0500	0.0750	0.1000	0.1250	0.1500	0.1750	0.2000
2.5	0.0036	0.0253	0.0501	0.0751	0.1001	0.1251	0.1500	0.1750	0.2000
5	0.0073	0.0260	0.0505	0.0754	0.1003	0.1252	0.1502	0.1752	0.2001
7.5	0.0109	0.0273	0.0512	0.0758	0.1006	0.1255	0.1504	0.1753	0.2003
10	0.0146	0.0290	0.0521	0.0764	0.1011	0.1258	0.1507	0.1756	0.2005
12.5	0.0182	0.0310	0.0532	0.0772	0.1017	0.1263	0.1511	0.1759	0.2008
15	0.0219	0.0332	0.0546	0.0781	0.1024	0.1269	0.1516	0.1764	0.2012
17.5	0.0255	0.0357	0.0561	0.0792	0.1032	0.1276	0.1522	0.1769	0.2016
20	0.0292	0.0384	0.0579	0.0805	0.1042	0.1284	0.1528	0.1774	0.2021

Error can also occur along the direction of the distribution parameter, θ^+ . With the way that the distribution parameter is defined, if all void fraction profile data points were shifted either up or down by a fixed relative amount, no error in the distribution parameter will occur. However, each void fraction data point could be

higher or lower than the actual value, independent of the other data points. The influence of this could be found by performing a numerical sensitivity analysis. One could assume that the data points measured are the mean value of the void fraction at that location. One could then assign some uncertainty of each point with a given distribution, such as a Gaussian distribution. One could then write a Monte Carlo program and sample the distribution for each data point. The program would sweep through each point along the vertical direction, sampling from the given distribution at each point, to generate a new and slightly different void fraction profile. Once swept through one pass, the distribution parameter could be calculated. The process would repeat many times (possibly 10,000 or more), which would find the mean phase distribution parameter along with the associated standard deviation. One would need to have a good idea of local void fraction error to properly implement this method.

In addition to the uncertainty of the local void fraction measurement, uncertainty in the position of where the data is collected will also factor into the error of the distribution parameter. There should also be at least a minimum number of data points across the channel. Having more data points will reduce the amount of error in the numerical integration that is performed to calculate the distribution parameter while achieving a better description of the actual void fraction profile.

The scatter within the data points shown may be due to other factors besides uncertainty in the experimental data. The scatter could be caused by the fact that the model is missing some aspect that is physically important (surface tension, viscosity, etc.). The other factor that could cause the apparent scatter is that the transition point from stratified flow to intermittent flow can occur at different liquid Froude numbers depending on void fraction, gas velocity, and liquid velocity.

4.6 COMPARISON OF MODEL TO PREVIOUS MODELS

The model created within this dissertation greatly enhances the hyperbolic nature of the one-dimensional two-fluid model with the use of a phase distribution parameter which creates a pressure difference between the two phases due to hydrostatic head. This model is physical in nature and works for a wide range of conditions for horizontal and inclined flows. Improving the stability of the vertical flow model still needs to be performed at a later time.

Other models investigated were found to only work under certain flow regimes, such as only stratified flows or just for bubbly flows. Many of the previous works relied on things such as incompressibility, surface tension, or viscosity to create an improved stability of the one-dimensional two-fluid model. However, these effects are often not included under typical flow calculations and should not be relied upon solely to create a stable flow situation.

This model, in conjunction with proper modeling of the phase distribution parameter, could be used to create a unified two-fluid model that would work over a wide range of flow conditions and eliminate the need of the more subjective flow regime maps. By eliminating the flow regime maps in conjunction with this model, the governing equations for the flow will remain hyperbolic and the unphysical oscillations caused by the sharp transitions within the current flow regime maps may be eliminated. Instead, a smoothly varying flow structure will exist over a wide range of conditions.

The use of the phase distribution parameter will also allow the bubbly flow condition to return back to the stratified condition due to the pressure difference between the two phases. Currently, bubbly flows are assumed to be in pressure equilibrium, which basically removes the influence of gravity. Because of this assumption, the model is not stable in a hyperbolic sense and the model is not able to transition back to stratified flow once it is in the bubbly flow regime.

5 DISCUSSION AND FUTURE WORK

A general two-pressure, two-fluid model was created. It was would that this model eliminates the non-hyperbolic nature of the single pressure two-fluid model. This particular model will aid in the hyperbolic nature for horizontal and inclined pipes. Further work will need to be performed in order to deal with the non-hyperbolic nature of the single pressure two-fluid model for vertical flows.

It was found that the model presented in this dissertation provides additional physical information into the one-dimensional, two-fluid model. This creates a pseudo-one-dimensional model because information of the transverse void fraction profile is built into the void distribution parameter. This additional information was found to greatly enhance the numerical stability of the problem (hyperbolic nature) as well as providing a possible way of unifying the stratified flow model and the fully-mixed two-fluid model. With this unification and proper modeling of the phase distribution parameter, the next generation multiphase computer codes could accurately calculate two-phase flows without the use of the more subjective flow regime maps. In addition to the flow regime maps being somewhat subjective, their use can also create unphysical oscillations in computer codes when the calculated flow is near one of the transition boundaries. At this point, small changes in gas flow, liquid flow, or void fraction, cause oscillations between two different flow regimes and the corresponding correlations used.

Future Work – This section will discuss the future work that needs to be performed in this area of research based on findings from this dissertation.

- Additional work regarding the unification of the stratified flow model and the fully-mixed condition needs to be performed. There needs to be additional work regarding interfacial area and transport between the liquid and gas phases

and how to implement this is a general sense to works with different flow structures.

- Further work needs to be performed in order to take care of the same hyperbolic problem for vertical applications of the two-fluid model.
- Additional theoretical work should be performed to create an analytical or semi-analytical model to predict the void fraction profile in a horizontal pipe in order to properly determine the phase distribution parameter in a numerical calculation.
- Additional experimental data to determine void fraction profiles for horizontal two-phase flows.
 - Data needs to be collected at very high liquid flow rates to determine at what point a flat distribution is achieved and to help determine a functional relationship between the distribution parameter and a non-dimensional number such as the liquid Froude number.
 - Data for different fluids should be obtained in order to determine what influences things like surface tension and viscosity have on the void fraction distribution. This experimental data will help to improve a model between the phase distribution parameter and known flow parameters.
- Once a good relationship between the distribution parameter and known flow parameters is created, one can implement a linear stability analysis to determine how the distribution parameter influences the transition between stratified wavy flow and intermittent flow.

- The interfacial pressure term should be further investigated. The simplification used in this dissertation works well for air-water flows and the void fraction range of interest. However, a more exact value of the interfacial pressure becomes important when the two phases have similar densities or if the void fraction is very high. As a subpart of this work, additional theoretical and experimental work will need to be performed to determine the transverse interfacial area concentration and corresponding interfacial pressure for horizontal two-phase flows.
- Additional work with interfacial area concentration needs to be performed for both the interfacial pressure term as well as for proper modeling of the exchange rates of mass, momentum, and energy between the two phases.
- Creation of a good model for the phase distribution parameter could eliminate the need for the more subjective flow regime maps and the unphysical oscillations that can be associated with them for numerical calculations near a transition boundary.

6 CONCLUSIONS

As part of this dissertation, an improved version of the one-dimensional two-fluid model for horizontal two-phase flow was developed. By incorporating the phase distribution parameter, additional information is included making this a pseudo-one-dimensional model. The incorporation of the distribution parameter allowed the one-dimensional two-fluid model to remain hyperbolic over a wide range of relative velocities between the gas and liquid phases, overcoming a major obstacle. It was found that the stratified flow condition is the most stable and the fully mixed flow case the least stable. The use of this phase distribution parameter will also allow for creating a unified two-fluid model that will work over a wide range of flow structures. Some methods of determining a calculated value of the distribution parameter was also shown. Additional work will need to be performed in the modeling of the distribution parameter and as well as interfacial area and mass, momentum, and energy transport rates between the two-phases in order to create a unified one-dimensional two-fluid model with smooth transitions between the various flow regimes.

BIBLIOGRAPHY

1. Andreussi, P., Bendiksen, K.H., Nydal, O.J., "Void Distribution in/ Slug Flow", *Int. J. Multiphase Flow*, Vol. 19, No. 5, pp. 817-828, 1993
2. Ansari, M.R., "Effect of Pressure on Two-Phase Stratified Flow Modeling", *Journal of Nuclear Science and Technology*, Vol. 41, No. 7, pp. 709-714, 2004
3. Beattie, D.R.H., "Flow Characteristics of Horizontal Bubbly Pipe Flow", *Nuclear Engineering and Design*, Vol. 163, pp. 207-212, 1996
4. Chen, I.Y., Downing, R.S., Parish, R., Keshock, E., "A Reduced Gravity Flight Experiment: Observed Flow Regimes and Pressure Drops of Vapor and Liquid Flow in Adiabatic Piping", *AIChE Symposium Series*, Vol. 84, pp. 203-216, 1988
5. Chen, Y.M., Fan, L.S., "Drift Flux in Gas-Liquid-Solid Fluidized Systems from the Dynamics of Bed Collapse", *Chemical Engineering Science*, Vol. 45, No. 4, pp. 935-945, 1990
6. Chung, M.S., Lee, S.J., Lee, W.J., Chang, K.S., "An Interfacial Pressure Jump Model for Two-Phase Bubbly Flow", *Numerical Heat Transfer, Part B*, Vol. 40, pp. 83-97, 2001
7. Chung, M.S., Pak, S.K., Chang, K.S., "A Numerical Study of Two-Phase Flow using a Two-Dimensional Two-Fluid Model", *Numerical Heat Transfer, Part A*, Vol. 45, pp. 1049-1066, 2004
8. Delhaye, J.M., "Jump Conditions and Entropy Sources in Two-Phase Systems: Local Instant Formulation" *Int. J. Multiphase Flow*, Vol. 1, pp. 395-409, 1974
9. Egely, G., Saha, P., "A Study of Momentum Transfer in Two-Fluid Formulation of Two-Phase Flow", *Multi-Phase Flow and Heat Transfer 3, Proceedings of the 3rd Symposium-Workshop, Part A: Fundamentals*, pp. 79-101, 1984
10. Franca, F., Lahey, R.T. Jr., "The Use of Drift-Flux Techniques for the Analysis of Horizontal Two-Phase Flows", *Int. J. Multiphase Flow*, Vol. 18, No. 6, pp. 787-801, 1992
11. Fukano, T., Ousaka, A., "Prediction of the Circumferential Distribution of Film Thickness in Horizontal and Near-Horizontal Gas-Liquid Annular Flows", *Int. J. Multiphase Flow*, Vol. 15, No. 3, pp. 403-419, 1989

12. Ghiaasiaan, S.M., Kamboj, B.K., Addel-Khalik, S.I., "Two-Fluid Modeling of Condensation in the Presence of Noncondensables in Two-Phase Channel Flows", Nuclear Science and Engineering, Vol. 119, pp. 1-17, 1995
13. Gidaspow, D., "Modeling of Two-Phase Flow", Round Table Discussion, Proceedings of the 5th International Heat Transfer Conference, VII, pp. 163-168, 1974
14. Gidaspow, D., Rasouli, F., Shin, Y.W., "An Unequal Velocity Model for Transient Two-Phase Flow by the Method of Characteristics", Nuclear Science and Engineering, Vol. 84, pp. 179-195, 1983
15. Hewitt, G.F., Roberts, D.N., "Studies of Two-Phase Flow Patterns by Simultaneous X-ray and Flash Photography", AERE-M2159, 1969
16. Hibiki, T., Hogsett, S., Ishii, M., "Local Measurement of Interfacial Area, Interfacial Velocity, and Liquid Turbulence in Two-Phase Flow", Nuclear Engineering and Design, Vol. 184, pp. 287-304, 1998
17. Hibiki, T., Ishii, M., "Experimental Study on Interfacial Area Transport in Bubbly Two-Phase Flows", Int. J. Heat Mass Transfer, Vol. 42, pp. 3019-3035, 1999
18. Hibiki, T., Ishii, M., "Two-Group Interfacial Area Transport Equations at Bubbly-to-Slug Flow Transition", Nuclear Engineering and Design, Vol. 202, pp. 39-76, 2000
19. Hibiki, T., Ishii, M., Zheng, X., "Axial Interfacial Area Transport of Vertical Bubbly Flows", Int. J. Heat Mass Transfer, Vol. 44, pp. 1896-1888, 2001
20. Hibiki, T., Takamasa, T., Ishii, M., "Interfacial Area Transport of Bubbly Flow in a Small Diameter Pipe", Journal of Nuclear Science and Technology, Vol. 38, No. 8, pp. 614-620, 2001
21. Ishii, M., "Thermally Induced Flow Instabilities in Two-Phase Mixtures in Thermal Equilibrium", Ph.D. Thesis, School of Mechanical Engineering, Georgia Institute of Technology, 1971
22. Ishii, M., "Thermo-Fluid Dynamic Theory of Two-Phase Flow", Eyrolles, Paris, 1975
23. Ishii, M., Mishima, K., "Two-Fluid Model and Hydrodynamic Constitutive Relations", Nuclear Engineering and Design, Vol. 82, pp. 107-126, 1984

24. Iskandrani, A., Kojasoy, G., "Local Void Fraction and Velocity Field Description in Horizontal Bubbly Flow", *Nuclear Engineering and Design*, Vol. 204, pp. 117-128, 2001
25. Jepson, W.P., Taylor, R.E., "Slug Flow and its Transitions in Large-Diameter Horizontal Pipes", *Int. J. Multiphase Flow*, Vol. 19, No. 3, pp. 411-420, 1993
26. Kaminaga, F., "Assessment of Void Fraction Correlations for Vertical Two-Phase Flow in Small Diameter Tube at Low Liquid Velocity", *Journal of Nuclear Science and Technology*, Vol. 29, pp. 695-698, July 1992
27. Kataoka, I., Ishii, M., "Drift Flux Model for Large Diameter Pipe and New Correlation for Pool Void Fraction", *Int. J. Heat Mass Transfer*, Vol. 30, pp. 1927-1939, 1987
28. Kataoka, Y., Suzuki, H., Murase, M., "Drift-Flux Parameters for Upward Gas Flow in Stagnant Liquid", *Journal of Nuclear Science and Technology*, Vol. 24, pp. 580-586, July 1987
29. Khan, H.J., Ye, W., Pertmer, G.A., "Numerical Calculation of Gas-Liquid Transient Flow in Channels and Bends", *American Society of Mechanical Engineers, Fluids Engineering Division (Publication) FED*, Vol. 144, Multiphase Flow in Wells and Pipelines, pp. 113-123, 1992
30. Kim, S., Fu, X.Y., Wang X., Ishii, M., "Study on Interfacial Structures in Slug Flows Using a Miniaturized Four-Sensor Conductivity Probe", *Nuclear Engineering and Design*, Vol. 204, pp. 45-55, 2001
31. Kocamustafaogullari, G., "Thermo-Fluid Dynamics of Separated Two-Phase Flow", Ph.D. Thesis, School of Mechanical Engineering, Georgia Institute of Technology, 1971
32. Kocamustafaogullari, G., "Two-Fluid Modeling in Analyzing the Interfacial Stability of Liquid Film Flows", *Int. J. Multiphase Flow*, Vol. 11, pp. 63-89, 1985
33. Kocamustafaogullari, G., Huang, W.D., "Internal Structure and Interfacial Velocity Development for Bubbly Two-Phase Flow", *Nuclear Engineering and Design*, Vol. 151, pp. 79-101, 1994
34. Kocamustafaogullari, G., Huang, W.D., Razi, J., "Measurement and Modeling of Average Void Fraction, Bubble Size and Interfacial Area", *Nuclear Engineering and Design*, Vol. 148, pp. 437-453, 1994

35. Kocamustafaogullari, G., Wang, Z., "An Experimental Study on Local Interfacial Parameters in a Horizontal Bubbly Two-Phase Flow", *Int. J. Multiphase Flow*, Vol. 17, No. 5, pp. 553-572, 1991
36. Kordyban, E., Okleh, A.H., "Interaction of Linear and Large Wave Instabilities in the Formation of Slugs", *American Society of Mechanical Engineers, Fluids Engineering Division (Publication) FED*, Vol. 165, Gas-Liquid Flows 1993, pp. 109-118, 1993
37. Kornienko, Y., Ninokata, H., "Development of Generalized Integral Forms for Two-Phase Flow Quasi-One-Dimension Closure Relationships of Distribution Parameters and Wall Friction, Heat and Mass Transfer Coefficients for Pipe, Annular and Subchannel Geometry", *The 10th International Conference on Nuclear Thermal Hydraulics (NURETH-10)*, Seoul, Korea, Oct. 5-9, 2003
38. Lafi, A.Y. and Reyes, J.N. Jr., "Phenomenological Models for Fluid Particles Coalescence and Breakage", *Technical Report, OSU-NE-9120*, Department of Nuclear Engineering, Oregon State University, Corvallis, Oregon, 1991.
39. Lahey, R.T. Jr., "Void Wave Propagation Phenomena in Two-Phase Flow", *AIChE J.*, Vol. 37, No. 1, pp. 123-135, 1991
40. Lamb, H., "Hydrodynamics", 6th edition, Cambridge University Press, 1932
41. Leung, W.H., Revankar, S.T., Ishii, Y., Ishii, M., "Axial Development of Interfacial Area and Void Concentration Profiles Measured by Double-Sensor Probe Method", *Int. J. Heat Mass Transfer*, Vol. 38, pp. 445-453, 1995
42. Lewis, S., Fu, W.L., Kojasoy, G., "Internal Flow Structure Description of Slug Flow-Pattern in a Horizontal Pipe" *Int. J. Heat Mass Transfer*, Vol. 45, pp. 3897-3910, 2002
43. Lopez de Bertodano, M., Lee, S-J., Lahey, R.T. Jr., Drew, D.A., "The Prediction of Two-Phase Turbulence and Phase Distribution Phenomena Using a Reynolds Stress Model", *J. of Fluids Engineering*, Vol. 112, pp. 107-113, 1990
44. Lopez de Bertodano, M., Lahey, R.T. Jr., Jones, O.C., "Phase Distribution in Bubbly Two-Phase Flow in Vertical Ducts", *Int. J. Multiphase Flow*, Vol. 20, No. 5, pp. 805-818, 1994
45. Lopez de Bertodano, M., Moraga, F.J., Drew, D.A., Lahey, R.T. Jr., "The Modeling of Lift and Dispersion Forces in Two-Fluid Model Simulations of a Bubbly Jet", *J. of Fluids Engineering*, Vol. 126, pp. 573-577, 2004

46. Lyczkowski, R.W., Gidaspow, D., Solbrig, C.W., Hughes, E.D., "Characteristics and Stability Analyses of Transient One-Dimensional Two-Phase Flow Equations and Their Finite Difference Approximations", *Nuclear Science and Engineering*, Vol. 66, pp. 378-396, 1978
47. Mandhane, J.M., Gregory, G.A., Aziz, K., "A Flow Pattern Map for Gas-Liquid Flow in Horizontal Pipes", *Int. J. Multiphase Flow*, Vol. 1, No. 4, pp. 537-553, 1974
48. Mishima, K., Ishii, M., "Theoretical Prediction of Onset of Horizontal Slug Flow", *Journal of Fluids Engineering, Transactions of the ASME*, Vol. 102, pp. 441-445, 1980
49. Morel, C., Goreaud, N., Delhay, J.M., "The Local Volumetric Interfacial Area Transport Equation: Derivation and Physical Significance", *Int. J. Multiphase Flow*, Vol. 25, pp. 1099-1128, 1999
50. Morriss, S.L., Hill, A.D., "Ultrasonic Imaging and Velocimetry in Two-Phase Pipe Flow", *Journal of Energy Resources Technology, Transactions of the ASME*, Vol. 115, No. 2, pp. 108-116, Jun, 1993
51. Murata, S., Minato, A., Yokomizo, O., "Development of Three-Dimensional Analysis Code for Two-Phase Flow Using Two-Fluid Model", *J. Nuclear Science and Technology*, Vol. 28, pp. 1029-1040, November 1991
52. Park, J.W., Drew, D.A., Lahey, R.T. Jr., "Void Wave Dispersion in Bubbly Flows", *Nuclear Engineering and Design*, Vol. 121, pp. 1-10, 1990
53. Pauchon C., Banerjee, S., "Interphase Momentum Interaction Effects in the Averaged Multifield Model, Part 1: Void Fraction Propagation in Bubbly Flows", *Int. J. Multiphase Flow*, Vol. 12, No. 4, pp. 559-573, 1986
54. Pauchon C., Banerjee, S., "Interphase Momentum Interaction Effects in the Averaged Multifield Model, Part 2: Kinematic Waves and Interfacial Drag in Bubbly Flows", *Int. J. Multiphase Flow*, Vol. 14, No. 3, pp. 253-264, 1988
55. Ransom, V.H., Hicks, D.L., "Hyperbolic Two-Pressure Models for Two-Phase Flow", *Journal of Computational Physics*, Vol. 53, pp. 124-151, 1984
56. Ransom, V.H., Hicks, D.L., "Hyperbolic Two-Pressure Models for Two-Phase Flow Revisited", *Journal of Computational Physics*, Vol. 75, pp. 498-504, 1988

57. Reinecke, N., Petritsch, G., Boddem, M., Mewes, D., "Tomographic Imaging of the Phase Distribution in Two-Phase Slug Flow", *Int. J. Multiphase Flow*, Vol. 24, No. 4, pp. 617-634, 1998
58. Revankar, S.T., Ishii, M., "Local Interfacial Area Measurement in Bubbly Flow", *Int. J. Heat Mass Transfer*, Vol. 35, pp. 913-925, 1992
59. Revankar, S.T., Ishii, M., "Theory and Measurement of Local Area Using a Four Sensor Probe in Two-Phase Flow", *Int. J. Heat Mass Transfer*, Vol. 36, pp. 2997-3007, 1993
60. Riznic, J.R., Lewis, S.P., Kojasoy, G., "Experimental Studies of Interfacial Area in Horizontal Slug Flow", American Society of Mechanical Engineers, Heat Transfer Division, (Publication) HTD, Vol. 334, No. 3, Proceedings of the ASME Heat Transfer Division, pp. 27-37, 1996
61. Sadatomi, M., Kawaji, M., Lorencez, C.M., Chang, T., "Prediction of Liquid Level Distribution in Horizontal Gas-Liquid Stratified Flows with Interfacial Level Gradient", *Int. J. Multiphase Flow*, Vol. 19, No. 6, pp. 987-997, 1993
62. Shi, J., Kocamustafaogullari, G., "Interfacial Measurements in Horizontal Stratified Flow Patterns", *Nuclear Engineering and Design*, Vol. 149, pp. 81-96, 1994
63. Song, J.H., Ishii, M., "The Well-Posedness of Incompressible One-Dimensional Two-Fluid Model", *Int. J. Heat Mass Transfer*, Vol. 43, pp. 2221-2231, 2000
64. Song, J.H., Ishii, M., "On the Stability of a One-Dimensional Two-Fluid Model", *Nuclear Engineering and Design*, Vol. 204, pp. 101-115, 2001
65. Song, J.H., "A Linear Stability Analysis for an Improved One-Dimensional Two-Fluid Model", *Journal of Fluids Engineering, Transactions of the ASME*, Vol. 125, No. 2, pp. 387-389, 2003
66. Taitel, Y., Dukler, A.E., "A Model for Predicting Flow Regimes Transition in Horizontal and Near Horizontal Gas-Liquid Flow", *AIChE J.*, Vol. 22, pp. 47-55, 1976
67. Trapp, J.A., "The Mean Flow Character of Two-Phase Flow Equations", *Int. J. Multiphase Flow*, Vol. 12, No. 2, pp. 263-276, 1986

68. Ulke, A., "Study of a Two-Component, Two-Phase Flow System in One Dimension", Multi-Phase Flow and Heat Transfer 3, Proceedings of the 3rd Symposium-Workshop, Part A: Fundamentals, pp. 59-77, 1984
69. Wallis, G.B., Dobson, J.E., "The Onset of Slugging in Horizontal Stratified Air-Water Flow", Int. J. Multiphase Flow, Vol. 1, pp.173-193, 1973
70. Wu, Q., Ishii, M., "Interfacial Wave Stability of Concurrent Two-Phase Flow in a Horizontal Channel", Int. J. Heat Mass Transfer, Vol. 39, No. 10, pp.2067-2075, 1996
71. Wu, Q., Ishii, M., "Sensitivity Study on Double-Sensor Conductivity Probe for the Measurement of Interfacial Area Concentration in Bubbly Flow", Int. J. Multiphase Flow, Vol. 25, pp.153-173, 1999
72. Zuber, N., Findley, J.A., "Average Volumetric Concentration in Two-Phase Flow Systems", J. Heat Transfer, pp. 453-468, Nov., 1965

NOMENCLATURE

A	flow area
a_i	interfacial area concentration
C_o	distribution parameter
C_{vk}	momentum covariance term
d_{sm}	Sauter mean diameter
g	acceleration due to gravity
H	flow channel height
j	superficial velocity
k	wave number
L_s	length scale at interface
\dot{m}	mass flux
n	surface normal vector
P	pressure
Q	volumetric flow rate
q	heat flux
t	time
u, v	velocity
V_{gj}	drift velocity of the j th interface
x	vapor quality
x, y, z	spatial coordinates

Greek Symbols

α	void fraction of gas phase
Δ	difference between two terms
Γ	mass generation rate per unit volume
ρ	density
θ	phase distribution parameter

σ	surface tension
τ	shear stress
ω	angular frequency
φ	angle from vertical, rates of change of the bubble number density
Φ	dissipation, rates of change of the interfacial area concentration
ξ	wetted perimeter
ψ	bubble shape factor

Subscripts

B, C	bubble breakup, bubble coalescence
P, V	phase change, void transport
f, g, i	liquid phase, gas phase, value at interface
m, n	index
r	relative
t	per unit time
x, y, z	spatial coordinates
0	reference

Mathematical operators

$\langle \rangle$	area averaged quantity
$\langle\langle \rangle\rangle$	void fraction weighted area averaged quantity
$-$	mean value
$-\text{t}$	time averaged quantity
$-\text{l}$	line averaged quantity
\cdot	perturbed quantity

APPENDICES

APPENDIX A: STRATIFIED TWO-FLUID MODEL DERIVATION

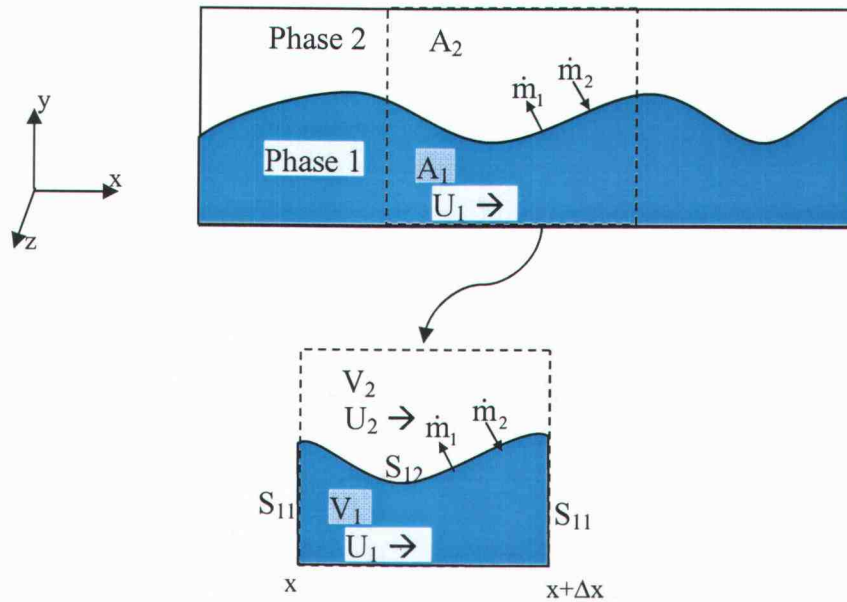


Figure A.1: Control volume for continuity equation

$S_{ff}(x, t)$ – liquid-liquid interface area

$S_{fg}(x, t)$ – liquid-gas interface area

$S_{fw}(x, t)$ – surface bounded by the wall

$V_f(x, t)$ – volume of liquid in control volume

$V_g(x, t)$ – volume of gas in control volume

Using the integral form of conservation of mass:

$$\frac{\partial}{\partial t} \left[\iiint_{V_f} \rho_f dV \right] + \iint_S \rho_f \vec{v} \cdot d\vec{S} = 0 \quad (\text{A.1})$$

$$\Rightarrow \frac{\partial}{\partial t} \left[\iiint_{V_f} \rho_f dV \right] + \iint_S \rho_f (u_f - u_i) \cdot n dS = 0 \quad (A.2)$$

$u_i(x, t)$ – velocity of the moving control volume surface

$n(x, t)$ – outward normal unit vector

Assumptions

- flow is incompressible
- 1-D flow
- at the wall, assume no-slip condition (i.e. $u_f = u_i = 0$)
- at S_{ff} (liquid-liquid interface) $u_i = 0$
- at S_{fg} , $\iint_{S_{fg}} \rho_f (u_f - u_i) \cdot n dS = \iint_{S_{fg}} \dot{m}_{fi} dS$
- assume that \dot{m}_{fi} is constant over the interface of the control volume

Now break up the surface integral into its components:

$$\begin{aligned} & \frac{\partial}{\partial t} \left[\iiint_{V_f} \rho_f dV \right] + \iint_S \rho_f (u_f - u_i) \cdot n dS = 0 \\ \Rightarrow & \frac{\partial}{\partial t} \left[\iiint_{V_f} \rho_f dV \right] + \iint_{S_{ff}} \rho_f (u_f - u_i) \cdot n dS + \iint_{S_{fg}} \rho_f (u_f - u_i) \cdot n dS + \iint_{S_{fw}} \rho_f (u_f - u_i) \cdot n dS = 0 \quad (A.3) \\ \Rightarrow & \frac{\partial}{\partial t} \left[\iiint_{V_f} \rho_f dV \right] + \iint_{S_{ff}} \rho_f u_f \cdot n dS + \iint_{S_{fg}} \rho_f (u_f - u_i) \cdot n dS = 0 \\ \Rightarrow & \frac{\partial}{\partial t} \left[\iiint_{V_f} \rho_f dV \right] + \iint_{S_{ff}} \rho_f u_f \cdot n dS = -\dot{m}_{fi} \iint_{S_{fg}} dS \end{aligned}$$

Since $n = (1, 0, 0)$ on the forward face of S_{ff} and $n = (-1, 0, 0)$ on the back face of S_{ff} , the second integral can be written as:

$$\iint_{S_{ff}} \rho_f u_f \cdot n dS = \iint_{S_{ff} \text{ (forward)}} \rho_f u_{fi} dS - \iint_{S_{ff} \text{ (backward)}} \rho_f u_{fi} dS \quad (A.4)$$

This is a definition of a derivative and can be written as:

$$\frac{\partial}{\partial x} \left[\iiint_{V_f} \rho_f u_{fi} dV \right] = \iint_{S_{ff} \text{ (forward)}} \rho_f u_{fi} dS - \iint_{S_{ff} \text{ (backward)}} \rho_f u_{fi} dS \quad (\text{A.5})$$

$$\Rightarrow \frac{\partial}{\partial t} \left[\iiint_{V_i} \rho_i dV \right] + \frac{\partial}{\partial x} \left[\iiint_{V_i} \rho_i u_{li} dV \right] = -\dot{m}_{li} S_{12} \quad (\text{A.6})$$

Dividing through by the total constant volume, V , we get:

$$\frac{\partial}{\partial t} \left[\frac{1}{V} \iiint_{V_i} \rho_i dV \right] + \frac{\partial}{\partial x} \left[\frac{1}{V} \iiint_{V_i} \rho_i u_{li} dV \right] = -\frac{\dot{m}_{li} S_{12}}{V} \quad (\text{A.7})$$

- Define liquid fraction as $V_i/V = \alpha_L$
- The phasic average is defined as $\bar{\psi}(x,t) = \frac{1}{V_k} \iiint_{V_k} \psi dV$

$$\frac{\partial}{\partial t} [\alpha_L \bar{\rho}_L] + \frac{\partial}{\partial x} [\alpha_L \overline{\rho_L u_{li}}] = -\frac{\dot{m}_{li} S_{12}}{V} \quad (\text{A.8})$$

Using $S_{12} = \xi_i dx$ and using the incompressible flow assumption, the continuity equation becomes:

$$\frac{\partial \alpha_L}{\partial t} + \frac{\partial}{\partial x} [\alpha_L u_L] = -\frac{\dot{m}_{li} \xi_i dx}{\rho_L V} = -\frac{\dot{m}_{li} \xi_i}{\rho_L A} \quad (\text{A.9})$$

For one-dimensional flow using area-averaged quantities:

$$\langle F \rangle = \frac{1}{A} \iint_A F dA \quad (\text{A.10})$$

Perform the area-average of the continuity equation:

$$\frac{1}{A} \iint_A \left[\frac{\partial \alpha_L}{\partial t_{[1]}} + \frac{\partial}{\partial x_{[2]}} [\alpha_L u_L] = - \frac{\dot{m}_{li} \xi_i}{\rho_L A_{[3]}} \right] dA \quad (A.11)$$

$$[1]. \frac{1}{A} \iint_A \frac{\partial \alpha_L}{\partial t} dA = \frac{\partial}{\partial t} \frac{1}{A} \iint_A \alpha_L dA = \frac{\partial \langle \alpha_L \rangle}{\partial t} \quad (A.12)$$

$$[2]. \frac{1}{A} \iint_A \frac{\partial}{\partial x} [\alpha_L u_L] dA = \frac{\partial}{\partial x} \frac{1}{A} \iint_A [\alpha_L u_L] dA = \langle \alpha_L u_L \rangle = \langle \alpha_L \rangle \langle u_L \rangle \quad (A.13)$$

$$[A]. \frac{1}{A} \iint_A - \frac{\dot{m}_{li} \xi_i}{\rho_L A} dA = - \frac{\dot{m}_{li} \xi_i}{\rho_L A} \frac{1}{A} \iint_A dA = - \frac{\dot{m}_{li} \xi_i}{\rho_L A} \quad (A.14)$$

The 1-D continuity equation for the liquid phase becomes:

$$\begin{aligned} \frac{\partial \langle \alpha_L \rangle}{\partial t} + \frac{\partial}{\partial x} [\langle \alpha_L \rangle \langle u_L \rangle] &= - \frac{\dot{m}_{li} \xi_i}{\rho_L A} \\ \Rightarrow \frac{\partial \langle 1 - \alpha_g \rangle}{\partial t} + \frac{\partial}{\partial x} [\langle 1 - \alpha_g \rangle \langle u_L \rangle] &= - \frac{\dot{m}_{li} \xi_i}{\rho_L A} \Rightarrow \frac{\partial \langle \alpha \rangle}{\partial t} + \frac{\partial}{\partial x} [\langle 1 - \alpha \rangle \langle u_L \rangle] = - \frac{\dot{m}_{li} \xi_i}{\rho_L A} \end{aligned} \quad (A.15)$$

The 1-D continuity equation for the gas phase is derived in the same manner with “g” subscripts replacing the “L” subscripts. The 1-D continuity equation for the gas phase becomes:

$$\begin{aligned} \frac{\partial \langle \alpha_g \rangle}{\partial t} + \frac{\partial}{\partial x} [\langle \alpha_g \rangle \langle u_g \rangle] &= - \frac{\dot{m}_{2i} \xi_i}{\rho_g A} \\ \Rightarrow \frac{\partial \langle \alpha \rangle}{\partial t} + \frac{\partial}{\partial x} [\langle \alpha \rangle \langle u_g \rangle] &= - \frac{\dot{m}_{2i} \xi_i}{\rho_g A} \end{aligned} \quad (A.16)$$

Now for the one-dimensional momentum equation:

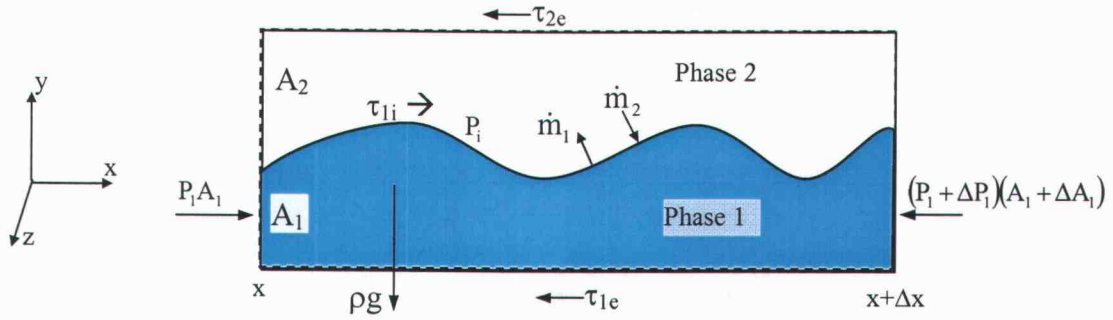


Figure A.2: Control volume for momentum equation

Using the integral form of the momentum equation:

$$\frac{\partial}{\partial t} \left[\iiint_{V_i} \rho_i u_i dV \right] + \iint_S \rho_i u_i (u_i - u_i) \cdot n dS = \iint_S [n_j \tau_{ji} - n_i P] dS + \iiint_{V_i} \rho_i F_i dV \quad (A.17)$$

Using the same assumptions as the continuity equation, the left hand side of the equation becomes:

$$\begin{aligned} & \frac{\partial}{\partial t} \left[\iiint_{V_i} \rho_i u_i dV \right] + \iint_S \rho_i u_i (u_i - u_i) \cdot n dS \\ & \Rightarrow \frac{\partial}{\partial t} \left[\iiint_{V_i} \rho_i u_i dV \right] + \iint_{S_{i1}} \rho_i u_i (u_i - u_i) \cdot n dS + \iint_{S_{i2}} \rho_i u_i (u_i - u_i) \cdot n dS + \iint_{S_{iw}} \rho_i u_i (u_i - u_i) \cdot n dS \quad (A.18) \\ & \Rightarrow \frac{\partial}{\partial t} \left[\iiint_{V_i} \rho_i u_i dV \right] + \iint_{S_{i1}} \rho_i u_i u_i \cdot n dS + \iint_{S_{i2}} \rho_i u_i (u_i - u_i) \cdot n dS \\ & \Rightarrow \frac{\partial}{\partial t} \left[\iiint_{V_i} \rho_i u_i dV \right] + \iint_{S_{i1}} \rho_i u_i u_i \cdot n dS + \dot{m}_{i1} u_i \iint_{S_{i2}} dS \end{aligned}$$

Following the same approach as with the continuity equation, the left-hand side of the one-dimensional momentum equation becomes:

$$\frac{\partial}{\partial t} \left[\iiint_{V_i} \rho_1 u_i dV \right] + \frac{\partial}{\partial x} \left[\iiint_{V_i} \rho_1 u_i u_i dV \right] + \dot{m}_{li} u_i \iint_{S_{12}} dS \quad (A.19)$$

The momentum equation now equals:

$$\frac{\partial}{\partial t} \left[\iiint_{V_i} \rho_1 u_i dV \right] + \frac{\partial}{\partial x} \left[\iiint_{V_i} \rho_1 u_i u_i dV \right] + \dot{m}_{li} u_i \iint_{S_{12}} dS = \iint_S (\tau_{li} - \tau_{le}) dS - \iint_S P \cdot ndS + \iiint_{V_i} \rho_1 g_x dV \quad (A.20)$$

Now divide through by V and assume the flow to be incompressible:

$$\rho_1 \frac{\partial}{\partial t} \left[\frac{1}{V} \iiint_{V_i} u_i dV \right] + \rho_1 \frac{\partial}{\partial x} \left[\frac{1}{V} \iiint_{V_i} u_i u_i dV \right] + \frac{\dot{m}_{li} u_i}{V} \iint_{S_{12}} dS = \frac{1}{V} \iint_S (\tau_{li} - \tau_{le}) dS - \frac{1}{V} \iint_S P \cdot ndS + \frac{\rho_1 g_x}{V} \iiint_{V_i} dV \quad (A.21)$$

Using the definition of liquid fraction, we get:

$$\rho_1 \frac{\partial}{\partial t} [\alpha_L \overline{u_i}] + \rho_1 \frac{\partial}{\partial x} [\alpha_L \overline{u_i u_i}] + \frac{\dot{m}_{li} u_i \xi_i}{A} = \frac{1}{V} \iint_S (\tau_{li} - \tau_{le}) dS - \frac{1}{V} \iint_S P \cdot ndS + \alpha_L \rho_1 g_x \quad (A.22)$$

[1] [2] [3] [4] [5] [6]

The first term in equation (A.22) becomes:

$$[1]. \rho_1 \frac{\partial}{\partial t} [\alpha_L \overline{u_i}] \rightarrow \rho_1 \frac{1}{A} \iint_A \frac{\partial}{\partial t} [\alpha_L \overline{u_i}] dA = \rho_1 \frac{\partial}{\partial t} \frac{1}{A} \iint_A [\alpha_L \overline{u_i}] dA = \rho_1 \frac{\partial}{\partial t} [\alpha_L u_i] = \rho_1 \frac{\partial}{\partial t} [\alpha_L \langle u_i \rangle] \quad (A.23)$$

The second term in equation (A.22) becomes:

$$[2]. \rho_1 \frac{\partial}{\partial x} [\alpha_L \overline{u_i u_i}] \rightarrow \rho_1 \frac{1}{A} \iint_A \frac{\partial}{\partial x} [\alpha_L \overline{u_i u_i}] dA = \rho_1 \frac{\partial}{\partial x} \frac{1}{A} \iint_A [\alpha_L \overline{u_i u_i}] dA = \rho_1 \frac{\partial}{\partial x} [\alpha_L u_i u_i] = \rho_1 \frac{\partial}{\partial x} [\alpha_L \langle u_i u_i \rangle] \quad (A.24)$$

note that:

$$\langle u_i u_i \rangle = \langle u_i \rangle^2 + \langle u_i^2 \rangle - \langle u_i \rangle^2 \quad (A.25)$$

$$\text{Cov}(u_i^2) \equiv \langle u_i^2 \rangle - \langle u_i \rangle^2 \quad (A.26)$$

The second term now becomes:

$$\rho_1 \frac{\partial}{\partial x} [\alpha_L \langle u_i u_i \rangle] \rightarrow \rho_1 \frac{\partial}{\partial x} [\alpha_L \langle u_i \rangle^2 + \text{Cov}(u_i^2)] \quad (A.27)$$

$$[3]. \frac{\dot{m}_{li} u_i \xi_i}{A} \rightarrow \frac{1}{A} \iint_A \dot{m}_{li} u_i \left(\frac{\xi_i}{A} \right) dA = \dot{m}_{li} u_i \left(\frac{\xi_i}{A} \right) \quad (A.28)$$

$$\begin{aligned} & \frac{1}{V} \iint_S (\tau_{li} - \tau_{le}) dS \rightarrow \frac{1}{V} \iint_S \tau_{li} dS - \frac{1}{V} \iint_S \tau_{le} dS \\ [4]. & \rightarrow \frac{1}{A} \iint_A \left[\frac{1}{V} \iint_S \tau_{li} dS - \frac{1}{V} \iint_S \tau_{le} dS \right] \rightarrow \frac{1}{A} \iint_A \left[\frac{\tau_{li}}{V} \iint_S dS - \frac{\tau_{le}}{V} \iint_S dS \right] \\ & \rightarrow \frac{1}{A} \iint_A \left[\tau_{li} \left(\frac{\xi_i}{A} \right) - \tau_{le} \left(\frac{\xi_{le}}{A} \right) \right] \rightarrow \tau_{li} \left(\frac{\xi_i}{A} \right) - \tau_{le} \left(\frac{\xi_{le}}{A} \right) \end{aligned} \quad (A.29)$$

The fifth term becomes:

$$[5]. -\frac{1}{V} \iint_S P \cdot n dS \rightarrow -\frac{1}{V} \iint_{S_{LL}} P_L n_1 dS - \frac{1}{V} \iint_{S_{LI} + S_{LW}} P_L n_1 dS \quad (A.30)$$

The fifth term is broken into two components:

$$\begin{aligned} [a]. & -\frac{1}{V} \iint_{S_{LL}} P_L n_1 dS \rightarrow -\frac{1}{V} \left(P_L A_L + \frac{\partial P_L A_L}{\partial x} dx - P_L A_L \right) \\ & \rightarrow -\frac{1}{A} \left(\frac{\partial P_L A_L}{\partial x} \right) \rightarrow -\left(\frac{\partial P_L \alpha_L}{\partial x} \right) \Rightarrow -\frac{1}{A} \iint_A \left(\frac{\partial P_L \alpha_L}{\partial x} \right) dA = -\frac{\partial \langle P_L \rangle \langle \alpha_L \rangle}{\partial x} \end{aligned} \quad (A.31)$$

$$\begin{aligned} [b]. & -\frac{1}{V} \iint_{S_{LI} + S_{LW}} P_L n_1 dS \rightarrow \frac{1}{V} P_{Li} \iint_{S_{LI} + S_{LW}} -n_1 dS + \frac{1}{V} P_{Li} \iint_{S_{LL}} -n_1 dS - \frac{1}{V} P_{Li} \iint_{S_{LL}} -n_1 dS \\ & \Rightarrow \frac{1}{V} P_{Li} \iint_{S_L} -n_1 dS + \frac{1}{V} P_{Li} \iint_{S_{LL}} n_1 dS \end{aligned} \quad (A.32)$$

using the divergence theorem, the first term on the right becomes :

$$\frac{1}{V} P_{Li} \iint_{V_L} \frac{\partial}{\partial x} (-1) dV = 0 \quad (A.33)$$

$$\begin{aligned} & \frac{1}{V} P_{Li} \iint_{S_{LL}} n_1 dS \Rightarrow \frac{1}{V} P_{Li} \left[\iint_{S_{LL}^{(forward)}} dS - \iint_{S_{LL}^{(back)}} dS \right] = \frac{1}{V} P_{Li} \frac{\partial}{\partial x} \left[\iiint_{V_L} dV \right] = P_{Li} \frac{\partial \alpha_L}{\partial x} \\ & \rightarrow \frac{1}{A} \iint_A P_{Li} \frac{\partial \alpha_L}{\partial x} dA \rightarrow P_{Li} \frac{\partial \langle \alpha_L \rangle}{\partial x} \end{aligned} \quad (A.34)$$

$$\begin{aligned}
-\frac{1}{V} \iint_S \mathbf{P} \cdot \mathbf{n} dS &= -\frac{\partial \langle \langle \mathbf{P}_1 \rangle \rangle \langle \alpha_L \rangle}{\partial x} + P_{Li} \frac{\partial \langle \alpha_L \rangle}{\partial x} = -\langle \langle \mathbf{P}_1 \rangle \rangle \frac{\partial \langle \alpha_L \rangle}{\partial x} - \langle \alpha_L \rangle \frac{\partial \langle \langle \mathbf{P}_1 \rangle \rangle}{\partial x} + P_{Li} \frac{\partial \langle \alpha_L \rangle}{\partial x} \\
&\rightarrow (P_{Li} - \langle \langle \mathbf{P}_1 \rangle \rangle) \frac{\partial \langle \alpha_L \rangle}{\partial x} - \langle \alpha_L \rangle \frac{\partial \langle \langle \mathbf{P}_1 \rangle \rangle}{\partial x}
\end{aligned} \tag{A.35}$$

$$[6]. \alpha_L \rho_1 g_x \rightarrow \frac{1}{A} \iint_A \alpha_L \rho_1 g_x dA = \langle \alpha_L \rangle \rho_1 g_x \tag{A.36}$$

The liquid phase momentum equation becomes:

$$\begin{aligned}
\rho_1 \frac{\partial}{\partial t} [\langle \alpha_L \rangle \langle \langle u_1 \rangle \rangle] + \rho_1 \frac{\partial}{\partial x} [\langle \alpha_L \rangle \langle \langle u_1 \rangle \rangle^2 + \text{Cov}(u_1^2)] \\
= -\dot{m}_{li} u_i \left(\frac{\xi_i}{A} \right) + \tau_{li} \left(\frac{\xi_i}{A} \right) - \tau_{le} \left(\frac{\xi_{le}}{A} \right) + (P_{Li} - \langle \langle \mathbf{P}_1 \rangle \rangle) \frac{\partial \langle \alpha_L \rangle}{\partial x} - \langle \alpha_L \rangle \frac{\partial \langle \langle \mathbf{P}_1 \rangle \rangle}{\partial x} + \langle \alpha_L \rangle \rho_1 g_x
\end{aligned} \tag{A.37}$$

The derivation of the gas phase momentum equation is performed in a similar manner with the exception that the sign on the interface shear term changes from a positive to a negative. The gas phase momentum equation becomes:

$$\begin{aligned}
\rho_2 \frac{\partial}{\partial t} [\langle \alpha_g \rangle \langle \langle u_2 \rangle \rangle] + \rho_2 \frac{\partial}{\partial x} [\langle \alpha_g \rangle \langle \langle u_2 \rangle \rangle^2 + \text{Cov}(u_2^2)] \\
= -\dot{m}_{2i} u_i \left(\frac{\xi_i}{A} \right) - \tau_{2i} \left(\frac{\xi_i}{A} \right) - \tau_{2e} \left(\frac{\xi_{2e}}{A} \right) + (P_{gi} - \langle \langle \mathbf{P}_2 \rangle \rangle) \frac{\partial \langle \alpha_g \rangle}{\partial x} - \langle \alpha_g \rangle \frac{\partial \langle \langle \mathbf{P}_2 \rangle \rangle}{\partial x} + \langle \alpha_g \rangle \rho_2 g_x
\end{aligned} \tag{A.38}$$

The one-dimensional two-fluid model equations for the fully-mixed flow condition can be derived using a similar procedure as above.

APPENDIX B: PHASE DISTRIBUTION PARAMETERS DERIVATION

Gas Phase Pressure

$$\langle\langle P_g \rangle\rangle = \frac{\frac{1}{A} \int_A (P_R + P_{grav}) \alpha dA}{\frac{1}{A} \int_A \alpha dA} \quad \text{with,} \quad P_{grav} = \int_0^y \rho_m g dy' \quad (B.1)$$

$$\langle\langle P_g \rangle\rangle = P_r + \frac{\frac{1}{A} \int_A \int_0^y \rho_m g dy' \alpha dA}{\frac{1}{A} \int_A \alpha dA} \rightarrow P_r + \frac{\frac{1}{A} \int_A \int_0^y [\rho_g \alpha + \rho_f (1-\alpha)] g dy' \alpha dA}{\frac{1}{A} \int_A \alpha dA} \quad (B.2)$$

Now, assume that the pressure variation due to the gravitational head is only a function of height. The phase-averaged gas pressure now becomes:

$$\langle\langle P_g \rangle\rangle - P_r = \frac{\frac{1}{H} \int_{H0}^y \int_0^y [\rho_g \alpha + \rho_f (1-\alpha)] g dy' \alpha dy}{\frac{1}{H} \int_H \alpha dy} \rightarrow \frac{\int_{H0}^y \int_0^y [\rho_g \alpha + \rho_f (1-\alpha)] g dy' \alpha dy}{\int_H \alpha dy} \quad (B.3)$$

$$\langle\langle P_g \rangle\rangle - P_r = g \frac{\int_H \left[\rho_g \int_0^y \alpha dy' + \rho_f \int_0^y (1-\alpha) dy' \right] \alpha dy}{\int_H \alpha dy} \quad (B.4)$$

$$\begin{aligned} \langle\langle P_g \rangle\rangle - P_r &= g \frac{\int_H \left[\rho_g \int_0^y \alpha dy' + \rho_f \left[\int_0^y dy' - \int_0^y \alpha dy' \right] \right] \alpha dy}{\int_H \alpha dy} \\ &\rightarrow g \frac{\int_H \left[\rho_g \int_0^y \alpha dy' + \rho_f \left[y - \int_0^y \alpha dy' \right] \right] \alpha dy}{\int_H \alpha dy} \end{aligned} \quad (B.5)$$

$$\begin{aligned}
\langle\langle P_g \rangle\rangle - P_r &= g \frac{\int_H \rho_g \int_0^y \alpha dy' \alpha dy}{\int_H \alpha dy} + g \frac{\int_H \rho_f \left[y - \int_0^y \alpha dy' \right] \alpha dy}{\int_H \alpha dy} \\
&\rightarrow \rho_g g \frac{\int_H \int_0^y \alpha dy' \alpha dy}{\int_H \alpha dy} + \rho_f g \frac{\int_H \left[y - \int_0^y \alpha dy' \right] \alpha dy}{\int_H \alpha dy}
\end{aligned} \tag{B.6}$$

$$\begin{aligned}
\langle\langle P_g \rangle\rangle - P_r &= \rho_g g \frac{\int_H \int_0^y \alpha dy' \alpha dy}{\int_H \alpha dy} + \rho_f g \frac{\int_H y \alpha dy - \int_H \int_0^y \alpha dy' \alpha dy}{\int_H \alpha dy} \\
&\rightarrow \rho_g g H \frac{\frac{1}{H} \int_H \int_0^y \alpha dy' \alpha dy}{\int_H \alpha dy} + \rho_f g H \left[\frac{\int_H \frac{y}{H} \alpha dy}{\int_H \alpha dy} - \frac{\frac{1}{H} \int_H \int_0^y \alpha dy' \alpha dy}{\int_H \alpha dy} \right]
\end{aligned} \tag{B.7}$$

$$\langle\langle P_g \rangle\rangle - P_r = \rho_g g H \left[\frac{\int_H \int_0^y \alpha dy' \alpha dy}{H^2 \bar{\alpha}^L} \right] + \rho_f g H \left[\frac{\int_H \frac{y}{H} \alpha dy}{H \bar{\alpha}^L} - \frac{\int_H \int_0^y \alpha dy' \alpha dy}{H^2 \bar{\alpha}^L} \right] \tag{B.8}$$

The average gas phase pressure becomes:

$$\langle\langle P_g \rangle\rangle - P_r = \rho_g g H \theta_2 + \rho_f g H [\theta_0 - \theta_2] \tag{B.9}$$

Where:

$$\theta_0 = \frac{\int_H \frac{y}{H} \alpha dy}{H \bar{\alpha}^L} \quad \theta_1 = \frac{\int_H \int_0^y \alpha dy' dy}{H^2 \bar{\alpha}^L} \quad \theta_2 = \frac{\int_H \int_0^y \alpha dy' \alpha dy}{H^2 \bar{\alpha}^L}$$

Liquid Phase Pressure

$$\langle\langle P_f \rangle\rangle = \frac{\frac{1}{A} \int_A (P_R + P_{\text{grav}})(1-\alpha) dA}{\frac{1}{A} \int_A (1-\alpha) dA} \quad \text{with,} \quad P_{\text{grav}} = \int_0^y \rho_m g dy' \quad (\text{B.10})$$

$$\langle\langle P_f \rangle\rangle = P_r + \frac{\frac{1}{A} \int_A \int_0^y \rho_m g dy' (1-\alpha) dA}{\frac{1}{A} \int_A (1-\alpha) dA} \rightarrow P_r + \frac{\frac{1}{A} \int_A \int_0^y [\rho_g \alpha + \rho_f (1-\alpha)] g dy' (1-\alpha) dA}{\frac{1}{A} \int_A (1-\alpha) dA} \quad (\text{B.11})$$

Now, assume that the pressure variation due to the gravitational head is only a function of height. The phase-averaged liquid pressure now becomes:

$$\langle\langle P_f \rangle\rangle - P_r = \frac{\frac{1}{H} \int_H^y \int_0^y [\rho_g \alpha + \rho_f (1-\alpha)] g dy' (1-\alpha) dy}{\frac{1}{H} \int_H (1-\alpha) dy} \rightarrow \frac{\int_H^y \int_0^y [\rho_g \alpha + \rho_f (1-\alpha)] g dy' (1-\alpha) dy}{\int_H (1-\alpha) dy} \quad (\text{B.12})$$

$$\langle\langle P_f \rangle\rangle - P_r = g \frac{\int_H^y \left[\int_0^y \rho_g \alpha dy' + \int_0^y \rho_f (1-\alpha) dy' \right] (1-\alpha) dy}{\int_H (1-\alpha) dy} \rightarrow g \frac{\int_H \left[\rho_g \int_0^y \alpha dy' + \rho_f \int_0^y (1-\alpha) dy' \right] (1-\alpha) dy}{\int_H (1-\alpha) dy} \quad (\text{B.13})$$

$$\langle\langle P_f \rangle\rangle - P_r = g \frac{\int_H \left[\rho_g \int_0^y \alpha dy' + \rho_f \left[\int_0^y dy' - \int_0^y \alpha dy' \right] \right] (1-\alpha) dy}{\int_H (1-\alpha) dy} \rightarrow g \frac{\int_H \left[\rho_g \int_0^y \alpha dy' + \rho_f \left[y - \int_0^y \alpha dy' \right] \right] (1-\alpha) dy}{\int_H \alpha dy} \quad (\text{B.14})$$

$$\langle\langle P_f \rangle\rangle - P_r = g \frac{\int_H \rho_g \int_0^y \alpha dy' (1-\alpha) dy}{\int_H (1-\alpha) dy} + g \frac{\int_H \rho_f \left[y - \int_0^y \alpha dy' \right] (1-\alpha) dy}{\int_H (1-\alpha) dy} \rightarrow \rho_g g \frac{\int_H \int_0^y \alpha dy' (1-\alpha) dy}{\int_H (1-\alpha) dy} + \rho_f g \frac{\int_H \left[y - \int_0^y \alpha dy' \right] (1-\alpha) dy}{\int_H (1-\alpha) dy} \quad (\text{B.15})$$

$$\langle\langle P_f \rangle\rangle - P_r = \rho_g g \frac{\int_H \int_0^y \alpha dy' (1-\alpha) dy}{\int_H (1-\alpha) dy} + \rho_f g \frac{\int_H y (1-\alpha) dy - \int_H \int_0^y \alpha dy' (1-\alpha) dy}{\int_H (1-\alpha) dy} \quad (\text{B.16})$$

$$\langle\langle P_f \rangle\rangle - P_r = \rho_g g \frac{\int_H^y \alpha dy' (1-\alpha) dy}{\int_H (1-\alpha) dy} + \rho_f g \left[\frac{\int_H^y y (1-\alpha) dy}{\int_H (1-\alpha) dy} - \frac{\int_H^y \alpha dy' (1-\alpha) dy}{\int_H (1-\alpha) dy} \right] \quad (B.17)$$

$$\begin{aligned} \langle\langle P_f \rangle\rangle - P_r = & \frac{\rho_g g}{\int_H (1-\alpha) dy} \left[\int_H^y \alpha dy' dy - \int_H^y \alpha dy' \alpha dy \right] \\ & + \frac{\rho_f g}{\int_H (1-\alpha) dy} \left[\int_H^y y dy - \int_H^y y \alpha dy - \int_H^y \alpha dy' dy + \int_H^y \alpha dy' \alpha dy \right] \end{aligned} \quad (B.18)$$

$$\begin{aligned} \langle\langle P_f \rangle\rangle - P_r = & \frac{\rho_g g H}{\int_H (1-\alpha) dy} \left[\frac{1}{H} \int_H^y \alpha dy' dy - \frac{1}{H} \int_H^y \alpha dy' \alpha dy \right] \\ & + \frac{\rho_f g H}{\int_H (1-\alpha) dy} \left[\frac{H}{2} - \int_H^y \alpha dy - \frac{1}{H} \int_H^y \alpha dy' dy + \frac{1}{H} \int_H^y \alpha dy' \alpha dy \right] \end{aligned} \quad (B.19)$$

$$\langle\langle P_f \rangle\rangle - P_r = \frac{\rho_g g H}{(1-\bar{\alpha}^L)} [\bar{\alpha}^L \theta_1 - \bar{\alpha}^L \theta_2] + \frac{\rho_f g H}{(1-\bar{\alpha}^L)} \left[\frac{1}{2} - \bar{\alpha}^L \theta_0 - \bar{\alpha}^L \theta_1 + \bar{\alpha}^L \theta_2 \right] \quad (B.20)$$

Using:

$$\theta_0 = \frac{\int_0^1 \eta \alpha d\eta}{\bar{\alpha}^L} \quad \theta_1 = \frac{\int_0^1 \int_0^\eta \alpha d\eta' d\eta}{\bar{\alpha}^L} \quad \theta_2 = \frac{\int_0^1 \int_0^\eta \alpha d\eta' \alpha d\eta}{\bar{\alpha}^L}$$

The simplifying relations were found to be:

$$\theta_0 = 1 - \theta_1 \quad \theta_2 = \frac{\bar{\alpha}^L}{2}$$

Substituting into the pressure equations:

$$\begin{aligned} \langle\langle P_g \rangle\rangle - P_r = & \rho_g g H \theta_2 + \rho_f g H [\theta_0 - \theta_2] \\ = & \rho_g g H \frac{\bar{\alpha}^L}{2} + \rho_f g H \left[\theta_0 - \frac{\bar{\alpha}^L}{2} \right] \end{aligned} \quad (B.21)$$

The gas phase pressure becomes:

$$\langle\langle P_g \rangle\rangle - P_r = \frac{\rho_g g H \bar{\alpha}^L}{2} + \rho_f g H \left[\theta - \frac{\bar{\alpha}^L}{2} \right] \quad (\text{B.22})$$

Now for the liquid phase with the simplifying relations:

$$\begin{aligned} \langle\langle P_f \rangle\rangle - P_r &= \frac{\rho_g g H}{(1 - \bar{\alpha}^L)} [\bar{\alpha}^L \theta_1 - \bar{\alpha}^L \theta_2] + \frac{\rho_f g H}{(1 - \bar{\alpha}^L)} \left[\frac{1}{2} - \bar{\alpha}^L \theta_0 - \bar{\alpha}^L \theta_1 + \bar{\alpha}^L \theta_2 \right] \\ &= \frac{\rho_g g H}{(1 - \bar{\alpha}^L)} \left[\bar{\alpha}^L (1 - \theta_0) - \frac{\bar{\alpha}^L \bar{\alpha}^L}{2} \right] + \frac{\rho_f g H}{(1 - \bar{\alpha}^L)} \left[\frac{1}{2} - \bar{\alpha}^L \theta_0 - \bar{\alpha}^L (1 - \theta_0) + \frac{\bar{\alpha}^L \bar{\alpha}^L}{2} \right] \\ &= \frac{\rho_g g H}{(1 - \bar{\alpha}^L)} \left[\bar{\alpha}^L (1 - \theta_0) - \frac{\bar{\alpha}^L \bar{\alpha}^L}{2} \right] + \frac{\rho_f g H}{(1 - \bar{\alpha}^L)} \left[\frac{1}{2} - \bar{\alpha}^L \theta_0 - \bar{\alpha}^L + \bar{\alpha}^L \theta_0 + \frac{\bar{\alpha}^L \bar{\alpha}^L}{2} \right] \\ &= \frac{\rho_g g H}{(1 - \bar{\alpha}^L)} \left[\bar{\alpha}^L (1 - \theta_0) - \frac{\bar{\alpha}^L \bar{\alpha}^L}{2} \right] + \frac{\rho_f g H}{2(1 - \bar{\alpha}^L)} [1 - 2\bar{\alpha}^L + \bar{\alpha}^L \bar{\alpha}^L] \\ &= \frac{\rho_g g H}{(1 - \bar{\alpha}^L)} \left[\bar{\alpha}^L (1 - \theta_0) - \frac{\bar{\alpha}^L \bar{\alpha}^L}{2} \right] + \frac{\rho_f g H}{2(1 - \bar{\alpha}^L)} [1 - \bar{\alpha}^L] [1 - \bar{\alpha}^L] \end{aligned} \quad (\text{B.23})$$

The liquid phase pressure becomes:

$$\langle\langle P_f \rangle\rangle - P_r = \frac{\rho_g g H}{(1 - \bar{\alpha}^L)} \left[\bar{\alpha}^L (1 - \theta) - \frac{\bar{\alpha}^L \bar{\alpha}^L}{2} \right] + \frac{\rho_f g H}{2} [1 - \bar{\alpha}^L] \quad (\text{B.24})$$

Where the distribution parameter, θ , the following range of values:

$$\frac{\bar{\alpha}^L}{2} \leq \theta \leq \frac{1}{2}$$